A
Thesis Submitted
in Partial Fulfillment of the Requirement

For the Degree of
Doctor of Philosophy

Synthesis, Characterization and Applications of Nanocomposite-MOFs of Cobalt with 4, 4'-oxy bis-benzoic acid and Metal Oxide Nanoparticles

Submitted by
Rupinder Kaur
(901209004)

Under the Supervision
Of

Dr. Susheel Mittal
Senior Professor

Dr. Manmohan Chhibber
Associate Professor

School of Chemistry & Biochemistry
Thapar Institute of Engineering and Technology (Deemed To Be University)
Patiala-147004, India

August, 2018

Candidate's Declaration

I, hereby declare that the work presented in the thesis entitled "**Synthesis, Characterization and Applications of Nanocomposite -MOFs of Cobalt with 4, 4'-oxy bis-benzoic acid and Metal Oxide Nanoparticles**" in partial fulfillment of the requirements for the award of the degree of Doctor of Philosophy, is an authentic record of my own work carried out under the joint supervision of Dr. Susheel Mittal (CChem, FRSc, Senior Professor) and Dr. Manmohan Chhibber (Associate Professor), School of Chemistry and Biochemistry, Thapar Institute of Engineering and Technology (Deemed To Be University), Patiala, India. The matter embodied in this thesis has not been submitted in part or full to any other university or institute for the award of any degree in India or abroad.

Rupinder Kaur

Reg. No.-901209004

Place: Patiala, India

Date:

Certificate

Certified that the thesis entitled "**Synthesis, Characterization and Applications of Nanocomposite -MOFs of Cobalt with 4, 4'-oxy bis-benzoic acid and Metal Oxide Nanoparticles**" which is submitted by Ms. Rupinder Kaur in partial fulfillment of the requirements for the award of the degree of Doctor of Philosophy at School of Chemistry and Biochemistry, Thapar Institute of Engineering and Technology (Deemed To Be University), Patiala, is a record of candidate's own independent and original research work carried out by her under our supervision and guidance. The matter embodied in this thesis has not been submitted in part or full to any other university or institute for the award of any degree in India or abroad.

Supervisors

Susheel Mittal

Dr. Susheel Mittal
(CChem, FRSc)
Senior Professor
School of Chemistry and Biochemistry,
Thapar Institute of Engineering and
Technology (Deemed To Be University),
Patiala-147004

Dr. Manmohan Chhibber
Associate Professor
School of Chemistry and Biochemistry,
Thapar Institute of Engineering and
Technology (Deemed To Be University),
Patiala-147004

Head

5/03/19

Dr. Amjad Ali
Associate Professor
School of Chemistry and Biochemistry,
Thapar Institute of Engineering and
Technology (Deemed To Be University),
Patiala-147004

ACKNOWLEDGEMENTS

Firstly, I would like to express my sincere gratitude to research supervisors Dr. Susheel Mittal (CChem, FRSc, Senior Professor) and Dr. Manmohan Chhibber (Associate Professor) for their continuous cooperation, patience, motivation and guidance throughout my research journey. The calm and supportive nature of Dr. Mittal makes him an ideal research guide for anyone who is willing to work under him. His ability to tackle any research problem and making a way out of it had always inspired me. Thank you Sir, for all that you have done for me. I am equally thankful to Dr. Chhibber for his positive attitude and able guidance. Doing every task with great perfection and devotion are few things which I have learnt from his personality.

I am also grateful to Dr. Partha Mahata (Associate Prof., Jadavpur University, Kolkata) for enlightening me with the first glance of research. Though from distance, he had always motivated and guided me with his positive attitude. His timely and well thought out interventions had greatly enriched my knowledge and research work.

Besides my advisors, I would like to thank the rest of my doctoral committee: Dr. Amjad Ali (Head of the department and Associate Prof.), Prof. Bonamali Pal, Prof. O.P. Pandey (Dean, R&SP and Sen. Prof.) not only for their insightful comments and encouragement, but also for the hard questions which incented me to widen my research from various perspectives.

I am thankful to Mr. Mayank Sharma and Mr. Chander Singh Thakur for their timely help and care.

I thank my fellow labmates- Ms. Manisha Pabbi, Ms. Sonia Rana, Mr. Sanjeev Kumar, Mr. Ashok Kumar and Ms. Shivali Gupta for the stimulating discussions, for the sleepless nights we were working together before deadlines and for all the fun we have had during this journey. Also my friends Ms. Manpreet Aulakh, Mr. Anirudh Sharma and Ms. Priyanka deserve a special mention for their support.

It is said that pillars of a person's life are the family members and my case is no exception. Right from the onset, my parents- Mr. Gurnam Singh and Mrs. Amarjit Kaur and my lovely brother-

Mr. Bikram Singh stood by my side and had always encouraged me to undertake this long journey with their love. All my worries and negative thoughts regarding my work used to disappear upon seeing the faces of my sweet little twin nephews-Nimratveer Singh and Samarveer Singh. I would like to attribute a special vote of thanks to my husband-Mr. Harpreet Singh for his unconditional love and patience. He had always put his faith in me and urged me to push on towards my goal. I am also thankful to my parents-in-laws for their cooperation and all the support.

The depths to which these people dove to support me are unfathomable. This thesis is a collective effort and a representation of the contribution that all these people made in my life.

Last but not the least; I would like to thank almighty, who gave me the strength and endurance to complete this chapter of my life.

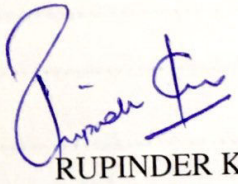

RUPINDER KAUR

TABLE OF CONTENTS

SUMMARY ……..1-11

CHAPTER 1……12-17

INTRODUCTION ……..12

Conclusions ……..14

References ……16

CHAPTER 2……18**-39**

LITERATURE BACKGROUND ……...18- 39

Preparation Methods for MOFs ……..... 19

Solvothermal synthesis …….. 19

Microwave synthesis …….. 20

Electrochemical Synthesis …… 21

Sonochemical Synthesis ……. 23

MOF Based Composites …….. 23

MOF-Organic Matrix composites …… 24

MOF-Inorganic Matrix composites …… 25

Nanoparticles@ MOF composites ……... 26

Wet Impregnation or Solution Infiltration Method …… 27

Chemical Vapour Deposition (CVD) method …… 28

Mechanical Grinding …… 29

Applications of NPs@MOF Composites …… 29

Heterogeneous catalysis …… 29

Hydrogen Storage …….. 31

Chemical Sensing ……... 32

Electrochemical Applications…… 33

References …… 35

CHAPTER 3……... 40-47

METHODS AND MATERIALS …… 40

Chemicals …… 40

Characterizations and Instruments …….. 40

Techniques Used …….. 41

Powder X-Ray Diffraction (PXRD) …….. 41

High Resolution Transmission Electron Microscopy (HR-TEM) …… 42

X-Ray Photoelectron Spectroscopy (XPS) …… 42

Raman Spectroscopy …….. 42

Scanning electron microscopy (SEM) ……... 42

Spectrophotometry …… 42

Spectroflourometry …… 43

Voltammetry …….. 43

Cyclic Voltammetry (CV) …….. 43

Linear Sweep Voltammetry (LSV) …… 43

Chronoamperometry ……..44

SYNTHETIC PROCEDURES …….. 44

Synthesis of $[Co(OBA)(H_2O)_2]$, 1 44

Synthesis of 4-(2, 4-Dinitrophenoxy)-3-methoxybenzaldehyde (DPE-1) …… 44

Synthesis of 4-(2, 4-Dintrophenoxy)-3-methoxybenzyl alcohol (DPE-2) …… 45

Synthesis of ZnO/MOF …… 45

Catalytic reduction using ZnO/MOF…….. 45

Synthesis of Ceria (CeO_2) nanoparticles ……... 45

Synthesis of Ceria loaded Co-MOF (CeO_2/MOF) ……..46

Preparation of Ceria/MOF modified electrode …….. 46

References …… 47

CHAPTER 4 …….. 48-97

RESULTS AND DISCUSSION

CHAPTER 4A ……... 48-60

Preparation of Materials ……..... 48

Synthesis and Characterization of Co-MOF …..……..... 48

Synthesis and Characterization of ZnO/MOF Composites …..…….. 50

Synthesis and Characterization of CeO_2/MOF Composite …….……...55

CHAPTER-4B..... 61-98

Applications of Co-MOF and its Composites ……. 61

Detection of nitro aromatic compounds ..…….. 61

Detection of organo-phosphate pesticides ……. 70

Catalytic reduction of nitro aromatic compounds (NACs) …….. 74

Electrocatalytic studies for oxygen evolution reaction (OER) …….. 85

References ……92

CHAPTER 5 ……..... 98-100

CONCLUSIONS ……98

References …….…… 100

ANNEXURE-1 ……101-107

LIST OF PUBLICATIONS ……... 108

SUMMARY

Chapter 1: Introduction

This chapter discusses origin of the problem and the versatile nature of metal organic frameworks and their nano-composites. Their versatility can be realized from the fact these materials can be used for numerous applications such gas storage, catalysis, ion exchange, drug delivery and many more. All these applications arise from their unique structural features such as pore size, pore volume, interlinked pore channels etc.

Chapter 2: Literature Review

This chapter is based upon the historical background related to the use of metal organic frameworks. The chapter also elaborates the different types of methods used so far for the synthesis of metal organic frameworks. Further, the types of composites and their utilities have been detailed. Composites are the multi-component mixtures of metal organic frameworks and other materials such as nanoparticles (NP), organic/inorganic matrices. Followed by this, the chapter is focused on the NP-MOF composites discussing their different synthetic methods and the applications of such composites.

The foundation stone of modern coordination chemistry was laid down long back in 1893 when Alfred Werner proposed the structure of octahedral complexes and provided a theoretical and experimental justification regarding the bonding in coordination complexes.[1] In the last two decades, metal organic frameworks (MOFs) have emerged as a new branch of coordination chemistry where metal centres are bridged through organic ligands giving rise to an infinite maze or array creating pores or cavities. The conventional method of MOF synthesis comprises a general process of dissolving the raw materials (metal salt and organic linker) in an appropriate solvent followed by heating in a sealed vessel under autogenous pressure above the boiling point of the solvent. This generally proceeds without any parallelization of reactions. The research group at BASF in 2005 did the pioneer work related to the electrochemical synthesis of metal organic frameworks. The prime objective of the work was to eliminate to use of anions such as sulphate, chloride or perchlorate for the synthetic procedure which are one of limiting factors for the large scale production of metal organic frameworks. Sonochemical synthesis is another method through which small MOF crystals can be produced in a short duration of time. The rate

of reaction is increased with the help of ultrasonic waves which causes the formation and collapse of bubbles in the reaction mixture.

Chapter 3: Materials and Methods

This chapter reports the materials and methods used to synthesize Co based metal organic framework and its composites with metal oxide nanoparticles and further their luminescent, catalytic studies by using spectroscopic, HPLC and electroanalytical techniques. Details about the techniques used throughout to carry out the catalytic and electrochemical studies such as spectrophotometry, spectrofluorimetry, PXRD, HR-TEM, SEM-EDS, XPS, Raman, cyclic voltammetry, linear sweep voltammetry and chronoamperommetry are also included in this chapter.

Chemicals needed for the synthesis, $CoCl_2.6H_2O$ (98%), NaOH (97%) benzene (BZ) (99%), nitrobenzene (NB) (99%), 4-nitrobenzoic acid (4-NBA) (97%), 3-nitrotoluene (NT) (98%), p-nitrophenol (PNP) (97%), 2,4-dinitrofluorobenzene (DNFB) (99%), 2, 4, 6-trinitrophenol (TNP) (98%), $Zn(NO_3)_2.6H_2O$ (98%), $NaBH_4$ (98%) and 4-fluoronitrobenzene (FNB) (98%)were used as received from SDFCL. Whereas 2,6-dintrotoluene (2,6-DNT) (98%), KOH (98 %), p-nitroanisole (p-NA) (98%), nitrobenzene (NB) (98%) , p-nitrobenzoic acid (p-NBA) (98%) and 1, 3- dinitrobenzene (1,3-DNB) (98%) were purchased from Loba Chemie, India and were used without further purification. Also 4, 4′-oxy bis(benzoic acid) (99%) was procured from Sigma-Aldrich and was used as received. Other solvents such as acetonitrile (99.5%) and toluene (Tol) (98%) were bought from Merck, India and were used without further purification. Pesticides, chlorpyrifos (94%), Malathion (96%), acephate (95%) and triazophos (90%) were procured from Markfed, India. $Ce(NO_3)_3.6H_2O$ (98%) and methanol (98%) were purchased from CDH, India All the electrochemical measurements were done in deionized water. The water used for luminescent studies and other synthesis was double distilled and filtered through a Millipore membrane. Stock solutions of compounds were prepared by using above mentioned solvents as per the analytical requirements. All the glassware was cleaned with HNO_3 and rinsed thoroughly with distilled water before use. Nitrogen purging was carried out for 5 minutes in the test solution to carry out all the electrochemical experiments.

Chapter 4: Results and Discussion

This chapter of the thesis summarizes various experimental results. The chapter is divided into two major parts. The first part focuses on the synthesis and characterization of MOF and its various composites with ZnO and ceria nanoparticles. The second part discusses the applications of the bare MOF and the composites.

Chapter 4A: Synthesis and Characterization of Co-MOF and its Composites

- **Co-MOF, 1**

This chapter begins with the synthesis and characterization of a Co based MOF, $Co(OBA)(H_2O)_2$] [OBA= 4,4'-oxybis(benzoate)], **1** and the various composites synthesized by the incorporation of ZnO nanoparticles (namely, ZnO/MOF-I, ZnO/MOF-II and ZnO/MOF-III) and ceria nanoparticles, i.e. CeO_2/MOF.

Co-MOF was prepared by using a convenient solvent evaporation method taking $CoCl_2.6H_2O$ and 4, 4'-oxy-bis (benzoic acid) as precursors by using an earlier reported protocol. The crystal structure of as-synthesized CP was characterized with the help of powder X-Ray diffraction technique (P-XRD) which was found in good agreement with the reported data.

- **ZnO/MOF Composites**

ZnO/MOF composites were synthesized using wet impregnation method where Zn^{2+} solution in methanol was hydrolyzed *in-situ* using NaOH to form ZnO nanoparticles in the presence of MOF, **1**, dispersion. Zn^{2+} salt was taken in different molar ratios to get three different compositions of ZnO nanoparticles doped MOF (ZnO/MOF-I, ZnO/MOF-II and ZnO/MOF-III). PXRD patterns observed for all the three composites- ZnO/MOF-I, ZnO/MOF-II and ZnO/MOF-III show sharp peaks and were similar to that of the parent MOF, **1,** indicating that the current synthesis protocol does not alter the crystallinity and proceed with the conservation of structural integrity of its framework. However, the slight shifting of the main peak to higher 2Θ from 6.97º (2Θ) to 7.7 º (2Θ) occurred during the calcinations in oven at 120 ºC to form ZnO nanoparticles from $Zn(OH)_2$. The morphology and composition of as-synthesized composites was investigated using HR-TEM, SEM-EDS and Microwave Plasma-Atomic Emission Spectroscopy (MP-AES). Further, the composites were characterized using X-Ray Photoelectron spectroscopy (XPS). The

peaks of O 1s for ZnO/MOF-I, II and III appear at 530.6 eV, 529.9 eV and 530.3 eV respectively, which is the standard peak for ZnO. Whereas the standard peak position for $Zn(OH)_2$ is usually located at 532 eV. Hence, this confirms the successful loading of ZnO nanoparticles onto the MOF. The room temperature Raman studies were also done in order to further confirm the incorporation of ZnO nanoparticles into the Co-MOF. The characteristic scattering peak at 437 cm^{-1} of the high frequency branch of E_2 mode of hexagonal wurtzite ZnO was observed in case of ZnO/MOF-I, ZnO/MOF-II and ZnO/MOF-III which confirms the successful incorporation of ZnO nanoparticles into Co-MOF.

- **CeO_2/MOF Composite**

Further, this chapter elaborates the synthesis and characterization of CeO_2/MOF composite where ceria nanoparticles were incorporated into Co-MOF, **1**, with the help of wet impregnation process. The aqueous solution of cerium nitrate is introduced into the MOF dispersion and the addition of hydroxide ions to the mixture leads to the formation of cerium hydroxide. Upon calcinations, it leads to the formation of a composite material having ceria nanoparticles incorporated into the Co-MOF. The powder XRD pattern of the synthesized Ceria/MOF hybrid indicated the conservation of overall structural framework of Co-MOF after the incorporation of ceria nanoparticles and the characteristic peaks for ceria nanoparticles as reported in the literature. HR-TEM and SEM-EDS studies were done to analyze the textural structures and composition of the composite material. The peak of O 1s for CeO_2/MOF observed at 530.2 eV in XPS measurements is the standard peak for the oxide oxygen which confirms the successful loading of ceria nanoparticles onto the MOF. Whereas the peak observed at 465 cm^{-1} in Raman spectra of CeO_2/MOF is attributed to the characteristic peak of cubic structured CeO_2 corresponding to the symmetrical stretching mode of Ce-O8 vibrational unit which confirms successful incorporation of ceria nanoparticles into Co-MOF.

Chapter 4B: Applications of Co-MOF and its Composites

Detection of Nitro Aromatic Compounds

The chapter further moves on to describe the potential applications of Co-MOF, **1** and its composites. Luminescence based studies of **1** were done and it was found that the nitro aromatics trinitro phenol (TNP), nitrobenzene (NB), p-nitrophenol (PNP), 1, 3-dinitro benzene

(1,3-DNB), 2,6-dinitro toluene (2,6-DNT), 4-nitrobenzoic acid (4-NBA), p-Nitrophenol (PNP), Diphenyl ether-1 (DPE-1) and DPE-2) behave as fluorescence quenchers with TNP being the most efficient quencher and NB being the least. It shows quenching constant [K_{SV}] value of 2.30 X 10^5 M^{-1} which is the highest among the known coordination polymers. An LOD of 43 ppb was achieved by the proposed method.

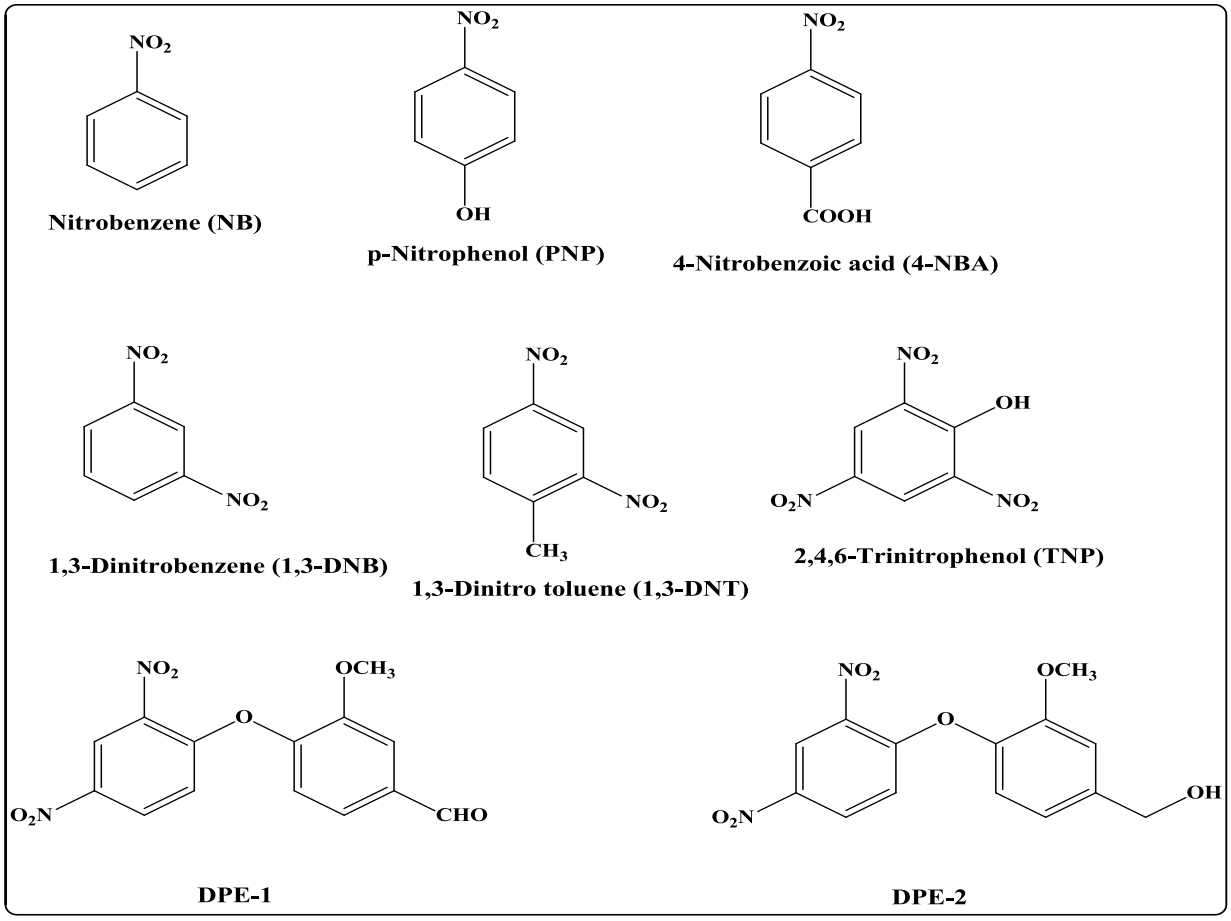

Fig.1. Chemical structures of the nitro aromatic compounds used

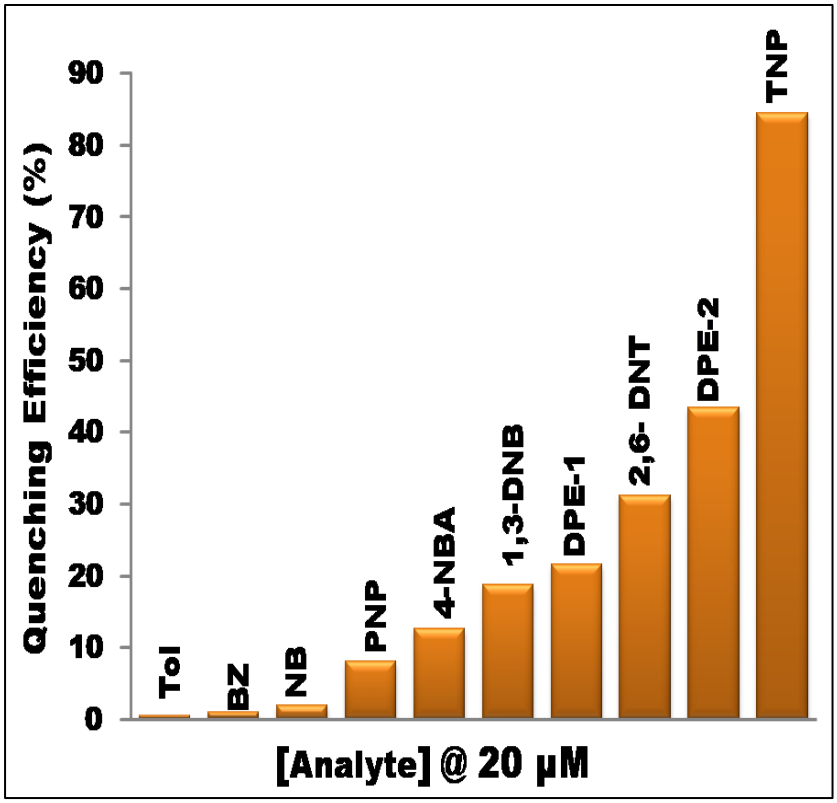

Fig.2. Percentage luminescence quenching at 411 nm of 1 with 20 µM of various nitro aromatics

Tab.1. Summary of results for various nitro aromatic analytes

S. No.	Analyte	Quenching Coefficient (K_{SV})	Detection Limit (ppm)
1.	**TNP**	**2.6×10^5 M^{-1}**	**0.043**
2.	**DPE-2**	**1.5×10^5 M^{-1}**	**0.64**
3.	**2,6-DNT**	**1.6×10^4 M^{-1}**	**1.09**
4.	**DPE-1**	**3.4×10^4 M^{-1}**	**1.12**
5.	**1,3-DNB**	**9.74×10^3 M^{-1}**	**1.27**
6.	**4-NBA**	**6.12×10^3 M^{-1}**	**1.31**
7.	**PNP**	**5.25×10^2 M^{-1}**	**1.39**
8.	**NB**	**-2.33×10^2 M^{-1}**	**1.23**

Detection of Organo-Phosphate Pesticides

Organophoshate pesticides namely triazophos (TZP) and chlorpyrifos (CPF) exhibit turn-on luminescence behaviour. The enhancement in emission intensity by 238% along with a red shift by ~70 nm was observed.

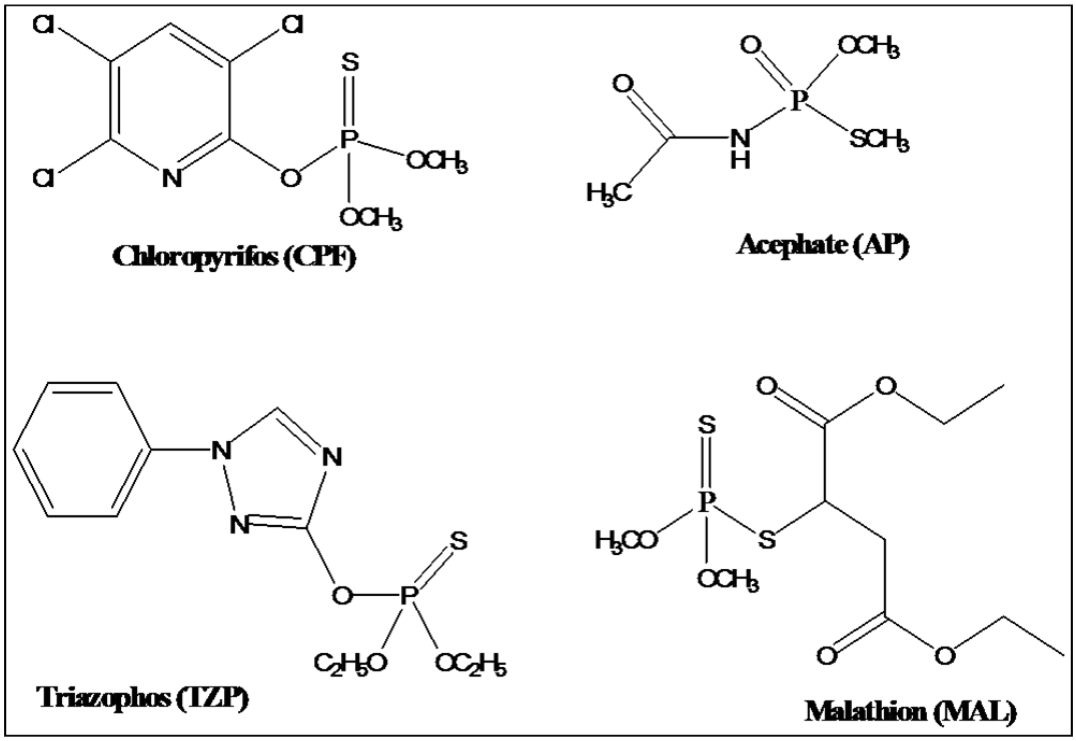

Fig.3. Chemical structures of the aromatic organo-phosphorous pesticides (chloropyrifos and triazophos) and non-aromatic organo-phosphorous pesticides (acephate and malathion)

Non aromatic pesticides like Malathion (MAL) and Acephate (ACP) did not show any increase in emission intensity. LOD for Triazophos (TZP) and Chlorpyrifos (CPF) were recorded as 0.62 and 0.7 ppm, respectively.

Catalytic Reduction of Nitro Aromatic Compounds (NACs)

The next part of the chapter explains the application of composites having ZnO nanoparticles incorporated into Co-MOF (ZnO/MOF-I, ZnO/MOF-II and ZnO/MOF-III) as a heterogeneous catalyst for the reduction of nitro aromatics (4-flouro nitrobenzene, p-nitro phenol, p-nitro benzoic acid and p-nitro anisole) to their corresponding amines under benign conditions, which cannot be realized using bare MOF. The catalytic studies were done and analyzed with the help

of HPLC. Out of the three cases, ZnO/MOF-I exhibits the highest catalytic activity with 97.78% and 96.8% yield of p-Aminophenol and of p-Anisidine respectively.

Scheme 1 General representation of catalytic reduction of various nitro aromatic compounds

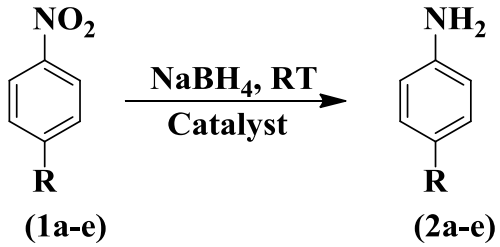

Table 2. Catalytic performance of the ZnO/MOF composites for the reduction reactions

Sr. No.	R	Reactant	Product	Catalyst	Time (min.)	Yield (%)	Rate constant, k (sec^{-1})
1.	F	1a	2a	ZnO/MOF-I	12	72.5	1.3×10^{-3}
				ZnO/MOF-II	12	64.9	6.4×10^{-4}
				ZnO/MOF-III	12	43.7	7.9×10^{-4}
2.	COOH	1b	2b	ZnO/MOF-I	15	80.1	1.4×10^{-3}
				ZnO/MOF-II	15	65.8	1.4×10^{-3}
				ZnO/MOF-III	15	56.5	9.0×10^{-4}
3.	OH	1c	2c	ZnO/MOF-I	5	97.78	1.0×10^{-2}
				ZnO/MOF-II	5	80.0	7.2×10^{-3}
				ZnO/MOF-III	5	70.6	5.6×10^{-3}
4.	OCH_3	1d	2d	ZnO/MOF-I	5	96.8	1.5×10^{-2}
				ZnO/MOF-II	5	91.0	9.6×10^{-3}
				ZnO/MOF-III	5	87.5	7.8×10^{-3}

Electrocatalytic studies for oxygen evolution reaction (OER)

In the end, this chapter describes the use of CeO_2/MOF composite as a thin film based electrocatalyst. The prepared composite material showed a satisfactory electrocatalytic activity towards oxygen evolution reaction (OER) with a low overpotential of 180 mV at 10 mA cm^{-2} of current density and a small Tafel slope of 39 mV dec^{-1}. The deposition of ceria nanoparticles played a vital role in enhancing the electrocatalytic activity for OER by changing the electronic environment around the Co core as evident by the shift in Co $2p_{3/2}$ and Co $2p_{1/2}$ peaks in XPS measurements. Moreover, this hetero structured catalyst exhibited long term stability for the duration of 16 h. The present work thus, reveals that ceria nanoparticles embedded into a MOF host might become a viable catalyst for the electrochemical water splitting reaction.

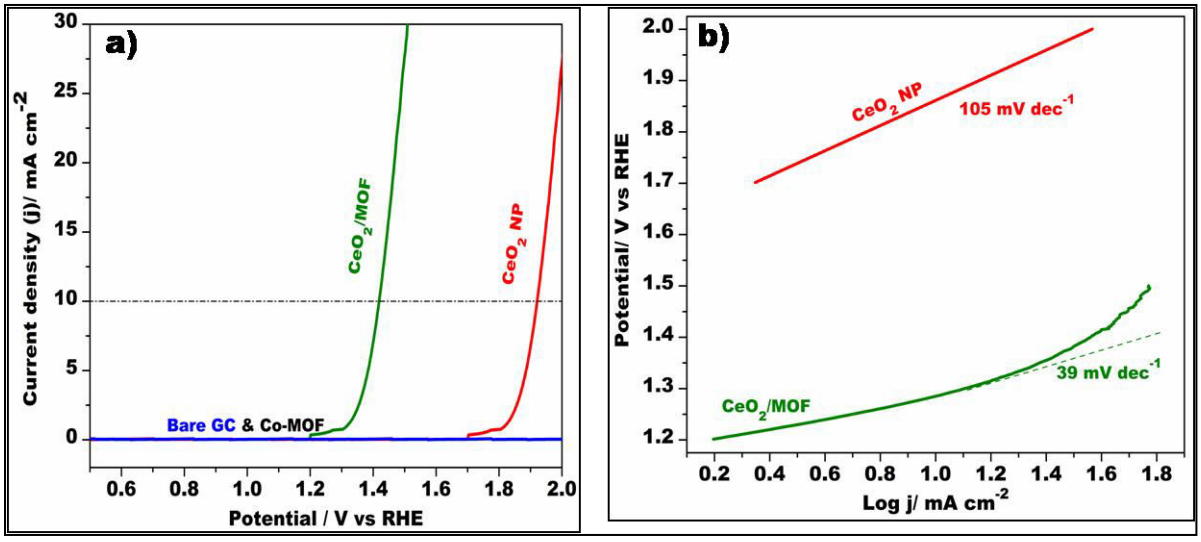

Fig. 4a) Linear sweep voltammetry (LSV) curves for glassy carbon electrode (GCE) modified with CeO_2/MOF (5mg), CeO_2 NPs, Co-MOF and bare GCE in O2-saturated 1.0 M KOH with a sweep rate of 1 mV s^{-1}. b) Tafel plot of the catalyst CeO_2/MOF and CeO_2 NPs recorded at sweep rate of 1 mV s^{-1}

Table 3. OER activities of some previously reported electrocatalysts in alkaline solutions with a current density at 10 mA cm^{-2}

Sr. No.	Catalyst	Electrolyte	Tafel slope (mV/dec)	η (mV)
1.	Co-MOF@CNTs	1.0 M KOH	69	340
2.	MOF-derived Co_3O_4C-NA	1.0 M KOH	61	1520
3.	Fe/Ni-BTC MOF	0.1 M KOH	47	270
4.	$Ni_xFe_{3-x}O_4$	1.0 M KOH	53	400
5.	$Co_xFe_{3-x}O_4$	1.0 M KOH	57	420
6.	20 wt% Ir/C	0.1 M KOH	-	380
7.	20 wt% Ru/C	0.1 M KOH	-	390
8.	Co-P/NC	1.0 M KOH	52	354
9.	**CeO_2/MOF**	**1.0 M KOH**	**39**	**180**

Chapter 5: Conclusions

This chapter includes the concluding remarks regarding the work done so far as discussed under the results and discussion chapter.

Two-dimensional luminescent cobalt based metal organic framework (MOF), **1**, has been synthesized on gram scale by simple solvent evaporation method. The MOF has been used for the detection of TNP through luminescence quenching. Experimental studies explained that static quenching as well as the excitation energy absorption and electron transfers are the mechanisms for the luminescence quenching in presence of TNP. The compound also demonstrates highly sensitive detection of aromatic organophosphate pesticides (triazophos and chlorpyrifos) through luminescence enhancement (turn-on). Further, cobalt based MOF,**1**, was used as a support to load ZnO nanoparticles with tunable sizes by wet infiltration method. The frameworks of the resulting composites retain their structural integrity which was confirmed by PXRD, TEM, EDX, MP-AES and Raman spectroscopic methods. The accessibility and catalytic activity of the

embedded ZnO nanoparticles was checked through the reduction of nitroarenes by $NaBH_4$ under ambient conditions. With this work, we established and validated the possibility of inducing the catalytic activity to the MOF using cheap ZnO nanoparticles for the first time substituting the corrosive and reactive catalysts as used conventionally. Afterwards, another composite material comprising Co-MOF and ceria nanoparticles was synthesized using same wet impregnation technique and its OER catalytic performance was investigated thoroughly by casting a thin film on glassy carbon electrode. Prior to this, the hybrid material was characterized and analyzed using PXRD, EDS, HR-TEM, XPS and Raman spectroscopy. This thin film based electrocatalyst shows high activity with lower overpotential value of 180 mV at 10 mA cm^{-2}, higher electrochemical surface area and a small Tafel slope of 39 mV dec^{-1}.

CHAPTER-1

INTRODUCTION

The foundation of metal organic frameworks (MOFs) can be dated back to late 1990s when two of these macromolecules- MOF-5[1] and HKUST-1[2] were synthesized by independent research groups in 1999. Metal organic frameworks are composed of metal ions bridged through organic linkers to form one, two, or three-dimensional structures. This subclass of coordination polymers has porosity as a special feature that open ways for their wide applicability for the purpose of catalysis,[3-7] molecular separations,[8-10] drug delivery,[11,12] sensing[13,14] and many others.[15-18] However, electrically non conductivity,[19] weak dispersive forces[20] and high chemical reactivity towards water vapors moisture resulting in distorted structures are some of the challenges for their utilization as industrial materials on a large scale. To overcome these challenges, loading or incorporating MOFs with nanoparticles has become a powerful tool in recent times.

Nanoparticle synthesis, on the other hand, has its own challenges like control on size distribution and agglomeration during synthesis that results in the loss of their extraordinary surface properties. The use of porous metal organic frameworks as a support provides a solution for the synthesis of size controlled nanostructures (also called confinement effect)[21] retaining their surface active sites. The approach has given birth to new materials that suppressed the pitfalls of the individual component and led to the development of synergistic properties.[22-24] In recent years, tremendous amount of work has been reported outlining the synthetic processes and the potential applications of these hybrid frameworks.

There are two broad approaches to synthesize MOF- nanoparticles composites. One is “Ship in the bottle” and the other one is “Bottle around the ship”. “Ship in the bottle” involves incorporating the nanoparticles into cavities of MOFs using methodologies like solution or wet impregnation,[25, 26] vapor deposition[27, 28] and mechanical grinding.[29-30]

Wet impregnation method is usually employed to load nanoparticles that have metal precursor solution in the form of inorganic salts. These salt solutions are added to the dispersion of MOF that infiltrates into the cavities of MOF due to capillary action. The precursors are then reduced using $NaBH_4$ or H_2 gas in the final step to form metal nanoparticles immobilized into the pores of MOF. In gas infiltration or vapor deposition technique the desolvated or dried MOF is

exposed to vapors of a volatile organometallic precursor of metal kept in a separate tighly sealed Schlenk tube under a constant pressure. After the precursor has been introduced into the MOF cavities by capillary forces after heating at a temperature just above the boiling point of volatile precursor under constant vacuum, it is finally reduced to zero valent metal nanoparticles by hydrogen gas or thermal decomposition. The method has been used for loading nanoparticles on flat surface[31] and also the internal surfaces[32] of the porous frameworks. Solvent free mechanical grinding is also a powerful strategy to deposit uniformly distributed nanoparticles into the accessible pores of MOF. The volatile organometallic precursor is grinded with an appropriate MOF for several minutes to allow the infusion of metal precursor into the MOF. This is followed by the treatment with H_2 gas at a mild temperature to form the metal nanoparticles.

'Bottle around ship" is also an equally useful approach to fabricate nanocomposites comprising nanoparticles and a MOF. The method is also termed as template based method where pre-synthesized nanoparticles are added to the solution containing molecular building blocks for constructing the whole framework around these nanoparticles. Usually the pre-fabricated nanoparticles are stabilized with the help of capping agents or surfactants. Unlike other methods, this technique generally prevents the agglomeration of nanoparticles on the external surface of MOF and also avoids the destruction of their overall structures caused by reduction in the final step to form metal nanoparticles from their respective precursors. Moreover, it offers an opportunity to control the size, morphology and compositon of the nanoparticles. But the controlled growth of MOF over the surface of nanoparticles instead of self nucleation in solution is an important factor to consider. Another major issue is that although the capping agents help to avoid the aggregation of nanoparticles but on the other hand may reduce their activity or performance and sometimes they are difficult to remove after the composite formation.

Followed by the synthetic part, the complexity of such hybrid systems having multiple components demands the careful analysis or characterization using different structure elucidation techniques. The techniques used should be such that they elaborate and clearly support the formation of the required hybrid material. The first major thing after the synthesis is to explore the structural framework of MOF after the deposition of NPs. Powder x-ray diffraction (P-XRD) method helps greatly in confirming that the synthesis occurred with the retention of framework or the level of destruction happened to the MOF structure. Moreover, if the loading ratio of NPs

is higher than 5 wt%, then the characteristic peaks for the NPs incorporated can be clearly observed.

Next important aspect of characterization is to explore and evaluate the size, morphology, distribution and the amount/weight percentages of the deposited nanoparticles. These can be confirmed using transmission electron microscopy (TEM), energy dispersive spectroscopy (EDS), inductively coupled plasma (ICP) spectroscopy or microwave plasma-atomic emission spectroscopy (MP-AES). Among these, TEM gives valuable information about the size distribution and morphology of the NPs deposited. Whereas, EDS, ICP and MP-AES confirm the loading ratios of nanoparticles. These give an exact idea of weight percentages of nanoparticles deposited, which is an important piece of information.

Similarly, the coordination environment and possible interactions between nanoparticles and MOF can be characterized using x-ray photoelectron spectroscopy (XPS) and nuclear magnetic resonance (NMR). XPS helps in providing the information about the oxidation states, elemental composition of nanoparticles and also indicates the change in electronic environment before and after the deposition of NPs. Also, Brunauer–Emmett–Teller (BET) measurements are also done complimentarily to evaluate the surface area before and after the deposition of nanoparticles. These studies are important for the analysis of NP@MOF composite systems for gas adsorption properties.

Conclusions

The last few decades had witnessed a geometrical hike in the number of publications related to MOFs. Most recently, the focus has been much drifted towards the fabrication and versatile applications of NP@MOF hybrid materials. The confined spaces inside MOFs exert a limiting effect during the in-situ synthesis of nanoparticles and also the organic moieties of MOF sometimes behave as a stabilizing agent for the metal nanoparticles. These factors make them a preferred choice for being used as a support for depositing NPs. In view of that, different synthetic strategies had been discussed. In addition to the conventional solution impregnation method, other techniques such as vapor deposition and mechanical grinding have also been explored. The next major requisite is their detailed characterization and analysis owing to the complexity of such composites. In this regard, multiple techniques such as P-XRD, HR-TEM, EDS, XPS, BET, solid state NMR etc. are used simultaneously for their characterization. The

future era should witness the development of more facile and cheaper synthetic methods and few more advanced characterization techniques should be developed in order to understand the mechanistic details.

In light of the above discussion, it can be summarized that the work presented in this thesis describes "Synthesis, Characterization and Applications of Nanocomposites-MOFs of Cobalt with 4, 4'-oxy bis-benzoic acid and Metal Oxide Nanoparticles". The initially synthesized MOF has been used for the detection of nitro aromatics and pesticides. However, the Co-MOF modified with nanoparticles has been used for the facile reduction of nitro arenes and oxygen liberation reaction.

References:

1. Li, H.; Eddaoudi, M.; O'Keeffe, M.; Yaghi, O. M., *Nature* **1999**, *402*, 276.
2. Chui, S. S.Y.; Lo, S. M. F.; Charmant, J. P. H.; Orpen, A. G.; Williams, I. D., *Science* **1999**, *283*, 1148.
3. Ma, L.; Abney, C.; Lin, W., *Chem. Soc. Rev.* **2009**, *38*, 1248.
4. Lee, J.; Farha, O. K.; Roberts, J.; Scheidt, K. A.; Nguyen, S. T.; Hupp, J. T., *Chem. Soc. Rev.* **2009**, *38*, 1450.
5. Corma, A.; Garcia H.; Llabresi Xamena, F. X., *Chem. Rev.* **2010**, *110*, 4606.
6. Yoon, M.; Srirambalaji, R.; Kim, K., *Chem. Rev.* **2012**, *112*, 1196.
7. Zhang,T.; Lin, W., *Chem. Soc. Rev.* **2014**, *43*, 5982.
8. Li, J. R.; Sculley, J.; Zhou, H. C., *Chem. Rev.* **2012**, *112*, 869.
9. Van de Voorde, B.; Bueken, B.; Denayer, J.; De Vos, D., *Chem. Soc. Rev.* **2014**, *43*, 5766.
10. Qiu, S.; Xue, M.; Zhu, G., *Chem. Soc. Rev.* **2014**, *43*, 6116.
11. Rocca, J. D.; Liu, D.; Lin, W. *Acc. Chem. Res.* **2011**, *44*, 957.
12. Horcajada, P.; Gref, R.; Baati, T.; Allan, P. K.; Maurin, G.; Couvreur, P.; Férey, G.; Morris, R. E.; Serre, C., *Chem. Rev.* **2012**, *112*, 1232.
13. Kreno, L. E.; Leong, K.; Farha, O. K.; Allendorf, M.; VanDuyne, R. P.; Hupp, J. T., *Chem. Rev.* **2012**, *112*, 1105.
14. Hu, Z.; Deibert, B. J.; Li, J., *Chem. Soc. Rev.* **2014**, *43*, 5815.
15. Murray, L. J.; Dinca, M.; Long, J. R., *Chem. Soc. Rev.* **2009**, *38*, 1294.
16. Sumida, K.; Rogow, D. L.; Mason, J. A.; McDonald, T. M.; Bloch, E. D.; Herm, Z. R.; Bae, T. H.; Long, J. R., *Chem. Rev.* **2012**, *112*, 724.
17. Wu, H.; Gong, Q.; Olson, D. H.; Li, J., *Chem. Rev.* **2012**, *112*, 836.
18. He, Y.; Zhou, W.; Qian, G.; Chen, B., *Chem. Soc. Rev.* **2014**, *43*, 5657.
19. Miyasaka, H., *Acc. Chem. Res.* **2013**, *46*, 248.
20. Petit, C.; Bandosz, T. J. J., *Colloid Interface Sci.* **2015**, *447*,139.
21. Meilikhov, M.; Yusenko, K.; Esken, D.; Turner, S.; VanTendeloo, G.; Fischer, R. A., *Eur. J. Inorg. Chem.* **2010**, 3701.
22. Zhu, Q. L.; Xu, Q., *Chem. Soc. Rev.* **2014**, *43*, 5468.
23. Ahmed, I.; Jhung, S. H., *Mater. Today* **2014**, *17*, 136.
24. Stock, N.; Biswas, S., *Chem. Rev.* **2012**, *112*, 933.

25. Zlotea, C.; Campesi, R.; Cuevas, F.; Leroy, E.; Dibandjo, P.; Volkringer, C.; Loiseau, T.; Ferey, G.; Latroche, M., *J. Am. Chem. Soc*. **2010**, *132*, 2991.
26. Jiang, H. L.; Akita, T.; Ishida, T.; Haruta, M.; Xu, Q., *J. Am. Chem. Soc.* **2011**, *133*, 1304.
27. Hermes, S.; Schroter, M. K.; Schmid, R.; Khodeir, L.; Muhler, M.; Tissler, A.; Fischer, R. W.; Fischer, R. A., *Angew. Chem. Int. Ed*. **2005**, *44*, 6237.
28. Schroder, F.; Esken, D.; Cokoja, M.; van den Berg, M. W. E.; Lebedev, O. I.; Van Tendeloo, G.; Walaszek, B.; Buntkowsky, G.; Limbach, H. -H.; Chaudret, B.; Fischer, R. A., *J. Am. Chem. Soc.* **2008**, *130*, 6119.
29. Ishida, T.; Nagaoka, M.; Akita, T.; Haruta, M., *Chem. Eur. J.* **2008**, *14*, 8456.
30. Ishida, T.; Kawakita, N.; Akita, T.; Haruta, M., *Gold Bull.* **2009**, *42*, 267.
31. Rocha, J.; Carlos, L. D.; Paz, F. A. A.; Ananias, D., *Chem. Soc. Rev.* **2011**, *40*, 926.
32. Schubert, U., *Chem. Soc. Rev.* **2011**, *40*, 575.

CHAPTER-2

LITERATURE BACKGROUND

The foundation stone of modern coordination chemistry was laid long back in 1893 when Alfred Werner proposed the structure of octahedral complexes and provided a theoretical and experimental justification regarding the bonding in coordination complexes.[1] Understanding of these concepts paved the way for the synthesis, reactivity and application of new types of coordination compounds and thus along the way, many novel and unconventional concepts of metal-metal bond, three centered-two electron (banana bond), back bonding etc. were widely accepted after initial discouragement for organo-metallic complexes. This took the understanding of coordination complexes to the next level.

In this era, metal organic frameworks (MOFs) have emerged as a new branch of coordination chemistry where metal centres are bridged through organic ligands leading to an infinite array. This automatically creates pores or cavities of varying size. Although the origin of MOFs stems from inorganic solids-zeolites, but there lies a basic difference. The most significant in being the factor of chemical tunability implanted through the organic counterparts of MOFs. Zeolites however, simply lack organic components as a part of their framework and thus lack variety. Zeolites are aluminosilicates that are commonly used as adsorbents and catalysts due to the presence of the micropores. Their synthesis usually requires an inorganic or organic template thus developing strong interactions between the inorganic framework and the template. Sometimes, removal of the template can result in collapse of the framework of the zeolites.

MOFs on the other hand, have vast applicability in the chemical catalysis,[2-6] drug delivery,[7-9] molecular separations,[10-12] gas adsorption,[13-14] ferroelectrics,[15] ion exchange[16] due to their intriguing and predictable topologies. Topologically, metal organic frameworks can be viewed as 1-D, 2-D and 3-D networks constructed by connecting metal nodes using organic spacers/ linkers through the coordination bonds.[17-20] Usually the metal ions dictate the final geometry of the frameworks which mainly depends upon their valency and the coordination environment. The advantage of MOF chemistry is to design and synthesize the pre-destined geometries around metal ions without causing any chemical decomposition of the organic counterparts present. An interesting aspect is that the same starting materials can lead to different MOF structures by

varying the physical parameters such as reaction temperature, pressure and time. The beginning era of MOF chemistry was much focused on achieving new synthesis protocols through the modification of older ones to form new architecturally diversified frameworks. Following sections describe different methods of MOF synthesis.

Preparation Methods for MOFs

The kinetic energy barrier to form MOF can be crossed through different means such as microwaves, ultrasonic waves, ultraviolet waves, mechanical grinding or by simple heating. Thus depending upon which source of energy has been used, the corresponding synthetic methods have been named.

Solvothermal synthesis

This conventional method comprises of dissolving the raw materials (metal salt and organic linker) in an appropriate solvent followed by heating in a sealed vessel under autogenous pressure above the boiling point of the solvent. The reaction generally proceeds without any parallelization. However, different conditions give rise to a number of metal organic frameworks in one, two or three dimensions (Fig. 1).

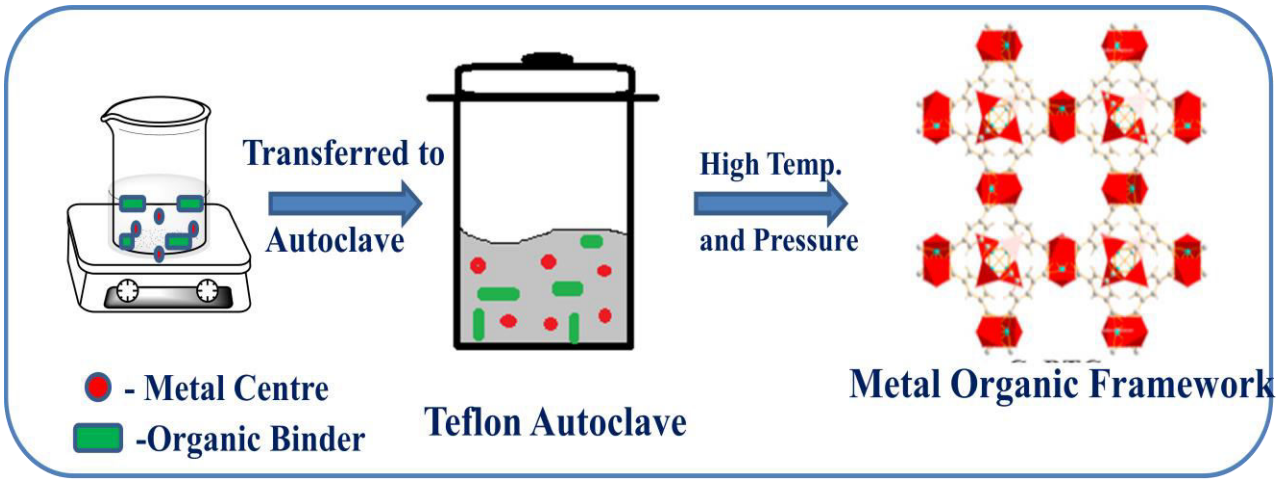

Fig.1. Diagrammatic representation of general conventional solvothermal synthesis

In 1999, two representative frameworks- MOF-5[21] and HKUST-1[22] were synthesized for the first time using the solvothermal technique which laid the foundation stone of this chemistry.

Temperature in this approach plays a key role where its variation can lead to new structural frameworks (Fig. 2). With advancement of time, an alternate approach was introduced where

pre-built inorganic building blocks were used instead of metal salts while all other parameters of conventional solvothermal synthesis remain the same.

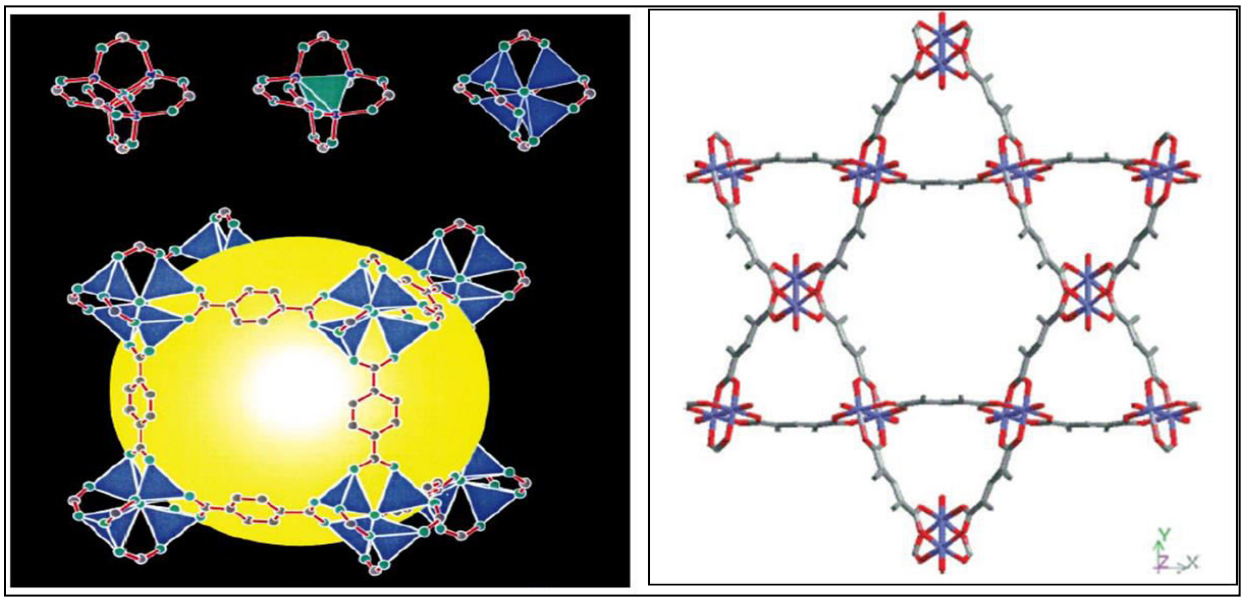

Fig.2. a) Construction of MOF-5 framework having eight clusters (only seven visible) constitute a unit cell and enclose a large cavity, indicated by a yellow sphere of diameter 18.5Å in contact with 72 C atoms b) $[Cu_3(TMA)_2(H_2O)_3]_n$, HKUST-1, viewed along the cell body diagonal [111], showing a hexagonal shaped 18Å window at the intersection of the nanopores

The monotopic ligands are replaced by polytopic ligands in this synthetic approach to give rise to three dimensional frameworks. For example, Zr based MOF was reported to be synthesized using zirconium methacrylate oxocluster, $[Zr_6O_4(OH)_4(OMc)_{12}]$ ($OMc=CH_2=CH(CH_3)COO$) as a precursor instead of zirconium salt.[23] This precursor approach has an edge over the conventional synthesis that the final topology of a MOF can be fine tuned as per requirement and it also requires the use of milder synthetic conditions.[23]

Microwave synthesis

Microwave energy is commonly used in organic chemistry where solvent plays an important part.[24-25] However, the field has been extended beyond its usual limits. The method relies on the use of dielectric or polar materials and such a mechanism of heating the dielectric material is named as dipolar loss or re-orientation loss mechanism.[26] During the reaction, the electromagnetic waves interact with the mobile electric charges and thus polar molecules try to re-orient themselves along with the applied field thereby colliding with each other which raises

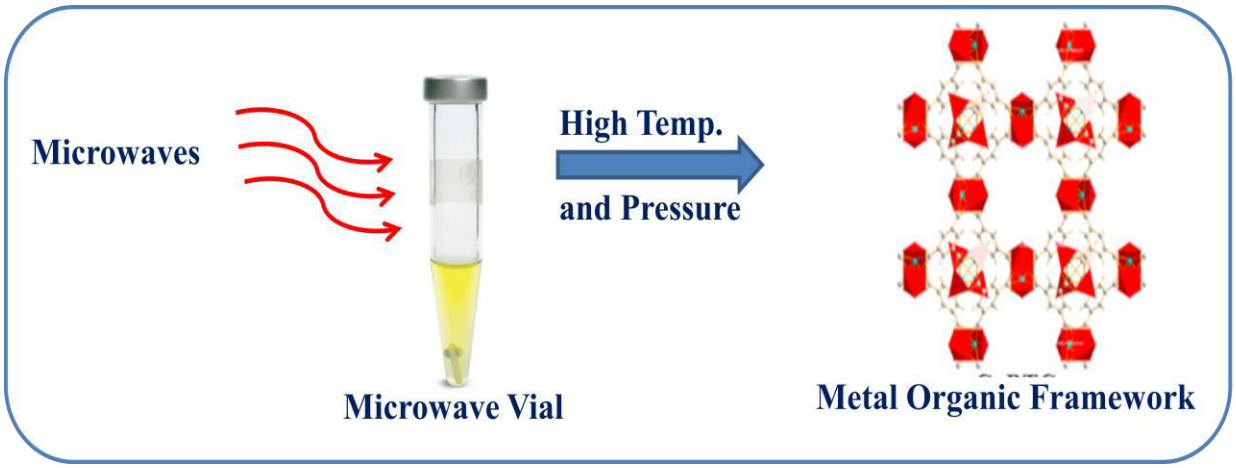

Fig.3. Diagrammatic representation of general microwave synthesis

their kinetic energy (Fig. 3). Hence the temperature elevates and the heating effect is produced. This is an energy efficient process as the radiation is directly interacting with the molecules and is also advantageous by the means that it causes homogenous heating of the sample. Moreover, shorter reaction times, formation of phase selective crystals[27] and faster crystallization[28] are few another attractive features of this synthetic approach. The first microwave assisted synthesis of a nanoporous Cr based MOF was reported by Chang and his co-workers.[29] The reaction yielded 44% in 4 hours using 220ºC which was comparable with that of the conventional synthetic route. Another report showed an increase in catalytic activity for cyclohexene oxidation when a pyrazolate based MOF was synthesized using microwaves in comparison with the conventional synthesis.[30]

Electrochemical Synthesis

The research group at BASF[31] in 2005 did the pioneer work related to the electrochemical synthesis of metal organic frameworks. The prime objective of the work was to eliminate to use of anions such as sulphate, chloride or perchlorate from the synthetic procedure which were one of limiting factors for the large scale production of metal organic frameworks. In principle, the method uses metal ions instead of metal salts which are constantly put into the solution through the anodic dissolution to the reaction medium having already dissolved organic linker molecules and a conducting salt (Fig. 4). Protic solvents are preferably used to avoid the deposition of metals at the cathode. Hydrogen gas evolved during the process can be taken care of by using

compounds that can be readily and preferentially reduced such as maleic esters, acrylonitrile etc. The possibility to run as a continuous process and to achieve higher yields of solid materials as

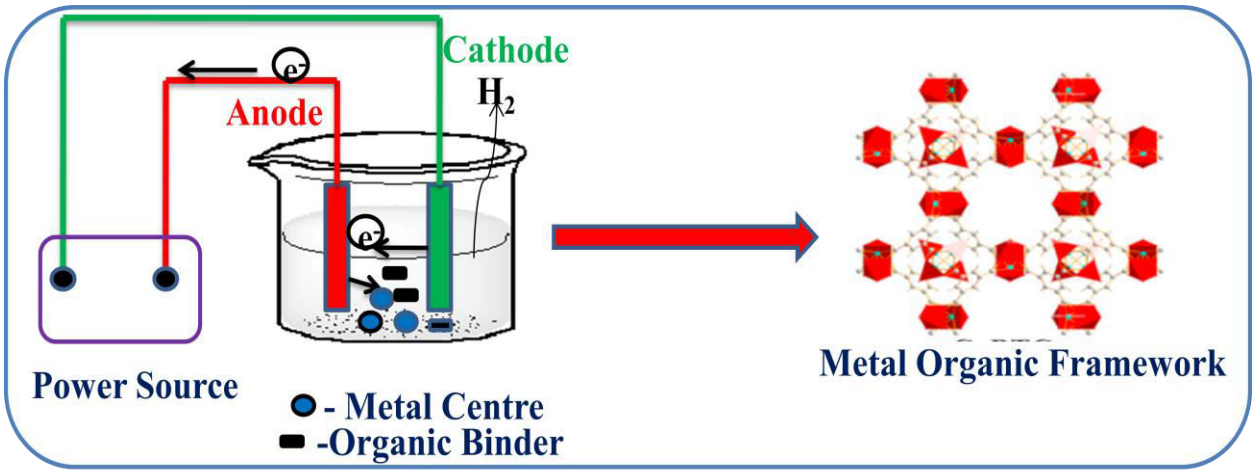

Fig.4. Diagrammatic representation of general electrochemical synthesis

compared to the regular batch reactions, gives the electrochemical route an edge over other methods to be used as an industrial process. The method has been efficiently used to prepare MOF films using metal oxide as a substrate.[32] These luminescent Tb containing MOF films exhibited sensing capability towards explosive aromatic nitro compounds (Fig. 5).

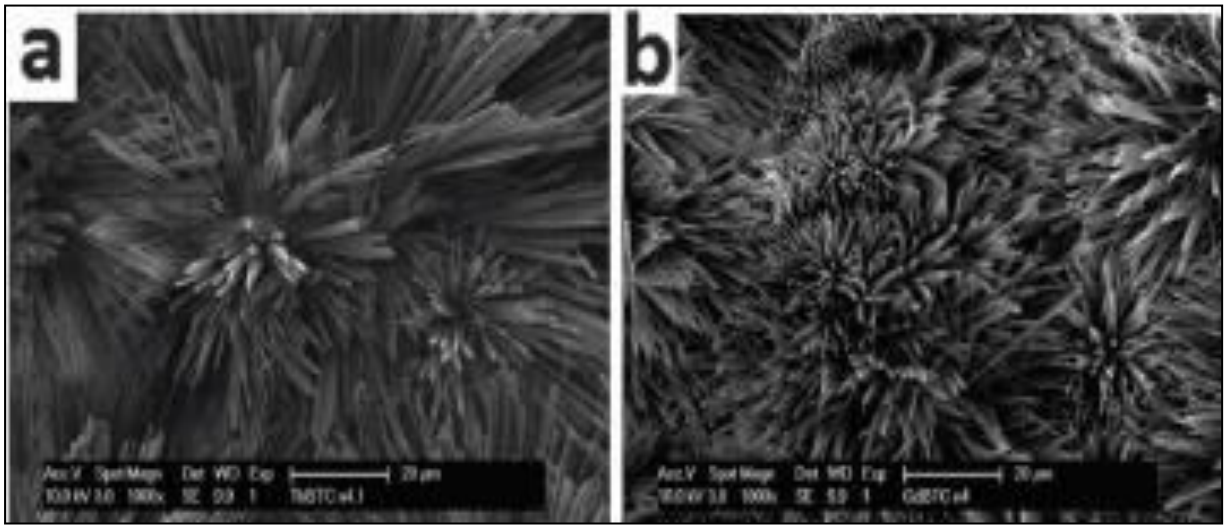

Fig. 5. SEM images of a) Tb-BTC and b) Gd-BTC

Sonochemical Synthesis

Sonochemical synthesis is another method through which small MOF crystals can be produced in a short duration of time. The rate of reaction is increased with the help of ultrasonic waves which causes the formation and collapse of bubbles in the reaction mixture. This phenomenon is termed as acoustic cavitation and results in the production of elevated local temperatures (usually greater than 5000 K) and pressures in a short duration of time (Fig.6). Sonochemical irradiation

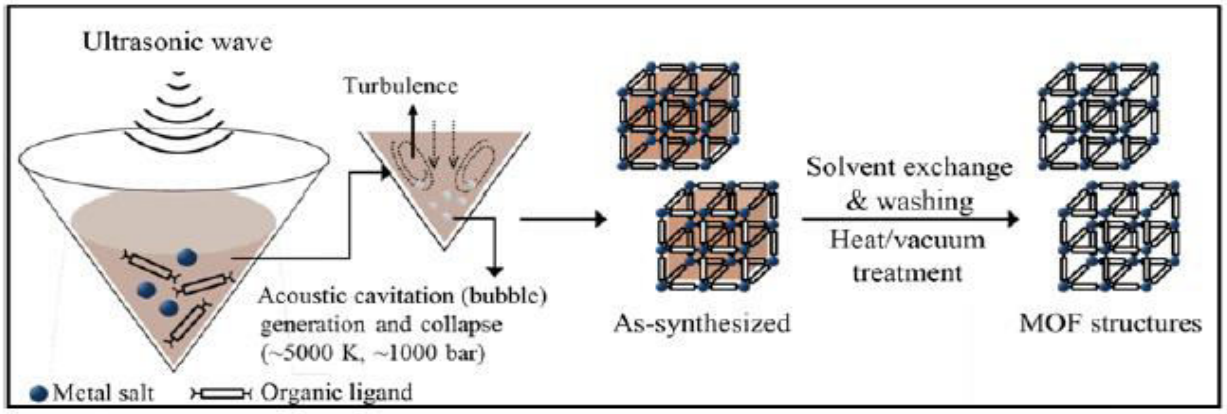

Fig.6. Diagrammatic representation of general sonochemical synthesis

was used to synthesize crystalline MOF-5 (having size range of 5-25 μm) in 1-methyl-2-pyrrolidinone. The MOF thus formed was observed to have properties similar to the MOF-5 synthesized using microwaves and conventional solvothermal method but in shorter duration of 30 minutes.[33] Similarly, different phases of $[Zn(1,4\text{-benzenedicarboxylate})(H_2O)]_n$ ranging from nano belts to microcrystals were synthesized using this method.[34] Though the technique eliminates the use of higher temperatures and achieves the desired results in short times, yet is new to explore its potential.

MOF Based Composites

Recently, new reports have started emerging where new materials have been synthesized using MOF as base material for the fabrication of composites. Composites are the multi-component materials containing different (nongaseous) phase domains in which at least one type of phase domain is a continuous phase.[35] They are widely used at industrial scale since they bring the properties of multiple components in a single material and their physico-chemical behavior can also be easily tuned. Following section discusses, three major types of composites (Fig.7).

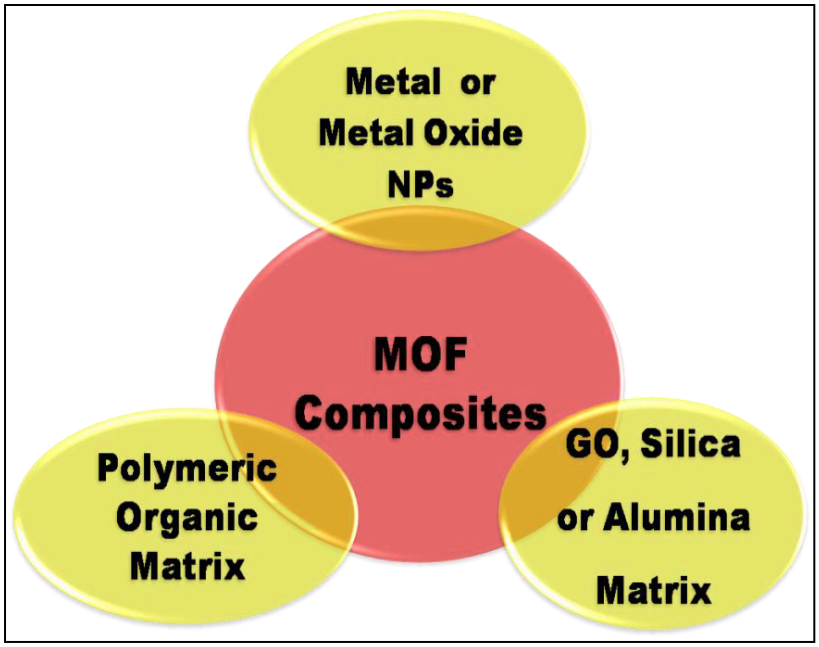

Fig. 7. The types of composites of MOFs

MOF-Organic Matrix composites

These types of composites have MOF in dispersed phase while polymeric organic matrix comprises the continuous phase. In one of the reports, composite membranes were synthesized using a polyimide (Matrimide) and a polysulfone polymer as a matrix while MOF-5 and ZIF-8 formed the dispersed phase. The desired hybrid material was prepared using solution blending approach.[36-37]

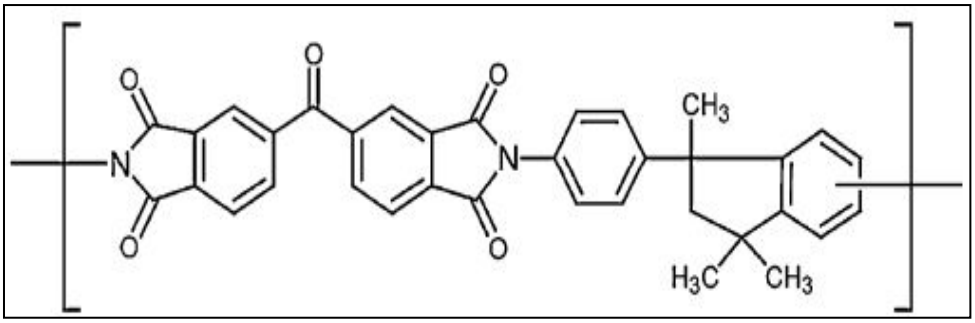

Fig.8. Structure of Matrimide® 5218

The dispersion of preformed MOF-5 or ZIF-8 was introduced to the solution of organic matrix and dissolved with the help of ultrasonication. The slow evaporation of the solvent resulted in the formation of membrane in the final step. Similar technique was applied to form composite

membranes of HKUST-1, MIL-47, MIL-53, and ZIF-8 with Matrimide or polysulfone.[38-39] The quality of membranes was improved when MOF crystals were pretreated with a silylating agent (N-methyl-N-(trimethylsilyl)trifluoroacetamide).

Likewise, natural polymer fibres were also used to form composite materials. Crystalline HKUST-1 was added to the slurry of pretreated pulp to get inhomogeneously distribution of the MOF.[40] While, the uniform distribution of HKUST-1 over the surface area of pulp was achieved with the help of direct growth method. This hybridization led to the increase in lignin content in the fibres which further resulted in the increase in degree of coverage.

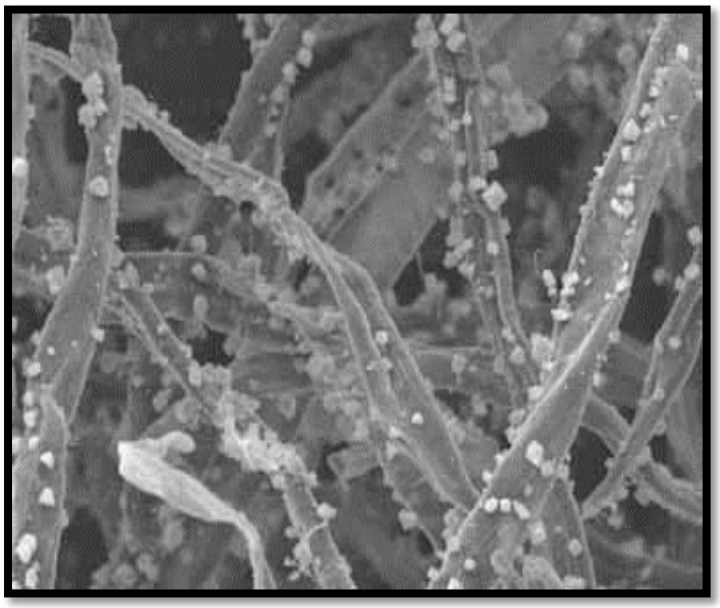

Fig.9. Scanning electron micrograph of $Cu_3(BTC)_2$ crystals on CMTP fibers

Similarly, PAM (Polyacrylamide) beads were also used to provide a matrix base in combination with HKUST-1[41] and Co-CPO-27[42] in order to improve mechanical stability. Solvothermal technique was used to fabricate HKUST-1/PAM composite and SEM images confirmed the formation of HKUST-1 cyrstals within the PAM beads. An alternate approach of immersing the PAM beads in ethanol/water (1:1) solution prior to the solvothermal treatment led to the deposition of HKUST-1 only over the external surface of PAM beads.

MOF-Inorganic Matrix composites

Graphene oxide (GO), silica and alumina are few common inorganic matrices used these days to incorporate MOF as dispersed phase. Bandosz *et al* synthesized the composites of HKUST-1[43]

and MOF-5[44] by introducing the Graphite oxide into the reaction mixture prior to the solvothermal treatment. The composites were synthesized with the aim of enhancing the gas adsorption capacity of graphite oxide. The composites of different ratios of GO and HKUST-1/MOF-5 were prepared. It was observed that microporosity decreased with increasing the ratio of GO in case of GO/MOF-5 hybrid material. Due to the chemical interactions between epoxy groups of graphene and the oxide clusters of MOF-5, the composite material acquired the lamellar structure which originated from the alternate layers of GO and MOF-5. While in case of GO/HKUST-1composite, the porosity was found to be more than that of the parent materials. Silica and alumina beads had also been used to fabricate the composite material with HKUST-1. The hybrid material showed promising separation properties as a stationary phase in HPLC. Monodisperse mesoporous silica beads (Nucleosil 100-3) were added to the reaction mixture along with the starting material for the synthesis of HKUST-1 and the solvent was evaporated in the final step to form the desired composite.[45]

Nanoparticles@ MOF composites

The porosity of MOFs has always been an attractive feature and has been exploited for number of purposes till date. Due to the presence of three dimensional framework and well defined pores, MOFs have great potential to act as a stabilizing/capping agent for thermodynamically unstable nano structures. These embedded nanoparticles can be easily accessed due to high porosity of MOFs. Such hybrid materials usually display better chemical and physical properties. For synthesis, there are two different approaches- first approach is analogous to building the bottle around ship which means it involves the preparation of metal nanoparticles individually, followed by the addition of precursors that can give rise to MOF around the preformed nanoparticles. Though it is less commonly followed but ensures the encapsulation of nano particles inside the MOF. Lu *et al* reported the successful encapsulation of PVP capped nanoparticles with varied compositions and shape in ZIF-8.[46] The preformed PVP capped nanoparticles were dissolved in methanolic solution of 2-methylimidazole and zinc nitrate at ambient conditions followed by centrifugation to produce NP@ZIF-8 hybrids. The second approach is the most commonly used one where MOF provides a confined space or cavity for the nucleation and growth of nanoparticles. It exerts a size limiting effect and also acts as a stabilizing agent to monodispersed nanoparticles. Various techniques such as wet impregnation,

chemical vapour deposition, solid grinding are used in this approach. Figure 10 shows the TEM image of ZIF-8 crystal encapsulating Au nanoparticles.

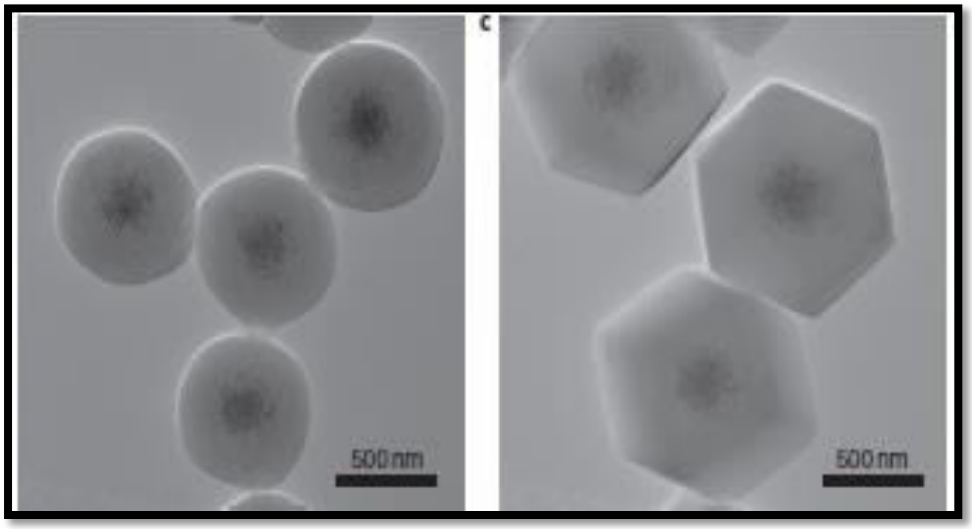

Fig.10. TEM analysis of the encapsulation of 13 nm Au nanoparticles in ZIF-8 crystals

Wet Impregnation or Solution Infiltration Method: The general protocol involves the impregnation of a metal precursor into the solution of porous MOF followed by the reduction of metal precursor to form metal (0) atoms. These zero valent atoms then aggregate into nanoparticles within the well defined cavities of the MOF matrix. Nitrate and chloride salts of metal are generally used as metal precursors for the synthesis of metal nanoparticles while hydrogen gas, hydrazine or $NaBH_4$ are frequently employed as reducing agents. Carefully choosing the conditions to avoid the decomposition of the host matrix, centrifugation and washing with appropriate solvent and then drying at an appropriate temperature gives the final composite material. The reaction parameters such as loading time and reducing agent exerts a great impact on the size of metal nanoparticles formed. Esken *et al* loaded different amounts of Pd nanoparticles onto MOF-5 using the wet impregnation method to reach the highest loading of 15.4 wt%[47] as shown in Fig.11.

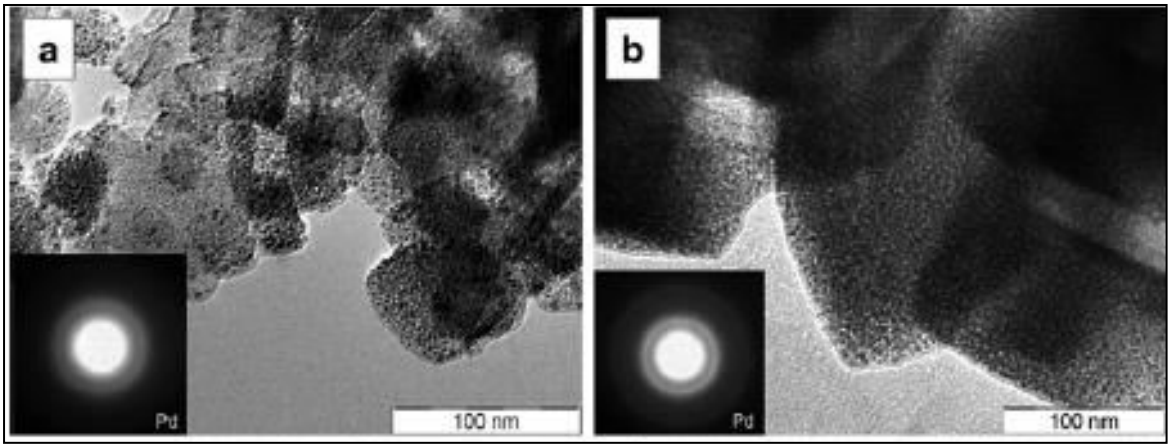

Fig.11. TEM micrographs and SAED patterns of selected samples of Pd_x@MOF-5

Another research group made an observation that the usage of high concentration of reducing agent (overwhelming reduction) can lead to the production of homogenously distributed AuNi nanoparticles with small size of 1.8 ± 0.2 nm inside the cavities of MIL-101. Whereas moderate concentrations of reductant led to the formation of agglomerated larger sized AuNi nanoparticles (›5 nm) and also on the outer surface of MOF.[48]

Chemical Vapour Deposition (CVD) method: This method implies the use of volatile organometallic precursors and a dried MOF which are kept in two different glass vials in a Schlenk tube. The tube is evacuated, sealed and maintained at an appropriate temperature which is decided by the vapour pressure of the precursor. The precursor molecules sublime and subsequently infiltrate into the channels of MOF followed by the thermal and photochemical decomposition.[49] As the process takes place in the absence of any solvent, it can load high amounts (30-40 wt %) of nanoparticles in a single step as compared to other methods. However, such high loading amounts can sometimes lead to partial of full degradation of host matrix. CVD technique was used to deposit Ru precursor, [Ru(cod)(cot)] (cod = 1,5-cyclooctadiene, cot = 1,3,5-cyclooctatriene) onto MOF-5.[50] TEM images and a cross sectional photo of the resultant material were taken which confirmed the homogenous deposition of cod and cot into MOF-5 while PXRD data showed the conservation of host framework after the deposition of precursor molecules. Further hydrogenolysis of the loaded Ru precursor yielded Ru NPs of size range of 1.5- 1.7 nm.

Mechanical Grinding: Loading of metal nanoparticles into the channels of porous MOF can also be done using mechanical grinding method. In this technique, an appropriate and activated

metal organic framework having easily accessible pores is grounded well with the volatile organometallic precursor using pestle and mortar in the absence of any solvent. The precusor sublimes during the grinding process and the vapors diffuse into the pores of MOF giving rise to the homogenous distribution of precursor molecules. Subsequent reduction with the help of H_2 gas at a certain high temperature produces metal nanoparticles. Xu *et al* reported a nanocomposite material which was prepared by grinding the volatile Au precursor with ZIF-8 in an agate mortar followed by reduction using a stream of H_2 gas at 230°C for 2.5 hours to yield Au NPs@ZIF-8.[51] The composite material exhibited a heterogeneous catalytic activity towards the oxidation of CO to produce CO_2.

Applications of NPs@MOF Composites

Amalgamating nanoparticles with metal organic frameworks is usually done in order to enhance the performance of the resultant materials. Consequently, these composites are being used in multiple arenas of chemistry. Some of the examples have been discussed in the following section.

Heterogeneous catalysis

Catalysis is one of the areas where nanocomposite materials find wide applications. Due to their heterogeneous nature, they can be easily separated from the reaction media after completion of the reaction. However, stability of incorporated nanoparticles and the host matrix is also an important factor which needs to be considered before its application in a particular reaction condition. The deposition of metal nanoparticles on to MOF matrix usually enhances the catalytic affect.

Hydrogenation is an important organic reaction holding commercial vitality. Nanoparticles of metals such as Pd, Pt and Ni loaded on different metal organic frameworks show evident catalytic performances in the reduction of various kinds of substrates including alkenes,[52-55] alkynes,[56-57] aromatics,[58] nitro-aromatics,[59-60] ketones,[61] and aldehydes.[62-63] Sabo and his group synthesized Pd@MOF-5 and used it as a heterogeneous catalyst for the hydrogenation of styrene. Catalytic activity was found to be comparable to previously reported catalysts having Pd supported on active carbon.[64] The catalyst also displayed the sieving effect for larger molecules such as 1-octene and cis-cyclooctene which could not diffuse through its pores. Another nanocomposite catalyst having Pd nanoparticles deposited on MIL-101 exhibited efficient catalytic activity towards the reduction of aryl alkyl ketones to form the corresponding alcohol

and/or aryl alkane by molecular hydrogen.[65] The catalyst had high stability as no leaching of Pd was observed even after the 11th cycle.

Similarly, Cu NPs of 1-3 nm when incorporated inside the MOF-5 showed catalytic activity for the methanol synthesis (70 $\mu mol_{MeOH}\ g_{cat}^{-1}\ h^{-1}$) without the use of any promoter (Zn or ZnO) which is usually required for such reactions.[66] This unusual behavior was thought to be due to Cu-O-Zn interaction within MOF-5. Another example of catalysis using nanocomposite material was reported by El-Shall *et al* for the oxidation of CO.[67] Pd@MIL-101 gave complete conversion at 100°C while Cu@MIL-101 also exhibited complete conversion but at elevated temperatures of about 289°C. It was also shown that catalytic activity vanished gradually with the increasing amount of Pd NPs and the removal of surface Pd NPs did not affect the conversion rates indicating that most of the catalytic activity is due to the incorporated Pd NPs.

C-C coupling form another class of organic transformation holding commercial importance. The formation and cleavage of C-C bond requires high energy, harsh conditions are normally applied to make it feasible. Sonogashira, Suzuki, Heck and many other reactions are well studied and explored and require Pd for their execution. Therefore, Pd@MOF hybrid catalysts brought this research to the spotlight.

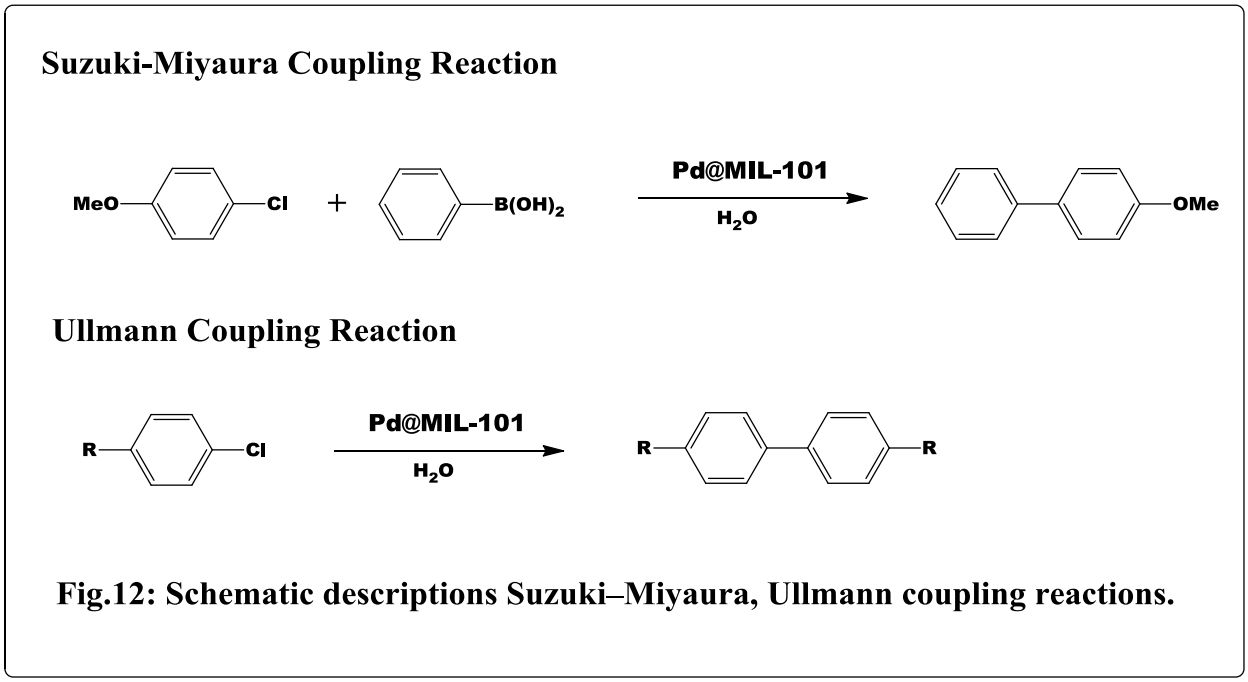

Fig.12: Schematic descriptions Suzuki–Miyaura, Ullmann coupling reactions.

Since MIL series exhibit an extraordinary stability in aqueous and organic solvents, therefore it has been extensively studied as a catalyst for various types of reactions. Pd@MIL-101(Cr) was

tested for catalysis in Ullmann homocoupling reactions of different aryl chlorides in air and under nitrogen atmosphere. Under both types of conditions, fairly good yields (>96%) were obtained (figure 12).[11] Moreover, the catalyst was easy to isolate from the reaction mixture and could be reused multiple times. Same catalyst was used for Suzuki-Miyaura coupling reaction of 4-chloroanisole and phenylboronic acid in the presence of different bases (Fig. 12). Thus, the catalyst displayed its efficiency to form C-C bond by the activation of C-Cl bond that requires harsher conditions than that for C-Br and C-I bonds.[66]

Hydrogen Storage

In 2003, Yaghi and his group reported hydrogen storage properties of MOF.[68] Since then, numerous reports based on hydrogen storage and adsorption properties of MOFs have appeared.[69-70] Although MOFs have porous structures but uptake of hydrogen at ambient conditions is still an issue in majority of the cases. Hence, the introduction of open and accessible metal centres through deposition of nanoparticles offers an opportunity for increasing the hydrogen uptake. In this regard, incorporation of Pd nanoparticles has been the most commonly used approach due to the spillover effect.[71] Pd nanoparticles catalyses the dissociation of H_2 to form the atomic hydrogen followed by the transfer of atomic hydrogen to the MOF framework thereby increasing the uptake capacity of MOF. The whole mechanism of spillover effect is yet to be clarified and therefore the possibility of PdH formation cannot be neglected.[71]

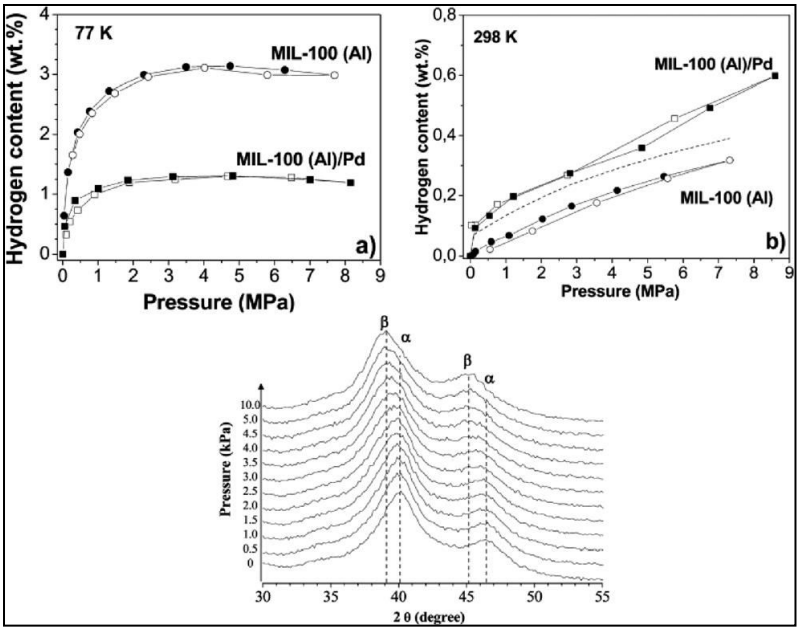

Fig. 13. Top: Comparison of H_2 adsorption (solid symbols) and desorption (open symbols) isotherms at 77 K (left) and 298 K (right) of MIL-101(Al) and Pd@MIL-101 (Al). The dashed line is calculated from the addition of the quantity of H_2 required for the formation of the bulk β-Pd hydride and the amount of physisorbed H_2 by Pd-free MIL-101(Al). Bottom: In situ XRD measurement, during hydrogen adsorption in Pd nanoparticles at room temperature and pressure upto 10 kPa, with phase transition to β-Pd hydride at high pressures

Latroche *et al* investigated the hydrogen storage properties of Pd/MIL-101(Al) at room temperature. The studies showed that the hydrogen uptake capacity was almost doubled from 0.19 to 0.35 wt% in comparison to Pd free MOF[72] (Fig. 13).

In another related study, hydrogen adsorption was investigated by Suh *et al* in Pd embedded redox active MOF, SNU-3. Hydrogen uptake was found to be dependent on the Pd content and showed a considerable enhancement from 1.03 to 1.48 wt% at 77 K, 1 bar as well from 0.13 to 0.30 wt% at room temperature and 95 bars. The enhanced adsorption was justified on the basis of the spillover effect.[73]

Chemical Sensing

Chemical sensing is one of the vital research topics these days due to its importance in homeland security, medical diagnosing and new materials for the trace level detection of hazardous materials, heavy metal ions and organic toxicants in food products and in biological systems as. Thus, there is a need to develop sensitive and selective sensors. For this purpose, the use of nanoparticle-MOF composite materials has gained attention due to specific pore size. This makes MOF moiety sense more selectively whereas nanoparticles through chemical interactions with

the analyte molecules makes the process sensitive. Chi and his co-workers incorporated the poly(ethyleneimine)-capped carbon quantum dots (BPEI–CQDs) into the framework of ZIF-8.[74]

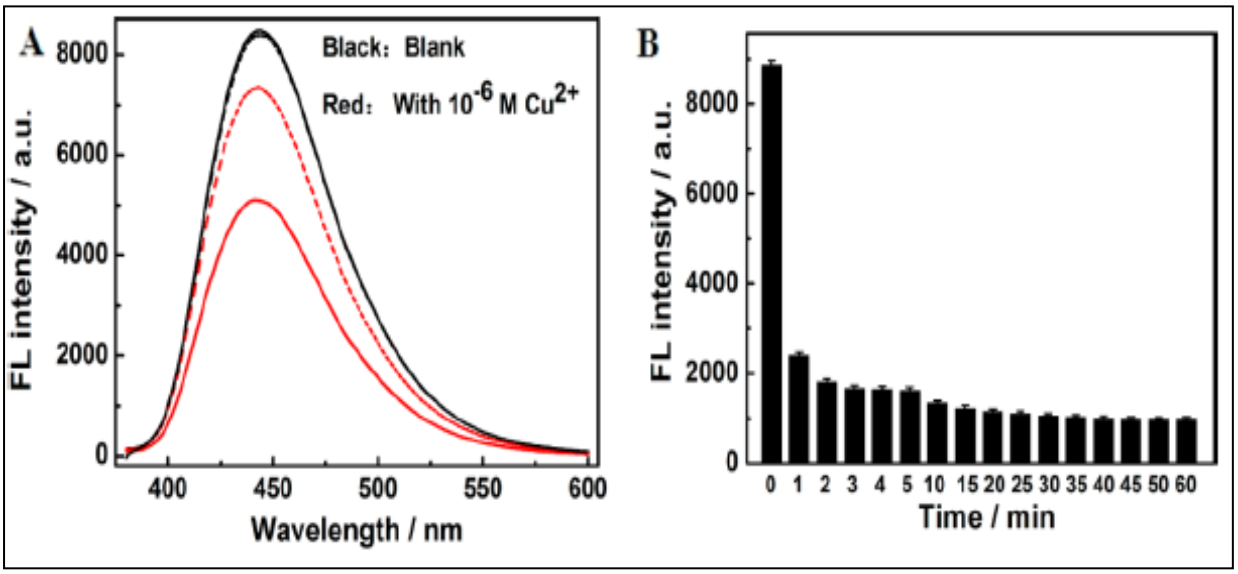

Fig. 14. A) FL spectra of BPEI-CQDs/ZIF-8 solution (solid line) and BPEI-CQDs (dash line) in the absence and presence of 1μM Cu^{2+} ions in pH 8 solution. B) Time dependent fluorescence response of 15 μg mL^{-1} BPEI-CQDs/ZIF-8 to 10μM Cu^{2+} ions in pH 8 solution

Due to synergistic behavior (porosity of MOF and complexation to CQDs), the composite showed highly sensitive and selective sensing of Cu^{2+} with a wide response range (2-1000 nm) and a very low detection limit of 80 pM. The composite exhibited accurate detection under laboratory and external conditions. Similarly, Li and coworkers have developed a non-enzymatic sensor for hydrogen peroxide.[75] The sensor is a composite containing Cu-MOF and CNTs and displayed a low detection limit of 0.46 mM and a broader response range (3–70 and 70–30 000 mM).

Electrochemical Applications

Metal organic frameworks have received much attention in the past decade and had been explored for applications in various fields. However, the use of single component MOFs is quite limited in electrochemistry due to their poor electronic conductivities, low mechanical stabilities and inferior electrocatalytic abilities.[76, 77] Hence, hybrid materials are prepared by incorporating the conducting nanostructures into the non-conducting MOFs. For example, Guo *et al* synthesized a novel nanocomposite material containing Graphene oxide nanoparticles

incorporated onto Cu-terephthalate MOF.[78] The nanocomposite was reported to behave as an excellent electrochemical sensor for drugs like dopamine (DA) and acetaminophen (ACOP).

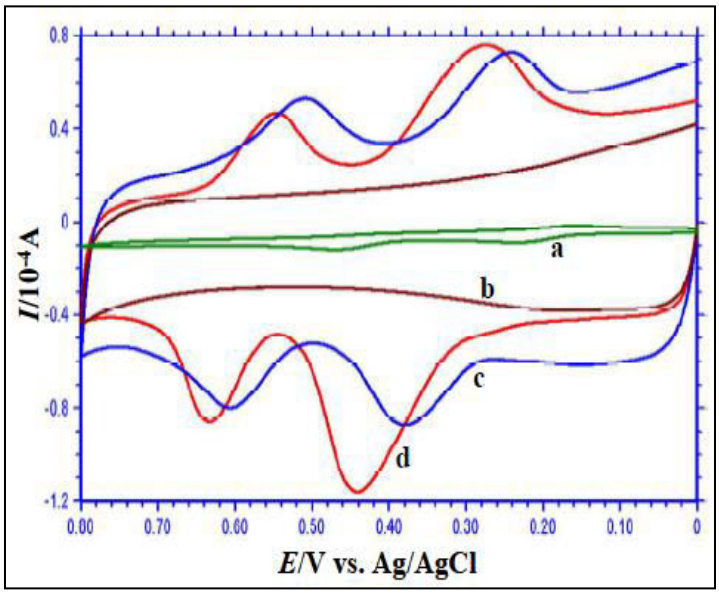

Fig.15. CVs of 0.1 mM ACOP and 0.1 mM DA mixture at Cu(tpa)-GO/GCE (a), EGR/GCE (c) and Cu(tpa)-EGR/GCE (d) in 0.1 M PBS (pH 5.0). Curve b is the CV of Cu(tpa)-EGR/GCE in 0.1 M PBS (pH 5.0) without ACOP and DA

Similarly, Sreedhar and his co-workers functionalized La BTC MOF with SPR active Au nanoparticles and CdSe quantum dots as a sensitizer.[79] The cumulative effect of three components rendered the composite material with exceptional activity for photo-electrochemical water splitting.

The work in the thesis describes new applications of a known MOF, $[Co(OBA)(H_2O)_2]$, **1**. The material has been used for the detection of nitro aromatics and aromatic organo phosphorous pesticides. Modifications have been made in MOF by incorporating ZnO and ceria nanoparticles to find their use in reduction reaction and for the electrochemical oxygen generation.

References:

1. Bowman-James, K. *Acc. Chem. Res.* **2005**, *38*, 671.
2. Lee, J.; Farha, O. K.; Roberts, J.; Scheidt, K. A.; Nguyen, S. T.; Hupp, J. T. *Chem. Soc. Rev.* **2009**, *38*, 1450.
3. Ma, L.; Abney, C.; Lin, W. *Chem. Soc. Rev.* **2009**, *38*, 1248.
4. Zhao, M.; Ou, S.; Wu, C. D. *Acc. Chem. Res.* **2014**, *47*, 1199.
5. Toyao, T.; Saito, M.; Horiuchi, Y.; Mochizuki, K.; Iwata, M.; Higashimura, H.; Matsuoka, M. *Cat. Sci. Tech.* **2013**, *3*, 2092.
6. Li, J.; Zhu, Q. L.; Xu, Q. *Chem. Comm*. **2014**, *50*, 5899.
7. An, J.; Geib, S. J.; Rosi, N. L. *J. Am. Chem. Soc.* **2009**, *131*, 8376.
8. Horcajada, P.; Serre, C.; Vallet-Regı, M.; Sebban, M.; Taulelle, F.; Ferey, G. *Angew. Chem. Int. Ed.* **2006**, *118*, 6120.
9. Taylor-Pashow, K. M. L.; Rocca, J. D.; Xie, Z.; Tran, S.; Lin, W. *J. Am. Chem. Soc.* **2009**, *131*, 14261.
10. Li, J. R.; Kuppler, R. J.; Zhou, H. C. *Chem. Soc. Rev.* **2009**, *38*, 1477.
11. Bae, Y. S.; Farha, O. K.; Spokoyny, A. M.; Mirkin, C. A.; Hupp, J. T.; Snurr, R. Q. *Chem. Comm.* **2008**, 4135.
12. An, J.; Geib, S. J.; Rosi, N. L. *J. Am. Chem. Soc.* **2010**, *132*, 38.
13. Murray, L. J.; Dinca, M.; Long, J. R. *Chem. Soc. Rev.* **2009**, *38*, 1294.
14. Hu, Y. H.; Zhang, L. *Adv. Mater.* **2010**, *22*, 117.
15. Ye, Q.; Fu, D. W.; Tian, H.; Xiong, R. G.; Chan, P. W. H.; Huang, S. D. *Inorg. Chem.* **2008**, *47*, 772.
16. Min, K. S.; Suh, M. P. *J. Am. Chem. Soc.* **2000**, *122*, 6834.
17. Liu, X.W.; Sun, T.J.; Hu, J. L.; Wang, S. D. *J. Mater. Chem. A* **2016**, *4*, 3584.
18. Ricco, R.; Malfatti, L.; Takahashi, M.; Hill, A. J.; Falcaro, P. *J. Mater. Chem. A* **2013**, *1*, 13033.
19. Li, S. Z.; Huo, F.W. *Nanoscale* **2015**, *7*, 7482.
20. Kitao, T.; Zhang, Y. Y.; Kitagawa, S.; Wang, B.; Uemura, T. *Chem. Soc. Rev.* **2017**, *46*, 3108.
21. Li, H.; Eddaoudi, M.; O'Keeffe, M.; Yaghi, O. M. *Nature*, **1999**, *402*, 276.

22. Chui, S. S.Y.; Lo, S. M. F.; Charmant, J. P. H.; Orpen, A. G.; Williams, I. D. *Science* **1999**, *283*, 1148.
23. Guillerm, V.; Gross, S.; Serre, C.; Devic, T.; Bauer, M.; Ferey, G. *Chem. Comm.* **2010**, *46* 767.
24. Kappe, C. O.; Dallinger, D.; Murphree, S. *In Practical Microwave Synthesis for Organic Chemists: Strategies, Instruments, and Protocols*; Wiley VCH: Weinheim, **2008**.
25. Kappe, C. O. *Chem. Soc. Rev.* **2008**, *37*, 1127.
26. Bradshaw, S. M.; Van Wyk, E. J.; de Swardt, J. B. *J. S. Afr. Inst. Min. Metall.* **1998**, 201.
27. (a) Jhung, S. H.; Chang, J. S.; Hwang, J. S.; Park, S. E. *Micropor. Mesopor. Mater.* **2003**, *64*, 33. (b) Jhung, S. H.; Lee, J.-H.; Yoon, J. W.; Hwang, J.-S.; Park, S.-E.; Chang, J.-S. *Micropor. Mesopor. Mater.* **2005**, *80*, 147.
28. Park, S.-E.; Chang, J.-S.; Hwang, Y. K.; Kim, D. S.; Jhung, S. H.; Hwang, J.-S. *Catal. Survey Asia* **2004**, *8*, 91.
29. Jhung, S. H.; Lee, J.-H.; Chang, J.-S. *Bull. Korean Chem. Soc.* **2005**, *26*, 880.
30. Tonigold, M.; Lu, Y.; Bredenkotter, B.; Rieger, B.; Bahnmuller, S.; Hitzbleck, J.; Langstein, G.; Volkmer, D. *Angew. Chem. Int. Ed*. **2009,** *48,* 7546.
31. Mueller, U.; Puetter, H.; Hesse, M.; Wessel, H. WO 2005/049892.
32. Campagnol, N.; Souza, E. R.; De Vos, D. E.; Binnemans, K.; Fransaer, J. *Chem. Comm*. **2014**, *50*, 12545.
33. Son, W. J.; Kim, J.; Ahn, W. S. *Chem. Comm.* **2008**, 6336.
34. Li, Z. Q.; Qiu, L. G.; Wang, W.; Xu, T.; Wu, Y.; Jiang, X. *Inorg. Chem. Comm.* **2008**, *11*, 1375.
35. Work, W. J.; Horie, K.; Hes, M.; Stepto, R. F. T. *Pure Appl. Chem.* **2004**, *76*, 1985.
36. Perez, E. V.; Balkus, K. J. Jr.; Ferraris, J. P.; Musselman, I. H. *J. Membr. Sci.* **2009**, *328*, 165.
37. Ordonez, M. J. C.; Balkus, K. J. Jr.; Ferraris, J. P.; Musselman, I. H. *J. Membr. Sci.* **2010**, *361*, 165.
38. Ordonez, M. J. C.; Balkus, K. J. Jr.; Ferraris, J. P.; Musselman, I. H. *J. Membr. Sci.* **2010**, *361*, 165.
39. Basu, S.; Cano-Odena, A.; Vankelecom, I. F. J. *J. Membr. Sci.* **2010**, *362*, 478.

40. Basu, S.; Maes, M.; Cano-Odena, A.; Alaerts, L.; De Vos, D. E.; Vankelecom, I. F. J. J. *Membr. Sci.* **2009**, *344*, 190.
41. Kusgens, P.; Siegle, S.; Kaskel, S. *Adv. Eng. Mater.* **2009**, *11*, 93.
42. Petit, C.; Burress, J.; Bandosz, T. J. *Carbon* **2011**, *49*, 563.
43. Petit, C.; Bandosz, T. J. *Adv. Mater.* **2009**, *21*, 4753.
44. Ameloot, R.; Liekens, A.; Alaerts, L.; Maes, M.; Galarneau, A.; Coq, B.; Desmet, G.; Sels, B. F.; Denayer, J. F. M.; De Vos, D. E. *Eur. J. Inorg. Chem.* **2010**, 3735.
45. Lu, G.; Li, S.; Guo, Z.; Farha, O. K.; Hauser, B. G.; Qi, X.; Wang, Y.; Wang, X.; Han, S.; Liu, X.; DuChene, J. S.; Zhang, H.; Zhang, Q.; Chen, X.; Ma, J.; Loo, S. C. J.; Wei, W. D.; Yang, Y.; Hupp, J. T.; Huo, F. *Nat. Chem.* **2012**, *4*, 310.
46. Esken, D.; Zhang, X.; Lebedev, O. I.; Schröder, F.; Fischer, R. A. *J. Mater. Chem.* **2009**, *19*, 1314.
47. Zhu, Q.-L.; Li, J.; Xu, Q.; *J. Am. Chem. Soc.* **2013**, *135,* 10210.
48. Hermes, S.; Schröter, M.-K.; Schmid, R.; Khodeir, L.; Muhler, M.; Tissler, A.; Fischer, R. W.; Fischer, R. A. *Angew. Chem. Int. Ed.* **2005**, *44*, 6237.
49. Schroder, F.; Esken, D.; Cokoja, M.; Van den Berg, M. W. E.; Lebedev, O. I.; Tendeloo, G. V.; Walaszek, B.; Buntkowsky, G.; Limbach, H.-H.; Chaudret, B.; Fischer, R. A. *J. Am. Chem. Soc.* **2008**, *130*, 6119.
50. Jiang, H. L.; Liu, B.; Akita, T.; Haruta, M.; Sakurai, H.; Xu, Q. *J. Am. Chem. Soc.* **2009**, *131*, 11302.
51. Sabo, M.; Henschel, A.; Frode, H.; Klemm, E.; Kaskel, S. *J. Mater. Chem.* **2007**, *17*, 3827.
52. Aguado, S.; El-Jamal, S.; Meunier, F.; Canivet, J.; Farrusseng, D. A. *Chem. Comm*. **2016**, *52*, 7161.
53. Jia, X.; Wang, S.; Fan, Y. *J. Catal.* **2015**, *327*, 54.
54. Zhang, W.; Lu, G.; Cui, C.; Liu, Y.; Li, S.; Yan, W.; Xing, C.; Chi, Y. R.; Yang, Y.; Huo, F. *Adv. Mater*. **2014**, *26*, 4056.
55. Liu, Y.; Zhang, W.; Li, S.; Cui, C.; Wu, J.; Chen, H.; Huo, F. *Chem. Mater*. **2014**, *26*, 1119.
56. Chen, L.; Li, H.; Zhan, W.; Cao, Z.; Chen, J.; Jiang, Q.; Jiang, Y.; Xie, Z.; Kuang, Q.; Zheng, L. *Appl. Mater. Interfaces* **2016**, *8*, 31059.
57. Chen, L.; Huang, B.; Qiu, X.; Wang, X.; Luque, R.; Li, Y. *Chem. Sci.* **2016**, *7*, 228.
58. Bi, H.; Tan, X.; Dou, R.; Pei, Y.; Qiao, M.; Sun, B.; Zong, B. *Green Chem.* **2016**, *18*, 2216.

59. Chen, L.; Huang, W.; Wang, X.; Chen, Z.; Yang, X.; Luque, R.; Li, Y. *Chem. Comm*. **2017**, *53*, 1184.
60. Chen, L. Y.; Chen, X. D.; Liu, H. L.; Li, Y. W. *Small* **2015**, *11*, 2642.
61. Hermannsdorfer, J.; Friedrich, M.; Miyajima, N.; Albuquerque, R.Q.; Kummel, S.; Kempe, R. *Angew. Chem. Int. Ed.* **2012**, *51*, 11473.
62. Lan, X.; Huang, N.; Wang, J.; Wang, T. *Catal. Sci. Tech.* **2017**, *7*, 2601.
63. Zhao, M.; Yuan, K.; Wang, Y.; Li, G.; Guo, J.; Gu, L.; Hu, W.; Zhao, H.; Tang, Z. *Nature* **2016**, *539*, 76.
64. Hermannsdorfer, J.; Kempe, R. *Chem.–Eur. J.* **2011**, *17*, 8071.
65. Hermes, S.; Schröter, M.-K.; Schmid, R.; Khodeir, L.; Muhler, M.; Tissler, A.; Fischer, R. W.; Fischer, R. A. *Angew. Chem. Int. Ed.* **2005**, *44*, 6237.
66. Yuan, B.; Pan, Y.; Li, Y.; Yin, B.; Jiang, H. *Angew. Chem. Int. Ed.* **2010**, *49*, 4054.
67. El-Shall, M. S.; Abdelsayed, V.; Khder, A. E. R. S.; Hassan, H. M. A.; El-Kaderi, H. M.; Reich, T. E. *J. Mater. Chem.* **2009**, *19*, 7625.
68. Rosi, N. L.; Eckert, J.; Eddaoudi, M.; Vodak, D. T.; Kim, J.; O'Keeffe, M.; Yaghi, O. M. *Science* **2003**, *300*, 1127.
69. Murray, L. J.; Dinca, M.; Long, J. R. *Chem. Soc. Rev*. **2009**, *38*, 1294.
70. Wang, Z.; Tanabe, K. K.; Cohen, S. M. *Chem. Eur. J.* **2010**, *16*, 212.
71. Kalidindi, S. B.; Oh, H.; Hirscher, M.; Esken, D.; Wiktor, C.; Turner, S.; Van Tendeloo, G.; Fischer, R. A. *Chem. Eur. J.* **2012**, *18*, 10848.
72. Zlotea, C.; Campesi, R.; Cuevas, F.; Leroy, E.; Dibandjo, P.; Volkringer, C.; Loiseau, T.; Férey, G.; Latroche, M. *J. Am. Chem. Soc.* **2010**, *132*, 2991.
73. Cheon, Y. E.; Suh, M. P. *Angew. Chem. Int. Ed.* **2009**, *48*, 2899.
74. Lin, X. M.; Gao, G. M.; Zheng, L. Y.; Chi, Y. W.; Chen, G. N. *Anal. Chem.* **2014**, *86*, 1223.
75. Zhou, E. C.; Zhang, Y. W.; Li, Y. J.; He, X. W. *Electroanalysis* **2014**, *26*, 2526.
76. Zhang, Y.; Bo, X.; Luhana, C.; Wang, H.; Li, M.; Guo, L. *Chem. Comm*. **2013**, *49*, 6885.
77. Hosseini, H.; Ahmar, H.; Dehghani, A.; Bagheri, A.; Tadjarodi, A.; Fakhari, A. R. *Biosens. Bioelectron.* **2013**, *42*, 426.
78. Wang, X.; Wang, Q.; Wang, Q.; Gao, F.; Gao, F.; Yang, Y.; Guo, H.-X. *ACS Appl. Mater. Interfaces* **2014**, *6*, 11573.

79. Vaddipalli, S. R.; Sanivarapu, S. R.; Vengatesan, S.; Lawrence, J. B.; Eashwar, M.; Sreedhar, G. *ACS Appl. Mater. Interfaces* **2016**, *8*, 23049.

CHAPTER-3

MATERIALS AND METHODS

Chemicals

Chemicals needed for the synthesis, cobalt (II) chloride hexahydrate (98%), sodium hydroxide (97%) benzene (99%), nitrobenzene (99%), 4-nitrobenzoic acid (97%), 3-nitrotoluene (98%), p-nitrophenol (97%), 2,4-dinitrofluorobenzene (99%), 2, 4, 6-trinitrophenol (98%), zinc (II) nitrate hexahydrate (98%), sodium borohydride (98%) and 4-fluoronitrobenzene (98%) were used as received from SDFCL. Whereas 2, 6-dintrotoluene (98%), potassium hydroxide (98 %), p-nitroanisole (98%), p-nitrobenzoic acid (98%) and 1, 3- dinitrobenzene (98%) were purchased from Loba Chemie, India and were used without further purification. Also 4, 4′-oxy bis(benzoic acid) (99%) was procured from Sigma-Aldrich and was used as received. Solvents such as acetonitrile (99.5%) and toluene (98%) were bought from Merck, India and were used without further purification. Pesticides, chlorpyrifos (94%), malathion (96%), acephate (95%) and triazophos (90%) were procured from Markfed, India. Cerium (III) nitrate hexahydrate (98%) and methanol (98%) were purchased from CDH, India All the electrochemical measurements were done with deionized water. The water used for luminescent studies and other synthesis was double distilled and filtered through a Millipore membrane. Stock solutions of compounds were prepared by using above mentioned solvents as per the analytical requirements. All the glassware was cleaned with nitric acid and rinsed thoroughly with distilled water before use. Nitrogen purging was carried out for 5 minutes in the test solution to carry out all the electrochemical experiments.

Characterizations and Instruments

Powder X-ray diffraction (PXRD) studies were done using XPERT PRO Diffractometer (Cu-Kα, λ=0.15406 nm, 45 KV, 40 mA, step size =0.013Å). The photoluminescence studies were done using Perkin Elmer Spectrofluorometer (LS-45). Surface morphologies and the particle size analysis were done using JEOL- 2100 high resolution-transmission electron microscope (HR-TEM) and the composition of synthesized composites was confirmed with the help of scanning electron microscopy (SEM) (JEOL, JSM-6510LV) and Energy Dispersive X-ray (EDX) using Oxford instrument (INCA X-act).The surface of the prepared composites was also examined

with the help of X-ray photoelectron spectroscopy (XPS) using using ESCA+, (omicron nanotechnology, Oxford Instrument Germany) equipped with monochromator Aluminum Source (Al Kα radiation having energy of 1486.7eV) operated at 15 kV and 20 mA. Samples taken in powder form were deposited on a Cu tape and degassed overnight in XPS FEL chamber to minimize the air contamination at the sample surface. All the reported binding energies were referenced to the main C 1s line at 285.0 eV.

Raman spectra were recorded on Renishaw InVia Raman microscope with an excitation wavelength of 785 nm from Argon laser focused on a sample by means of 100 X objective of 0.9 numerical aperture. Optical studies were done using Analytica Jena UV-Vis spectrophotometer having slit width 1 cm was for monitoring the progress of catalytic reduction. Catalytic conversions were monitored using HPLC (Thermofisher Ultimate Dionex 3000) by reverse phase chromatography using C-18 column (Thermo Scientific Acclaim^{TM} 120, 5 µm, 120 Å, 4.6 X 250 mm) having UV-VIS detector (λ= 254 nm) and flow rate of 1 mL/min (MeOH: H_2O = 70:30).

All the electrochemical studies were performed using potentiostat (Autolab/ PGSTAT12/Eco Chemie/Netherlands) in O_2 saturated 1.0 M KOH aqueous solution at room temperature. An electrochemical cell (V= 10 mL) having standard three electrode system with glassy carbon (GC, diameter=3 mm) as a working electrode, Pt wire as a counter electrode and KCl (1.0 M)-Ag/AgCl (Metrohm make) as a reference electrode was used for all the electrochemical measurements. Cyclic voltammetric measurements were done with optimized concentration of the electrocatalyst (5 mg) and the scan rate was set at 40 mV s^{-1}. The OER activity was also investigated using linear sweep voltammetric technique at scan rate of 1 mVs^{-1}. Current- time responses were recorded with the help of chronoamperometric method having set potential of +0.8V vs RHE in O_2 saturated 1.0 M KOH aqueous solution for 1000 minutes.

Techniques Used:

Powder X-Ray Diffraction (PXRD)

X-ray powder diffraction (XRD) is an analytical technique primarily used for phase identification of a crystalline material and provides information on unit cell dimensions. The sample under analysis was finely grounded and homogenized before analysis with the help of pestle and mortar to determine of crystal structure and atomic spacing.

High Resolution Transmission Electron Microscopy (HR-TEM)

It is a powerful imaging technique that gives information about the atomic structure of a sample under investigation. The samples were dissolved in ethanol and homogenized with the help ultrasonicator for 2 hours prior to the analysis gave a clear image due to proper transmission of electrons.

X-Ray Photoelectron Spectroscopy (XPS)

X-ray photoelectron spectroscopic technique is used to investigate the elemental composition and is known as electron spectroscopy for chemical analysis (ESCA). The spectrum is generated by bombarding the sample with X-rays of definite energy which interact with core electrons of the sample located around the nucleus leading them to escape from the sample at a well defined kinetic energy. The photoelectrons ejected from different atomic orbitals have different binding energies and thus determine the elemental composition. Here, photoelectrons ejected from the top 0 to 10 nm layer were investigated.

Raman Spectroscopy

Raman spectroscopy is the vibrational spectroscopy that provides insight about the molecular vibrations and the crystal structure. The sample was finely grounded before analysis with the help of pestle and mortar and was used to study chemical bonding and crystallographic orientation of the materials.

Scanning electron microscopy (SEM)

SEM is also an imaging technique that is used to provide information about the surface morphology, chemical composition and crystalline structure of the material. Metals or conducting materials can be used as such but the non-conducting materials were coated by a thin layer deposition of Gold/Palladium with the help of sputter coater prior to the analysis. The samples were then mounted on a support or stub with help of conductive double coated carbon tape used as an adhesive. Finally the sample was then observed under electron microscope.

Spectrophotometry

It is a quantitative measurement of the amount of light being absorbed or emitted by a chemical compound to determine the composition and properties. The samples dissolved in an appropriate

solvent were made to a specific concentration (10^{-2} M, 10^{-3} M) and their absorbance/emission was measured using a cuvette by scanning UV light over the required range.

Spectroflourometry

It is one of the types of electromagnetic spectroscopy that deals with the fluorescence phenomenon. Flourescence occurs when the molecules of an analyte are excited by providing the light of certain wavelength and it then emits the radiation of different wavelength usually the longer wavelength. The photoluminescence studies were done using MOF dispersed in water (5 mg of MOF into 100 mL water followed by ultrasonic agitation for 30 minutes) at room temperature. The analytes were added into the dispersion using micro pipette.

Voltammetry

Voltammetry is one of the types of electroanalytical method which investigates the redox properties of the analyte by measuring current as a function of applied potential. It also provides information about the adsorption process and electron transfer mechanisms taking place at the surface that has been chemically modified. Voltammetry used in the current work were linear sweep voltammetry (LSV) and Cyclic Voltammetry (CV).

Cyclic Voltammetry (CV)

It is a type of potentiodynamic electroanalytical technique which measures the current that develops in an electrochemical cell under conditions where voltage is in excess of that predicted by the Nernst equation. CV is usually applied to study redox reactions, to determine the stability of reaction products, to know the electron stochiometry, electron transfer kinetics,[1] the formation of reaction intermediates,[2] diffusion coefficient of analyte and also the reversibility of the reaction.[3]

Linear Sweep Voltammetry (LSV)

Linear sweep voltammetry generally involves scanning the potential of the working electrode linearly with respect to the time. The current is plotted as a function of potential to produce a voltammogram. LSV is simply a cyclic voltammetry without vertex potential and reverse scan. A typical LSV experiment utilizes a standard three electrode cell setup to deliver a potential to the solution and monitor its change in current. It is more useful in case of irreversible redox reactions and gives better insight about the kinetics of such irreversible redox reactions.

Chronoamperometry

Chronoamperometry is an electrochemical technique in which the potential of the working electrode is stepped and the resulting current from faradaic processes occurring at the electrode (caused by the potential step) is monitored as a function of time. The technique can be used to measure concentration by measuring I *Vs* conc. at any fixed time and can analyze the shape of the current-time curve in order to study coupled chemical reactions. It also gives information about the stability of the working electrode.

SYNTHETIC PROCEDURES

Synthesis of [Co(OBA)(H_2O)$_2$], 1

MOF was prepared through convenient solvent evaporation method by a known procedure.[4] In a beaker was taken $CoCl_2.6H_2O$ (3.8 g, 16 mmol) and dissolved in water (80 ml). In another beaker was taken 4, 4'-oxy-bis (benzoic acid) (4.2 g, 16 mmol) and NaOH (1.3 g, 32 mmol) and dissolved in water (80 ml) by heating to a temperature of 100ºC. The transparent solution of 4,4'-oxy-bis (benzoate) from second beaker was poured into cobalt solution of first beaker and the resulting solution kept at 80ºC in water bath. After two days, pink colored product was observed, filtered and washed with deionized water till neutral (pH paper) and dried at ambient conditions. Product yield was 85% (4.76 g) and it was characterized by PXRD.

Synthesis of 4-(2, 4-Dinitrophenoxy)-3-methoxybenzaldehyde (DPE-1)

DPE-1 was prepared using an earlier reported procedure.[5] 1-Fluoro-2, 4 dinitrobenzene (0.48g, 2.5 mmol) and vanillin (0.5g, 3.2 mmol) in presence of K_2CO_3 (1.48g, 10.8 mmol) were taken in 250 ml round bottom flask. To this was added DMF (10 ml), 18-crown-6 (25 mg, 0.1 mmol) and stirred under the room temperature for 12 hrs. TLC was done to monitor the progress of reaction using toluene as a solvent. After completion of reaction, was washed with aqueous NaOH (0.1 M). Resulting solid was filtered and was neutralized with 2% HCl followed by washing with water (3-4 times) to remove excess of the solvent. The crude product was dried under vacuum and was purified by column chromatography using toluene as an eluent. Light yellow colored solid (0.7207g, 66 %) was obtained. ^{1}H-NMR (400 MHz, $CDCl_3$): δ 3.8 (s, 3H), 6.9 (d, J=9.16 Hz, 2H), 7.3 (m, 1H), 7.6 (m, 2H), 8.3 (dd, 1H), 8.9 (d, J=2.76 Hz, 1H), 10.0 (s, 1H).

Synthesis of 4-(2, 4-Dintrophenoxy)-3-methoxybenzyl alcohol (DPE-2)

DPE-1 (0.5g, 1.5mmol) was taken in 250 ml round bottom flask in methanol (100 mL). To this was added slowly sodium borohydride (0.028g, 0.75mmol) in methanol (150 ml). The reaction mixture was stirred for about 2-3 hrs at room temperature and TLC was monitored. A new spot indicated the product formation. Methanol was evaporated using rotary evaporator and the crude product obtained was purified by column chromatography using petroleum ether and ethyl acetate as solvents. Yellow colored solid was analyzed by ^{1}H-NMR (400MHz, CDCl3): δ 3.78(s, 3H), 4.75(s, 2H), 6.87(d, J=9.6 Hz, 1H),7.11(d, 1H), 7.17(d, J=8.2 Hz, 1H), 8.25(d, J=2.8, 1H), 8.28(s,1H), 8.8(d, J=2.8, 1H).

Synthesis of ZnO/MOF

To a dispersion of Co-MOF (500 mg) in 20 mL of methanol was added dropwise the required amount of methanolic solution of $Zn(NO_3)_2.6H_2O$ followed by vigorous stirring at room temperature. After ten minutes, NaOH (0.1 M) dissolved in methanol was added to the reaction mixture and allowed to stir for another hour to allow the complete formation of $Zn(OH)_2$. The product thus obtained was centrifuged at 5,000 rpm, washed with methanol (10 mL X 4), subsequently dried under vacuum and calcined in oven at 120 ℃ leading to the formation of ZnO/MOF-I, ZnO/MOF-II and ZnO/MOF-III composites.

Catalytic reduction using ZnO/MOF

The ZnO/MOF catalysts were activated at 90-100℃ (1 hour) before each reduction reaction. For catalytic reduction, ZnO/MOF catalyst (1 mg) was suspended into the methanolic solution of a nitro aryl compound (5 mM) taken in a stoppered test tube. To this was added freshly prepared solution of $NaBH_4$ (0.36 mM) in methanol (5mL) and the test tube sealed with parafilm. After the given reaction time, a sample was withdrawn and the catalyst was separated from the reaction mixture using Millipore filter (pore size 0.22 μm) to monitor the progress of the reduction reactions at different time intervals with the help of UV-Vis spectroscopy and HPLC.

Synthesis of Ceria (CeO_2) nanoparticles

To the deionized water (30 mL) was added, CTAB (83 mg) under vigorous stirring at room temperature. To this solution was added dropwise, an aqueous solution of $Ce(NO_3)_3.6H_2O$ (500 mg, 20 mL) and allowed to stir at room temperature. After an hour, aqueous solution of NaOH

(0.1 M, 10 mL) was added and the mixture heated at 80ºC for another two hours. The yellow coloured product was then allowed to age for 30 minutes at ambient temperature followed by centrifugation at 5,000 rpm and washing with deionized water (10 mL X 4). The nanoparticles were subsequently dried under vacuum and calcined at 70 ºC.

Synthesis of Ceria loaded Co-MOF (CeO_2/MOF)

An aqueous solution of $Ce(NO_3)_3.6H_2O$ (0.1M, 1.42 mL) was added dropwise to the Co-MOF (500 mg) dispersed in water (20 mL) and the mixture stirred vigorously at room temperature. After about an hour, aqueous solution of NaOH (0.1 M, 5 mL) was added to the reaction mixture and allowed to stir for another two hours at 80 ºC to allow the complete formation of CeO_2. The product formed was then allowed to age for 30 minutes at ambient temperature and centrifuged at 5,000 rpm followed by washing with deionized water (10 mL X 4). The product was subsequently calcined at 70 ºC.

Preparation of Ceria/MOF modified electrode

Electrocatalyst powder (5 mg) was dispersed in solution having 1:1(v/v) water and ethanol (1 mL) and 200 µL of Nafion solution (5% Nafion w/w in propanol) was added. The mixture was sonicated for 30 minutes to form suspension. Above suspension was dropcast (5 µL) onto the surface of the glassy carbon electrode and was allowed to dry in air at room temperature. Before use, the surface was polished well with alumina powder (Al_2O_3) followed by washing with ethanol and was dried in air in order to obtain a mirror like surface.

References:

1. DuVall, S.; McCreery, R. *Anal. Chem.* **1999**, *71*, 4594.
2. Nicholson, R. S. *Anal. Chem.* **1965**, *37*, 1351.
3. Bond, A. M.; Feldberg, S. *J. Phys. Chem.* **1998**, *102*, 9966.
4. Mahata, P.; Drazneiks, C. M.; Roy, P.; Natarajan, S. *Cryst. Growth Des.* **2013**, *13***,** 155.
5. Chhibber, M.; Kumar, G.; Parasuraman, P.; Ramya, T. N. C.; Surolia, N.; Surolia, A. *Bioorg. Med. Chem.* **2006**, *14*, 8086.

CHAPTER-4

RESULTS AND DISCUSSION

CHAPTER-4A

PREPARATION OF MATERIALS

Synthesis and Characterization of Co-MOF

The metal organic framework (MOF), [Co(OBA)(H_2O)$_2$] [OBA= 4,4'-oxybis(benzoate)], **1** was prepared using a convenient solvent evaporation method taking $CoCl_2.6H_2O$ and 4,4'-oxy-bis (benzoic acid) as precursors and water as a solvent.[1] The crystal structure of as-synthesized MOF was characterized with the help of powder X-Ray diffraction technique (P-XRD) (Fig.1). The diffraction pattern of the Co-MOF was found to be in complete agreement with the simulated pattern generated from the single crystal data and with that of the earlier reported literature.[1] The pattern shows two sharp and major peaks at 2Θ = 6.97º, 13.8º suggesting its highly crystalline nature and a multiplet ranging from 18.1º -21º.

The properties of MOF, **1**, can be described on the basis of its crystal structure where, the Co^{2+} ions are connected by the OBA unit forming a two-dimensional layer structure. Inter-layer hydrogen bond interactions between coordinated water molecules of one layer and the carboxylate oxygens of another layer give rise to a supra-molecularly organized three-dimensional structure (Fig.2).

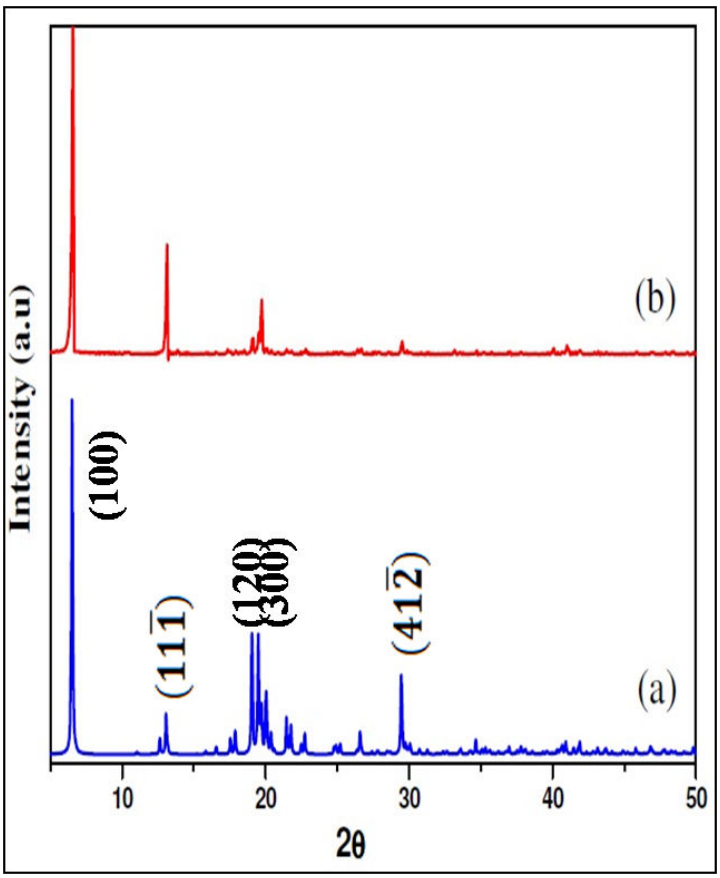

Fig. 1. Powder XRD (CuKα) patterns: (a) Earlier reported (b) As-synthesized sample of [Co(OBA)(H_2O)$_2$], **1**

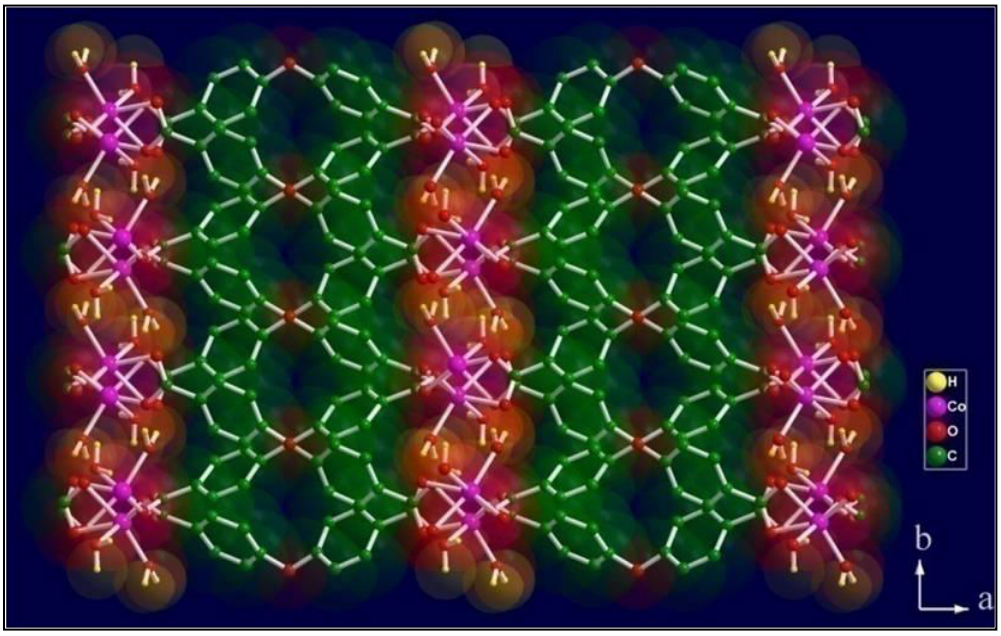

Fig. 2. Two-dimensional layered structure of MOF with inter-layer hydrogen bond interactions

Synthesis and Characterization of ZnO/MOF Composites

ZnO/MOF composites were prepared by wet impregnation method using Zn^{2+} ions in three different molar ratios. A suspension of Zn^{2+} ions and pre synthesized MOF (**1**) was hydrolyzed using NaOH to form corresponding ZnO nanoparticles impregnated on the later. Final material in all the three cases (ZnO/MOF-I, ZnO/MOF-II and ZnO/MOF-III) was isolated by centrifugation followed by calcinations at 120 °C.

Diffraction patterns observed for all the three composites (ZnO/MOF-I, ZnO/MOF-II and ZnO/MOF-III) displayed sharp peaks that were similar to that of the parent MOF, **1,** indicating alteration in crystallinity and conservation of structural integrity of its framework (Fig.3). However, a slight shifting of the peak from 6.97º to 7.7º occurred due to the incorporation of ZnO nanoparticles. The peak at 7.7° (2Θ) indicated the presence of MOF with open structure, due to its value lower than 10° (2Θ). It is hypothecated that incorporation of ZnO nanoparticles in the interplanar positions of the MOF followed by calcinations at 120ºC results in the release of two coordinated water molecules[1] due to which, the inter layer separation and the distance

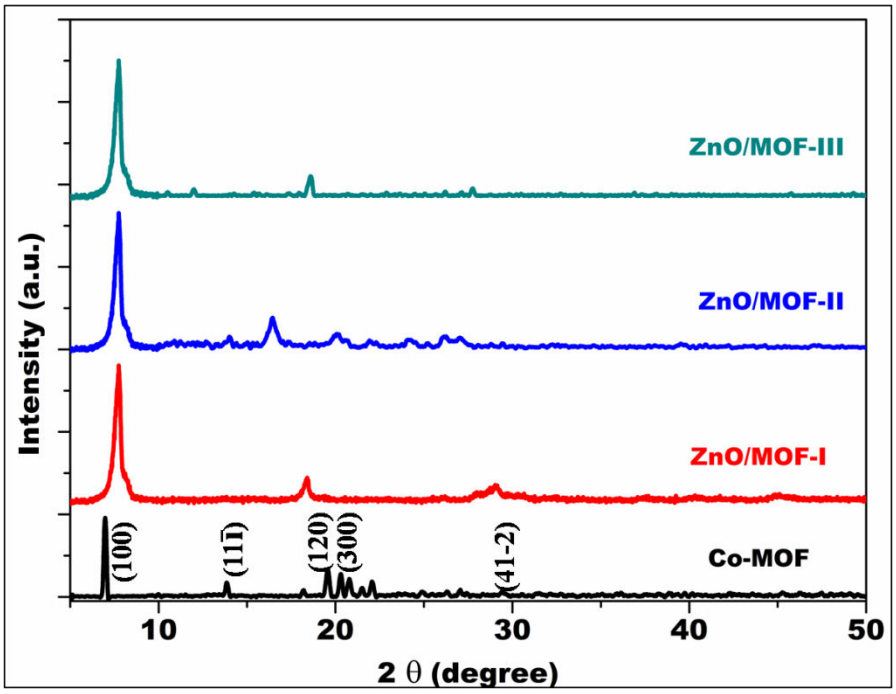

Fig.3. Experimental PXRD pattern of Co-MOF showing no major change in the diffraction pattern as the loading wt% of ZnO nanoparticles is very low and also the particle size is very small

between the two planes of the MOF decreases resulting in a slightly condensed structure without changing the main framework of the composites. However, no diffraction peaks corresponding to the ZnO NPs were observed suggesting that the ZnO loadings were too low in all the composites.[2, 3]

In order to confirm that Co-MOF structure was intact after the incorporation of ZnO nanoparticles, room temperature Raman spectra was recorded and compared for all the synthesized materials. Figure 4 shows the comparison of spectra for 100-3200 cm^{-1} range. Multiple bands associated with the vibration modes of carboxylate group and aromatic ring were observed. The band at 1618 cm^{-1} in case of Co-MOF, **1** corresponds to -C=O stretching whereas the band at 1451 cm^{-1} signifies the presence of –C=C– group present in the aromatic ring of the OBA ligand moiety. Aromatic C-H vibrations at 643 cm^{-1} are attributed to its out-of-plane deformation mode. The ether linkage (-C-O-C-) of OBA present in the MOF appears at 878 cm^{-1} and 1161 cm^{-1} (asymmetric stretch) while a relatively small band at 428 cm^{-1} for Co-O indicates the successful formation of Co-MOF. In case of ZnO/MOF-I, ZnO/MOF-II and ZnO/MOF-III; a characteristic scattering peak at 437 cm^{-1} corresponds to high frequency branch of E_2 mode of hexagonal wurtzite ZnO which confirmed successful incorporation of ZnO nanoparticles into Co-MOF.[4] The peak at 437 cm-1 is missing in case of bare MOF as shown in Fig. 7b. The weak intensity of the peak can be attributed to the low content of the nanoparticles. Thus, overall structural framework of Co-MOF is conserved which is confirmed by the appearance of characteristic peaks of bare Co-MOF in case of ZnO/MOF-I, ZnO/MOF-II and ZnO/MOF-II. But the broadening of signals along with a slight shift of the peaks can be attributed to the incorporation of ZnO nanoparticles into MOF.

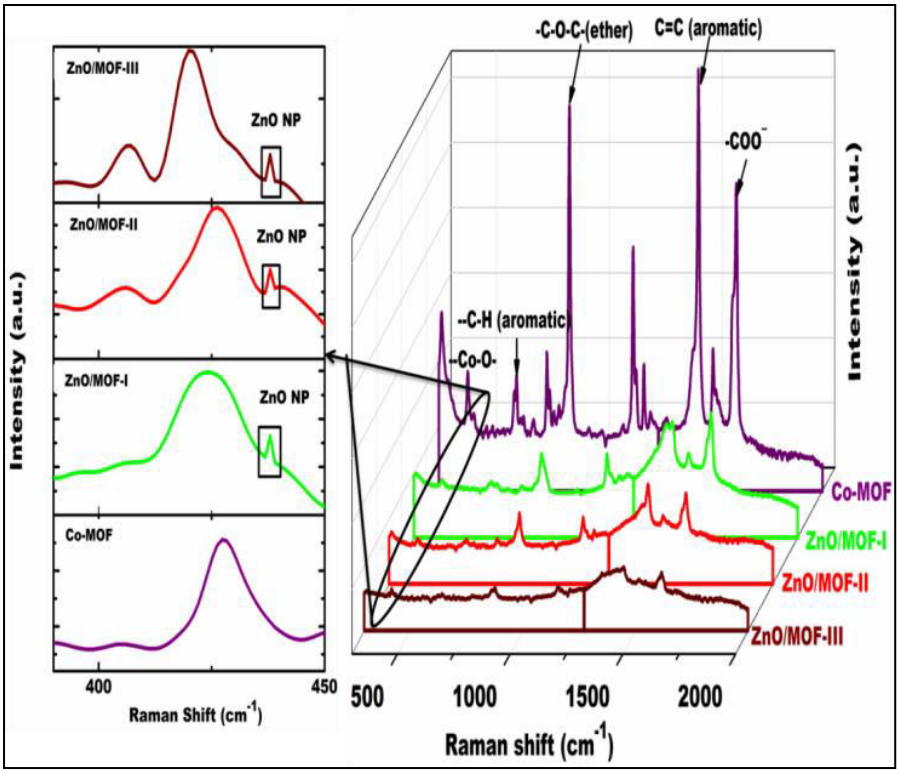

Fig.4. Raman spectra of Co-MOF and ZnO/MOF-I/II/III composites

The incorporation of ZnO nanoparticles in MOF as hypothecated earlier was confirmed by high resolution transmission electron microscopy (HR-TEM). Figure 5 shows three different sizes of NPs that were dependent upon the loading ratios of Zn^{2+} ions. Lowest loading of the Zn^{2+} resulted in the incorporation of spherical nanoparticles (ZnO/MOF-I) having size 4-8 nm (Fig.5a). Lattice fringes of 0.24 nm and 0.28 nm matched with 101 and 100 planes of ZnO respectively. The results are in good agreement with XRD data (JCPDS 75-1526) of wurtzite ZnO having the hexagonal structure (Fig.5b). For ZnO/MOF-II samples (Fig.5c) the incorporated nanoparticles were of 7-14 nm size range. The lattice fringes of 0.24 nm corresponding to 101 plane (fig. 5d) were also observed here. The image also shows continuous deposition of small range nanoparticles in case of ZnO/MOF-II along with higher sized particles. Needle shaped nanoparticles of dimensions 80-90 nm in case of highest loading (ZnO/MOF-III, Fig.5e) with lattice fringes of 0.19 nm and 0.26 nm corresponding to 102 and 002 planes respectively (Fig.5f). Thus, the size of incorporated nanoparticles in MOF can be controlled or tuned by varying the metal loading ratio of Zn^{2+} salt. Highlight of this method is absence of surfactant in the preparation of nanoparticles that keep the surface active for further applications (chapter 4B).

The composition of all the three samples was confirmed using energy dispersive X-ray spectroscopy (EDX) which showed the presence of both ZnO along with MOF. The weight percentage of zinc in the composites, ZnO/MOF-I, ZnO/MOF-II and ZnO/MOF-III was found to be 0.51, 1.34 and 2.57 against the initial loading of 1, 2 and 5 weight percentage respectively (Fig. 6).

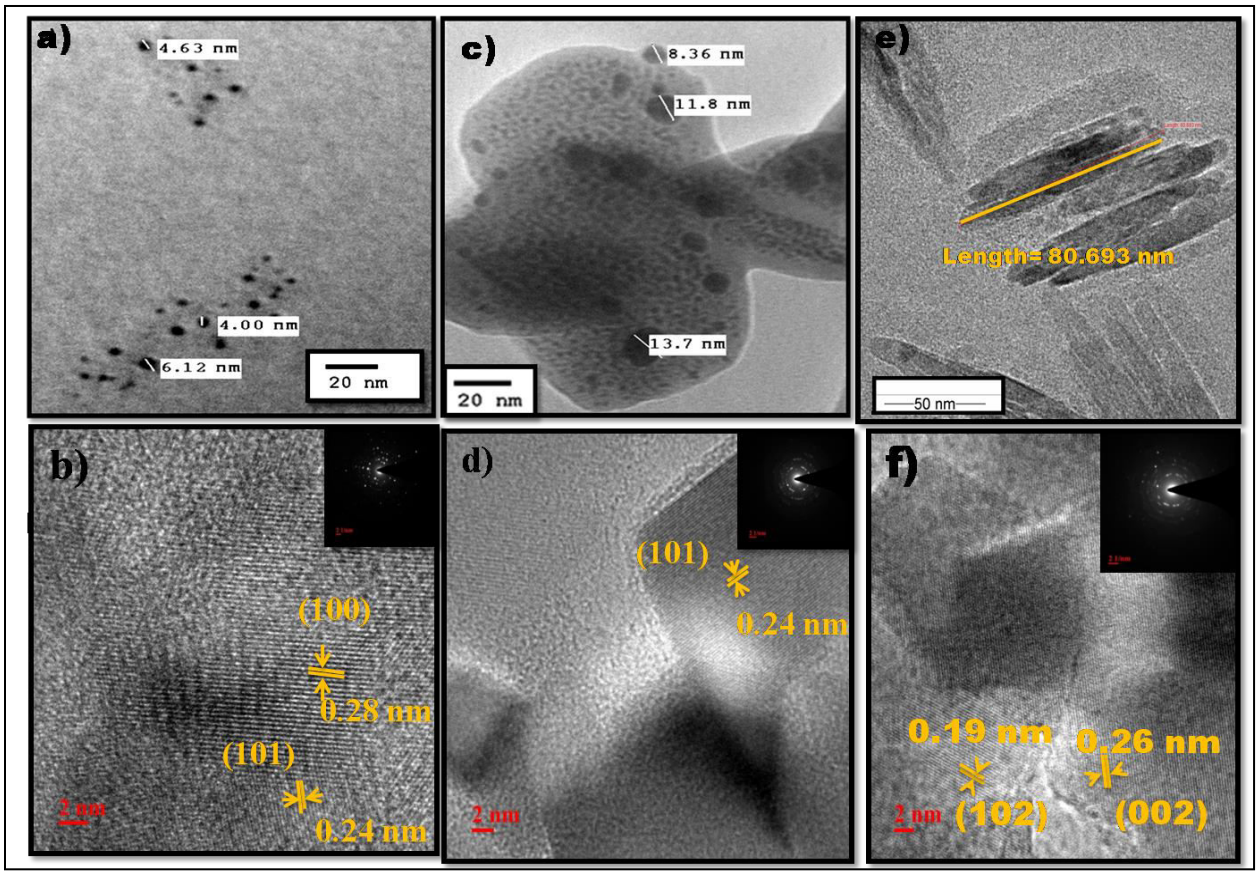

Fig. 5. TEM images of composites having different loading weight percent of ZnO nanoparticles a-b) ZnO/MOF-I (quantum dots) showing lattice fringes of 0.24 nm and 0.28 nm corresponding to 101 and 100 planes respectively c-d) ZnO/MOF-II showing lattice fringes of 0.24 nm corresponding to 101 plane e-f) ZnO/MOF-III (nano needles) showing lattice fringes of 0.19 nm and 0.26 nm corresponding to 102 and 002 planes respectively

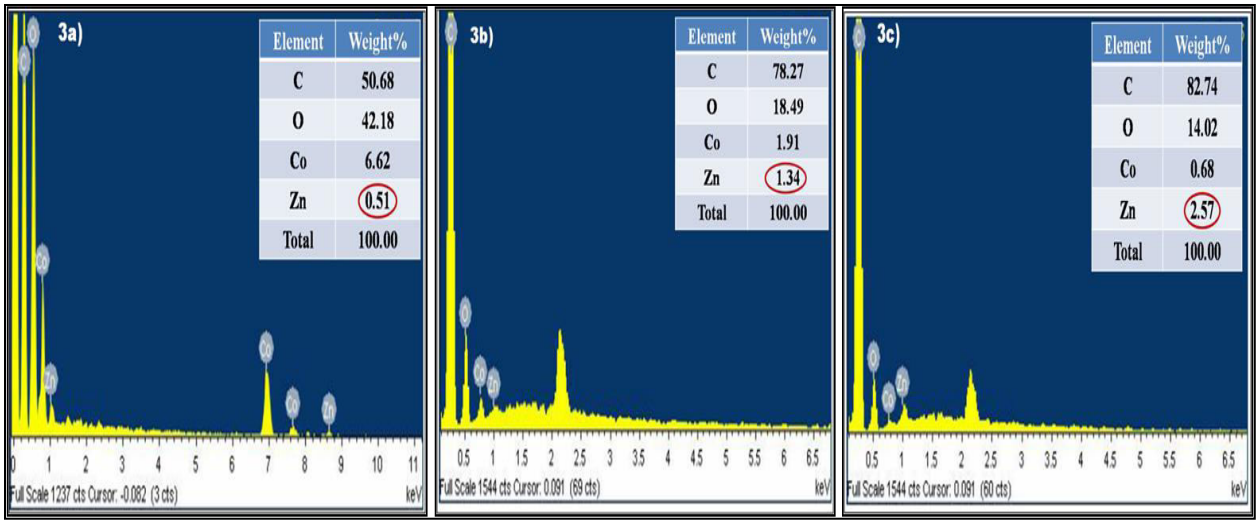

Fig. 6. EDX images of a) ZnO/MOF-I b) ZnO/MOF-II and c) ZnO/MOF-III showing weight percentages of different elements

Microwave Plasma Atomic Emission Spectroscopy (MP-AES) was used to further confirm the weight percentage of zinc in composites. The results as described in Table 1 were corroborated with data obtained from EDX analysis.

Table 1: Comparison of zinc analysis (in terms of weight percent) by MP-AES and EDX

Sr. No.	**Composite**	**Zinc**	
		MP-AES	**EDX**
1.	ZnO/MOF-I	0.86	0.51
2.	ZnO/MOF-II	1.10	1.34
3.	ZnO/MOF-III	2.50	2.57

The conditions used for the synthesis of ZnO nanoparticles can also lead to the formation of $Zn(OH)_2$ species. XPS is one of the most reliable means to analyze the different chemical states of an element based on their characteristic binding energies. Figure 6 shows the XPS spectra of oxygen 1s for all the three composites. The peaks appearing at 530.6 eV, 529.9 eV and 530.3 eV correspond to ZnO/MOF-I, II and III respectively (Fig.7a). These were in line with the ZnO species whereas the standard peak corresponding to oxygen (1s) for $Zn(OH)_2$ appears at 532 eV.[5] This confirmed the successful loading of ZnO nanoparticles onto the MOF. The peaks of

ZnO/MOF-I, II and III for Zn $2p_{3/2}$ appeared at 1022.3 eV, 1022.1 eV and 1022.4 eV respectively (Fig.7b). The XPS spectra of Co 2p and C 1s for bare MOF and the three composites have also been shown in Fig. 7 which is corroborated with the literature values.

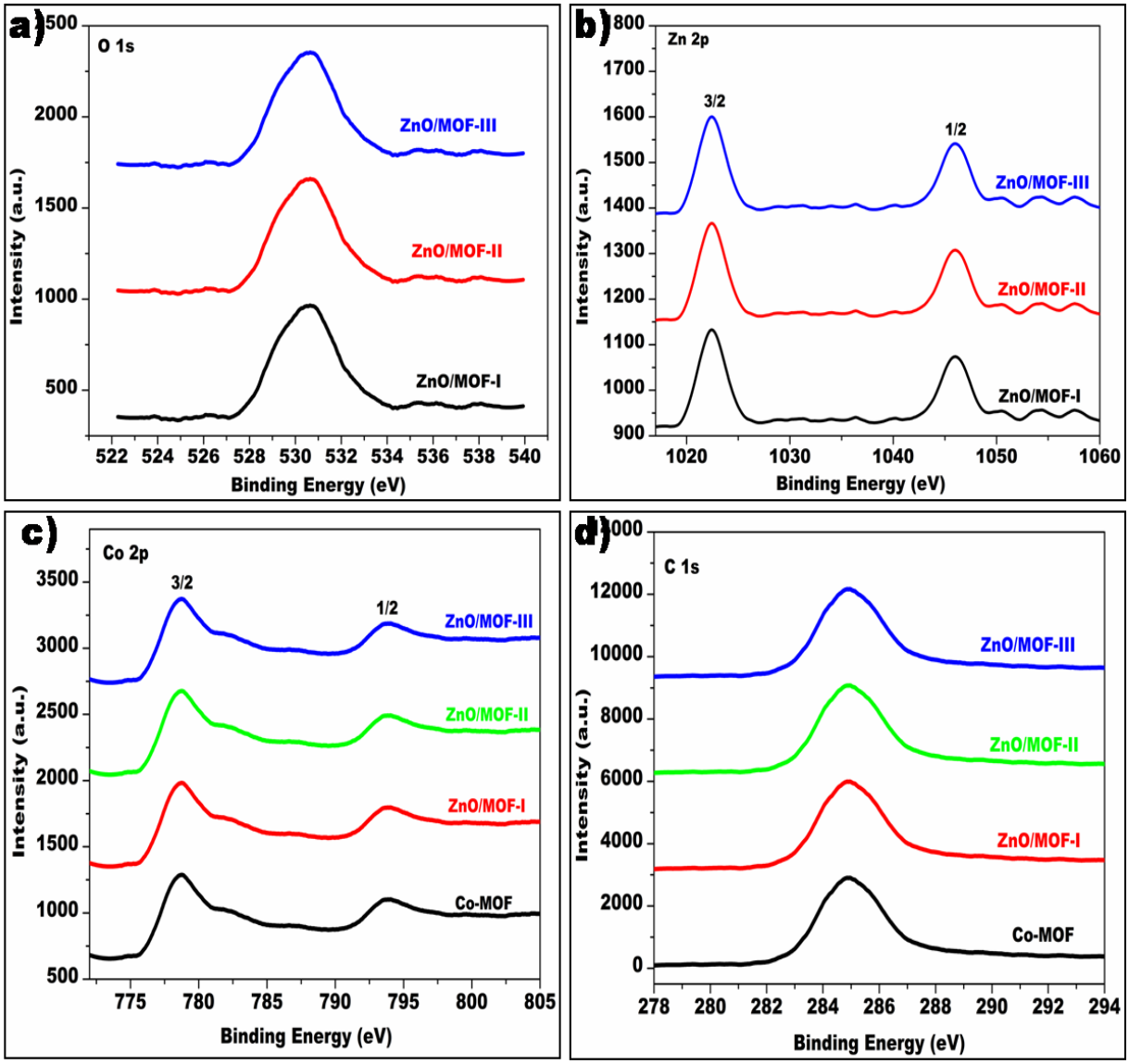

Fig.7. XPS spectra of ZnO/MOF composites

Synthesis and Characterization of CeO_2/MOF Composite

Cerium is one of the promising materials due to its lower reduction potential and ability to easily interconvert between two oxidation states [Ce(IV)↔ Ce(III)].[6-8] It was envisaged to use cerium nanoparticles for making composite with Co-MOF to further explore their properties. Ceria/MOF

composites were fabricated with the help of wet impregnation method. An aqueous solution of cerium nitrate was introduced into the MOF dispersion followed by the addition of sodium hydroxide that led to the formation of cerium hydroxide. Calcination of the reaction mixture gave of ceria nanoparticles incorporated onto the Co-MOF. Ceria nanoparticles were also synthesized independently using surfactant (CTAB) assisted method for structural comparison purposes. The crystal structures of the synthesized ceria nanoparticles and Ceria/MOF composite were analyzed using powder X-ray crystallography.

X-ray diffraction pattern with 2Θ ranging from 5º-90º for the ceria nanoparticles revealed the formation of pure cubic phase (JCPDS- 34-0394) with space group *Fm*3*m*. The characteristic peaks corresponding to *111, 200, 220, 311, 420* planes were identified at 29.2°, 33.1°, 47.5° and 59.0° (2Θ) using standard data.[9,10] The powder XRD pattern for Ceria/MOF composite overlapped with 2Θ values of bare Co-MOF and pure ceria nanoparticles (Fig.8). Thus, it can be concluded from Fig. 8 that the overall structural framework of Co-MOF after the incorporation of ceria nanoparticles remained intact.

Further structural investigations for CeO_2/MOF composite were carried out using high resolution TEM (HR-TEM). Figure 9a shows dark coloured blocks of ceria nanoparticles against the light background of Co-MOF. A d-spacing distance of 0.4 nm was observed for the nanoparticles (Fig. 9b-c). Additional, SEM images taken along with EDS elemental analysis maps revealed the insight into the chemical composition of CeO_2/MOF hybrid material. The results showed a homogenous distribution of Co, O, C and Ce as the main elements (Fig. 10) with Ce having weight percentage of 4.07.

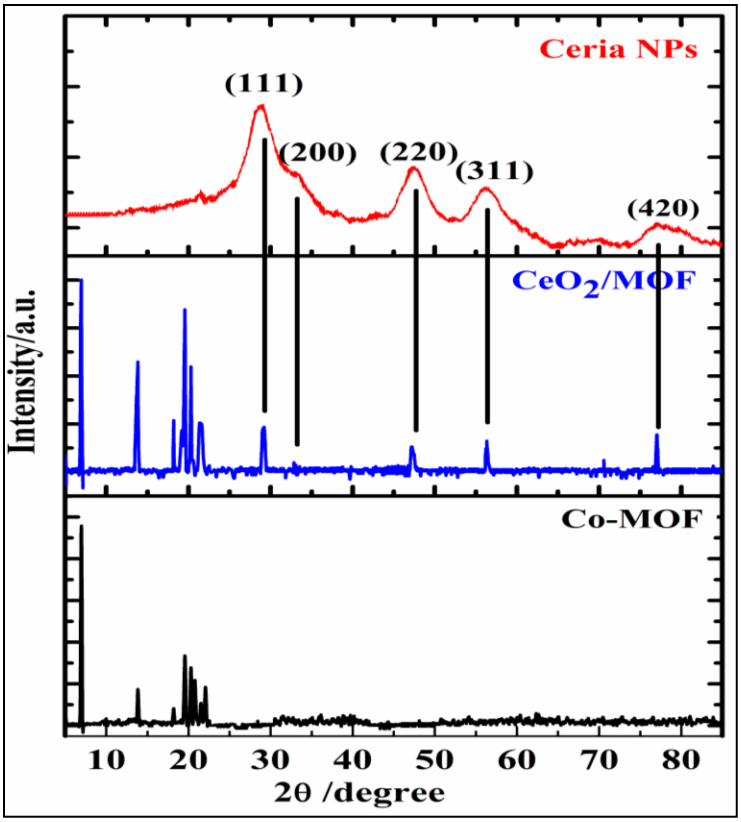

Fig. 8. An overlay showing the experimental PXRD pattern of Co-MOF, CeO_2/MOF and CeO_2 nanoparticles

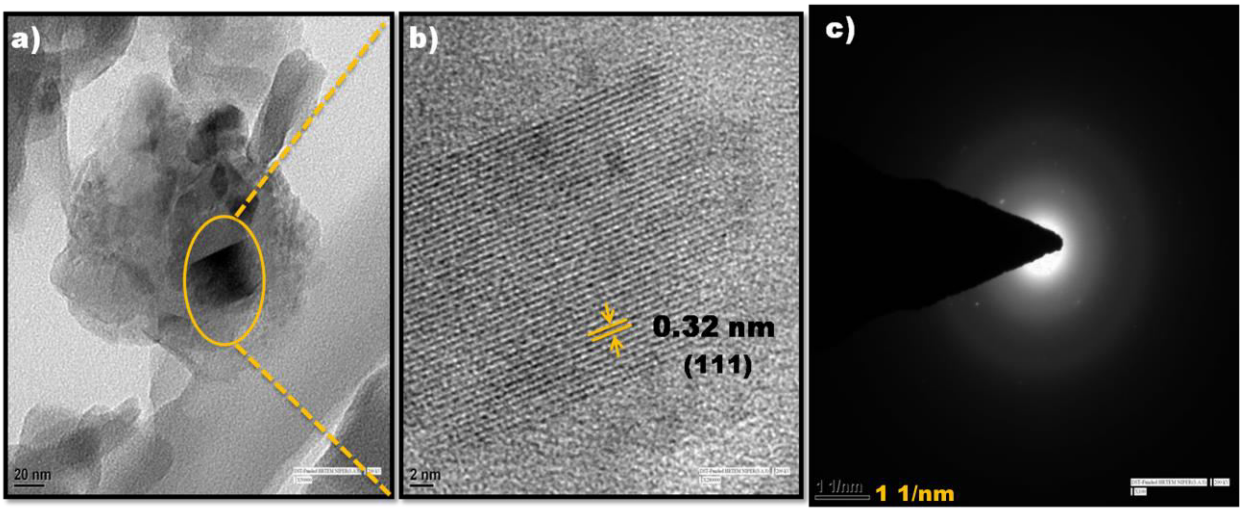

Fig. 9. HR-TEM images of composite material having ceria nanoparticles incorporated onto Co-MOF

In order to investigate the ceria and oxygen species present in CeO_2/MOF composites, XPS measurements were carried out. The peaks for Ce $3d_{5/2}$ and $3d_{3/2}$ were observed at 880.5 eV and

899.3 eV respectively for CeO_2/MOF (Fig. 11a). Similarly, the peak of O 1s appeared at 530.2 eV as seen in figure 11b. The later confirmed the absence of cerium hydroxide as the corresponding peak for O 1s appears at 532 eV.[5] Additionally, binding energies for Co in bare Co-MOF and ceria incorporated Co-MOF (CeO_2/MOF) were compared using XPS. A blue shift of 1 eV in case of CeO_2/MOF (Fig. 12) confirmed the incorporation of ceria nanoparticles into Co-MOF skeleton.

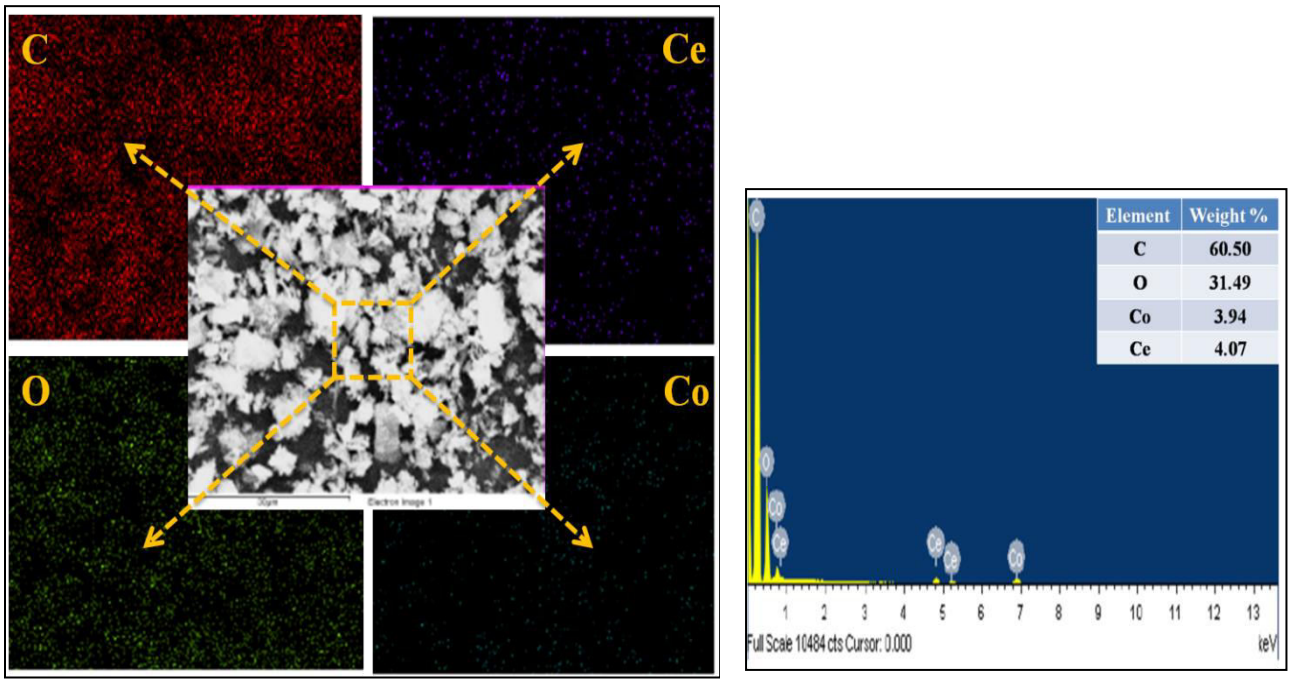

Fig. 10.a) EDX maps showing the presence of the elements C, Ce, Co and O b) EDX spectrum indicating the weight percentages of various elements

This may be attributed to alteration by the incorporation of ceria nanoparticles. Cerium has a tendency to get readily interconverted between the +IV and +III states, hence this shift in binding energy values implies the electron transfer from ceria nanoparticles to the Co-MOF. The changes in the electronic environment of the Co core are believed to be the reason for the enhancement of its electrochemical activity[11] (chapter-4B).

Room temperature Raman studies done onto the CeO_2/MOF revealed a peak at 465 cm^{-1} that was absent in case of bare Co-MOF is attributed to CeO_2/MOF. The peak corresponds to the cubic structured CeO_2 with symmetrical stretching mode of Ce-O_8 vibrational unit. This confirmed successful incorporation of ceria nanoparticles into Co-MOF.[12] The intactness of overall structural framework of Co-MOF was confirmed by the appearance of characteristic peaks of

bare Co-MOF in case of CeO_2/MOF. The broadening of the signals can be attributed to the incorporation of ceria nanoparticles into MOF as suggested by PXRD patterns as well.

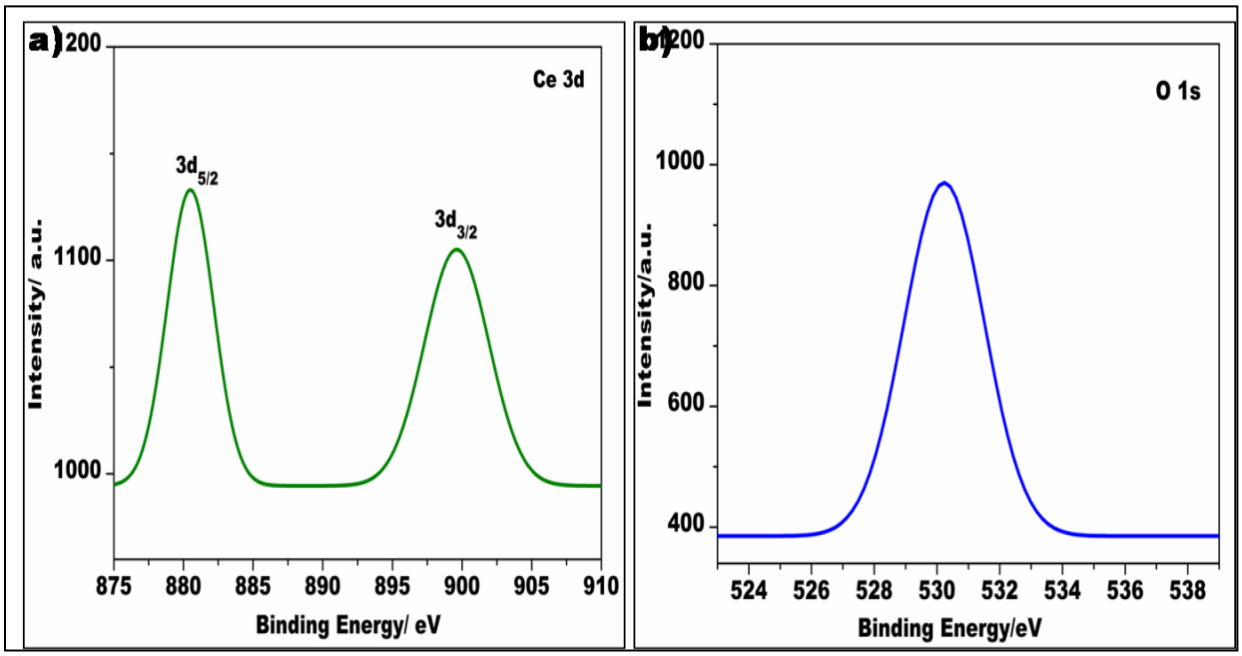

Fig. 11a) Ce 3d XPS spectra of CeO_2/MOF composite b) O 1s XPS spectra of CeO_2/MOF composite

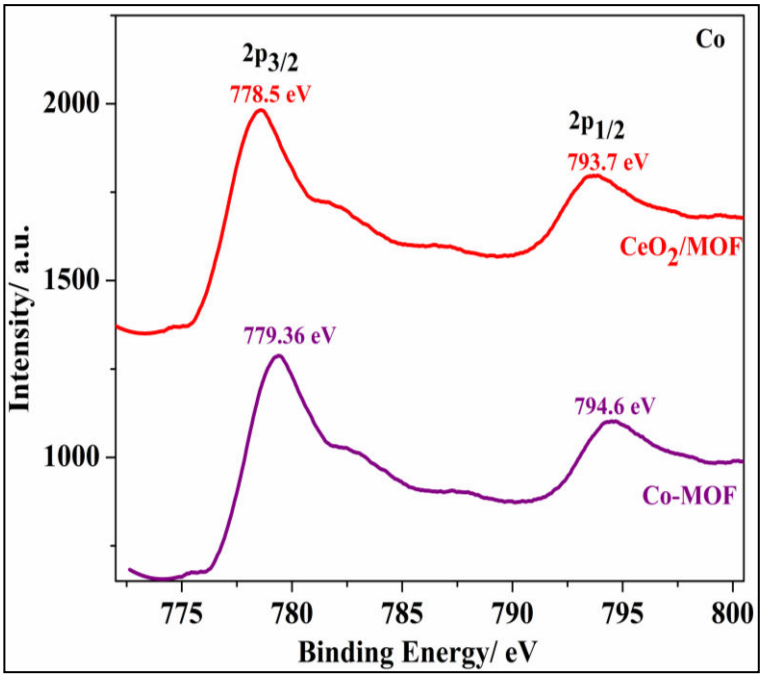

Fig.12.Co 2p XPS spectra of CeO_2/MOF composite and Co-MOF

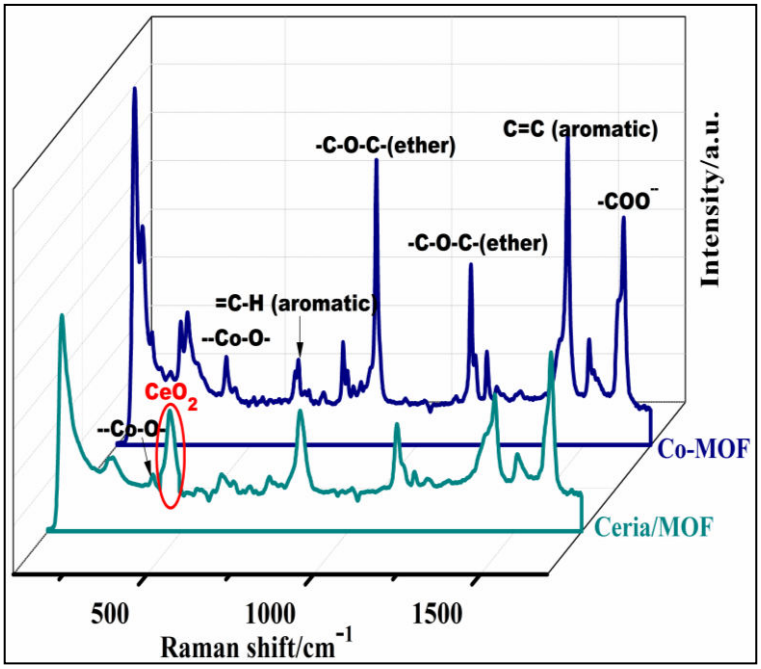

Fig.13. Raman spectra of Co-MOF and CeO_2/MOF composite

CHAPTER-4B

APPLICATIONS OF CO-MOF AND ITS COMPOSITES

Metal organic frameworks are comparatively a new class of hybrid crystalline solids with diverse structural characteristics having organic ligands connected by metal ions or clusters. These materials have shown a variety of potential applications such as heterogeneous catalysis,[13] gas storage,[14,15] drug delivery,[16,17] and molecular sensing.[18-21] The property of luminescence is responsible for various potential applications of MOFs.[22] This includes molecular sensing of the substances that are hazardous to the environment, health and homeland security.[23] Following section describes the use of Co-MOF and its composites synthesized (as described in previous section) for four different applications. This includes the detection of nitro aromatic compounds and pesticides, reduction of nitro aromatics and electrochemical evolution of oxygen from water. While first two applications use bare Co-MOF, the latter two use Co-MOF composites.

DETECTION OF NITRO AROMATIC COMPOUNDS

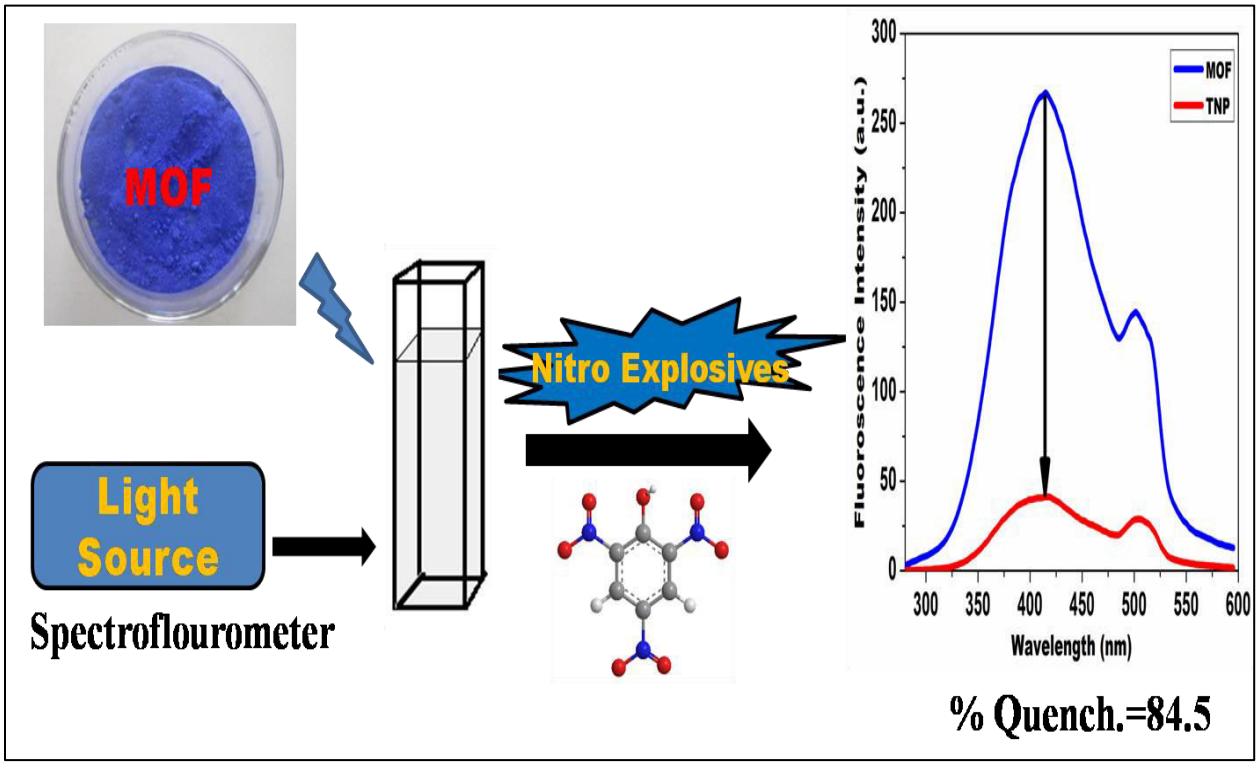

Explosives find their use and misuse in various activities of any state or disruptive forces. The principle ingredient of all the explosives is 2, 4, 6-trinitrophenol (TNP) and 2, 4, 6-trinitro

toluene (TNT). Although TNT is more popular among the two, TNP is more destructive [24] and used in landmines, improvised explosive devices (IED)[25] and many others. [25-27] TNP is also known to causes adverse effects on human heath like skin and eye irritation and respiratory problems.[28] Therefore, the detection of nitro aromatics is of great significance to check their presence, transportation and use. Current explosive detection methods include trained canines[29] or use of high end instruments, such as ion mobility spectrometry (IMS), [30] energy dispersive X-ray diffraction (EDXRD),[31] plasma desorption mass spectrometry (PDMS),[32] surface-enhanced Raman spectroscopy (SERS)[33-35] and various imaging technologies.[36] Although these methods establish high sensitivity and accuracy, they suffer from a number of shortcomings such as high cost, complex functioning and lack of portability. Following work demonstrates the detection of nitro aromatics using Co-MOF by optical method.

Compound **1** when dispersed in water exhibits violet emission at 411 nm due to the intra-ligand transitions (л*→n and л*→ л) of OBA ligands. The excitation has to be done at 255 nm. Attenuation in the luminescence intensity of **1** was observed upon addition of trace amount of nitro aromatics.

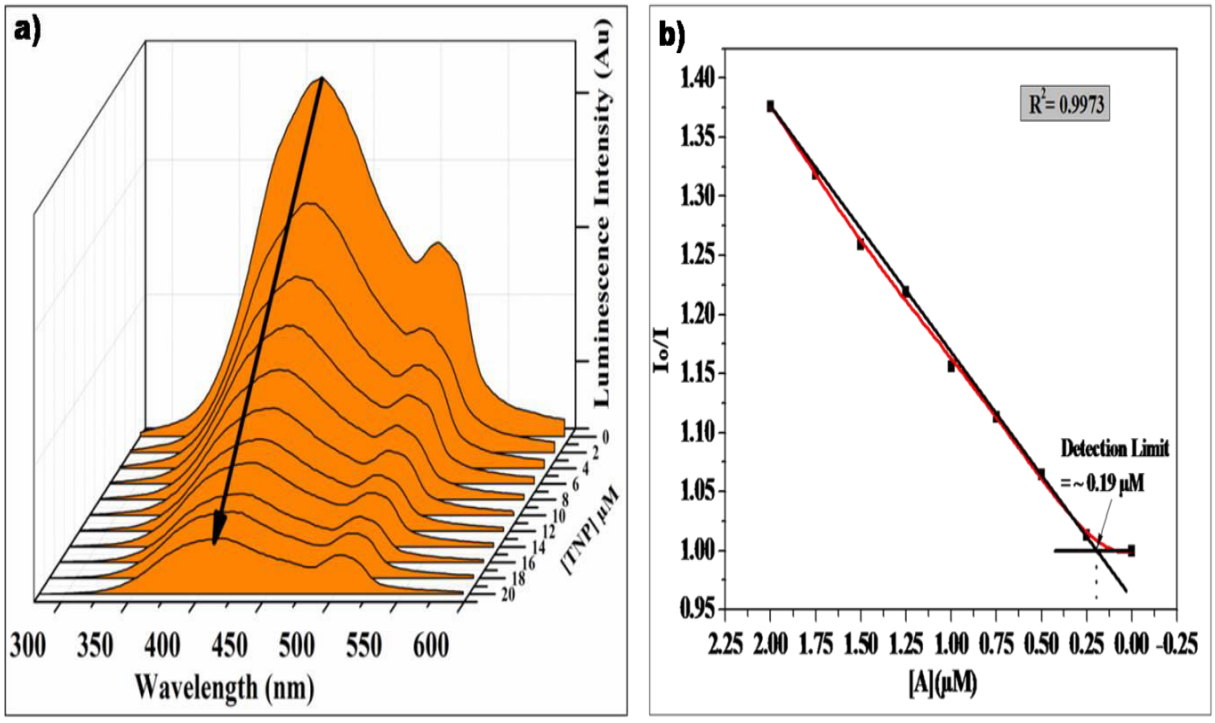

Fig. 14. a) Emission spectra of **1** dispersed in water upon incremental addition of 2, 4, 6-trinitrophenol solution (λ_{ex} = 255 nm). b) Luminescence quenching *vs*. concentration of TNP plot indicating the detection limit (where I_o is the luminescence intensity in absence of analyte and I is the luminescence intensity with incremental addition of TNP)

Compounds shown in Fig. 15 were tested for their ability to quench luminescence. Figure 16 and 17 shows attenuation in luminescence intensity of **1** upon incremental additions of each of the analytes. Among all the nitro aromatic compounds, the response of TNP, a major explosive compound was exceptional. It quenched the emission intensity of **1** to about 84.5% of its initial and could be detected as low as to the concentration of 43 ppb (Fig. 14).

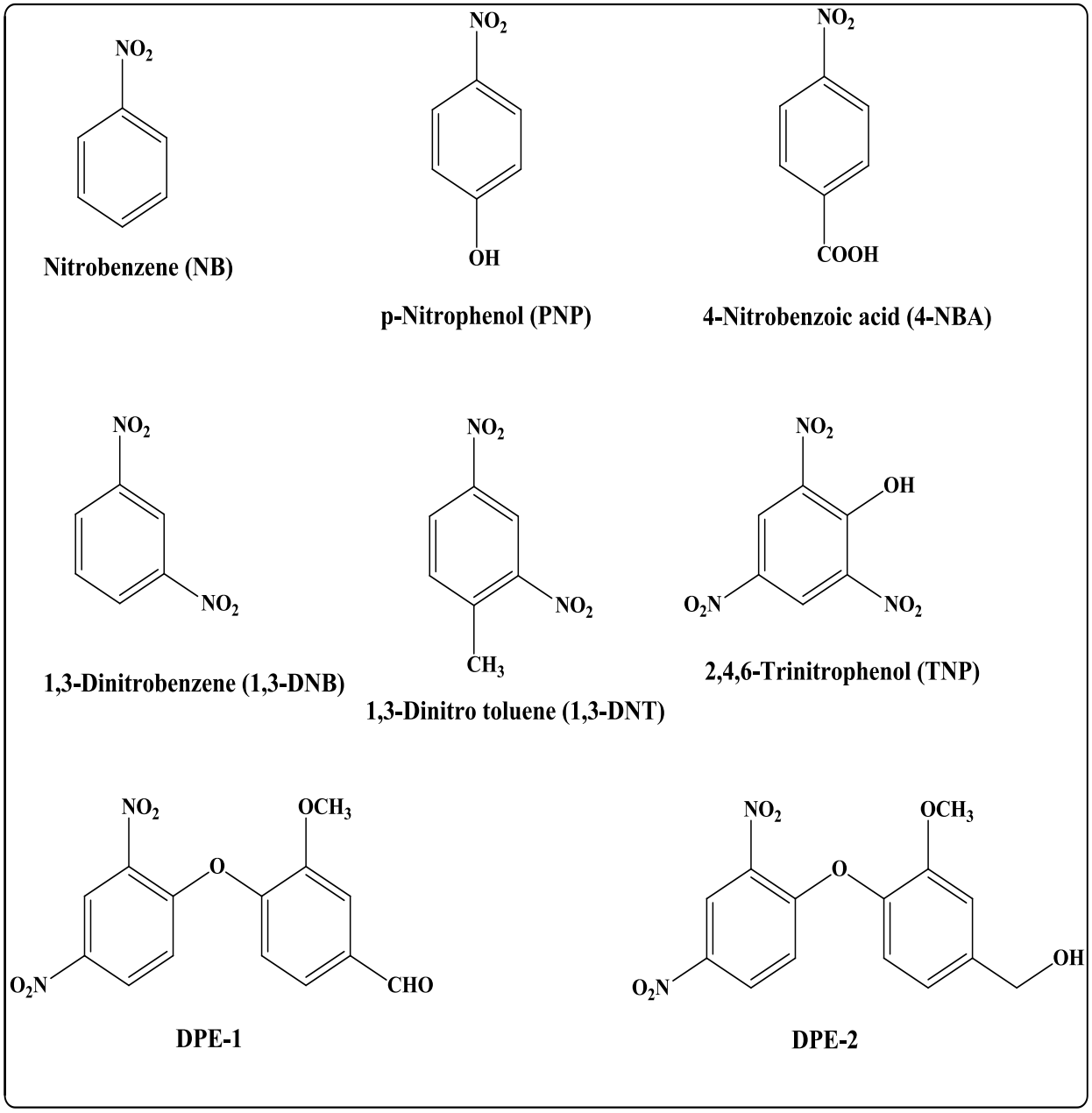

Fig.15. Chemical structures of the nitro aromatic compounds used

The quenching efficiency (%) was estimated using the formula $(I_o - I)/I_o \times 100\%$, where I_o is the fluorescence intensity without the addition of analyte and I being the intensity after the addition of analyte. The quenching efficiency of the analytes after addition of 20 μM is shown in Figure 19 as bar diagram. The quenching efficiency of **1** for other nitro aromatic compounds was found to be as follows: DPE-2 (73.5%), DPE-1(41.6%), 1, 3- dinitrobenzene (1, 3-DNB) (18.8%) and 2, 6-dinitrotoluene (2, 6-DNT) (31.2%). While compounds with single nitro group such as 4-nitrobenzoic acid (4-NBA) (12.6%), nitrobenzene (NB) (2%) and p-nitrophenol (PNP) (8.15%) showed negligible quenching behavior. Benzene and toluene did not any quenching behavior. Thus, it can be concluded that quenching behavior is controlled by the presence of nitro groups on the aromatic ring.

The luminescence quenching efficiency of TNP was analyzed by fitting the experimental data to the Stern-Volmer (SV) equation**,** $(I_o/I) = K_{SV}[A] + 1$, in which I_o and I are the luminescence intensities before and after the addition of analyte, [A] is the molar concentration of the analyte and K_{SV} is the quenching constant. As shown in figure 18, at low concentration (upto 10 μM) of TNP a linear increase in (I_0/I)-1 was observed. With the increase in concentration SV plot diverged from linearity and began to bend upwards in the case of TNP (Fig. 19). The linear variation at lower concentration are mainly due to static quenching, whereas the steep curves at higher concentration are presumably due to dynamic quenching. The static quenching can be accredited due to the ground state interaction between the analytes and the compound **1**. The dynamic quenching is due to the energy and electron transfer processes between the analytes and the compound **1**. Apart from these mechanisms, absorption of excitation light by the analyte itself may also contribute to the quenching effect. Fitting of the linear parts of the plots allow the determination of the quenching coefficients, (K_{SV}) to be $2.30 \times 10^5\ M^{-1}$. The larger observed K_{SV} values correlate to extremely high sensitive systems indicating that **1** is one of the best reported luminescence probe to be used for the detection of TNP.

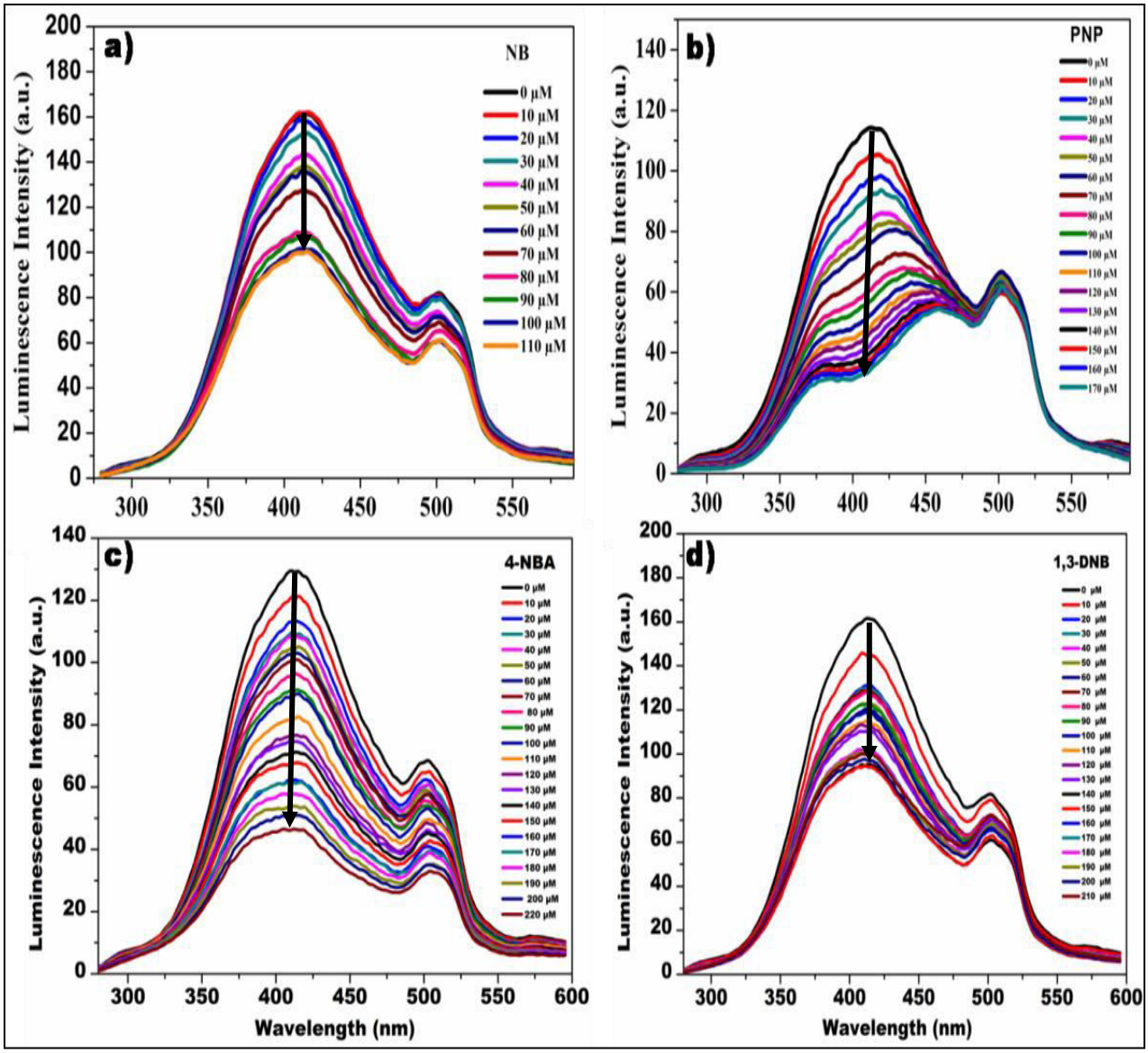

Fig. 16. Emission spectra of 1 (λ_{ex}=255 nm) upon incremental addition of a) Nitrobenzene (NB) b) p-Nitrophenol (PNP) c) 4-Nitrobenzoic acid (4-NBA) and d) 1,3-Dinitrobenzene (1,3-DNB). All the spectra are measured using PerkinElmer LS-45 spectrofluorometer

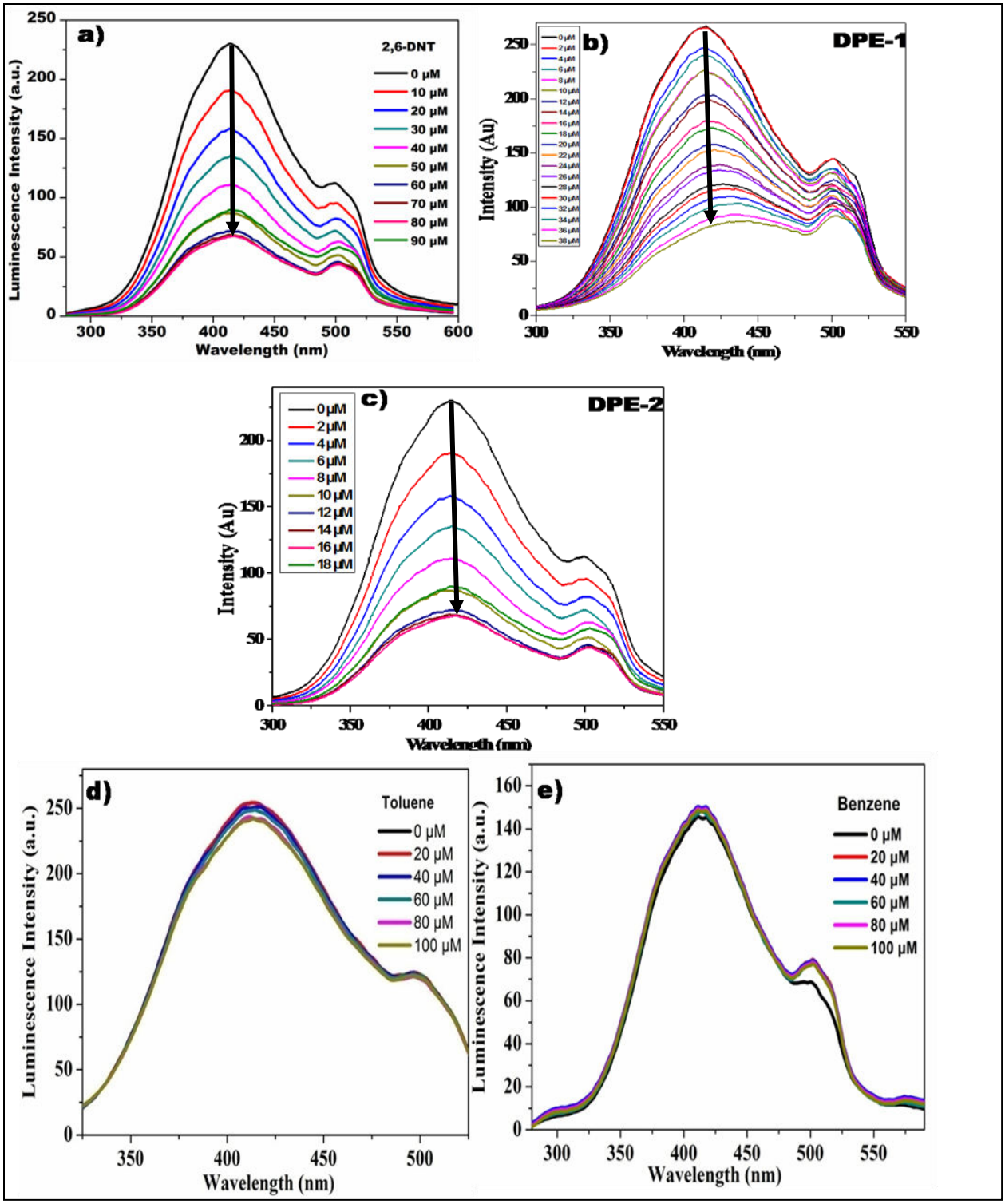

Fig. 17. Emission spectra of 1 (λ_{ex}=255 nm) upon incremental addition of a) 2, 6-Dinitrotoluene (2,6-DNT) b) Diphenyl ether-1 (DPE-1) c) Diphenyl ether-2 (DPE-2) d) Toluene e) Benzene . All the spectra are measured using Perkin Elmer LS-45 spectrofluorometer

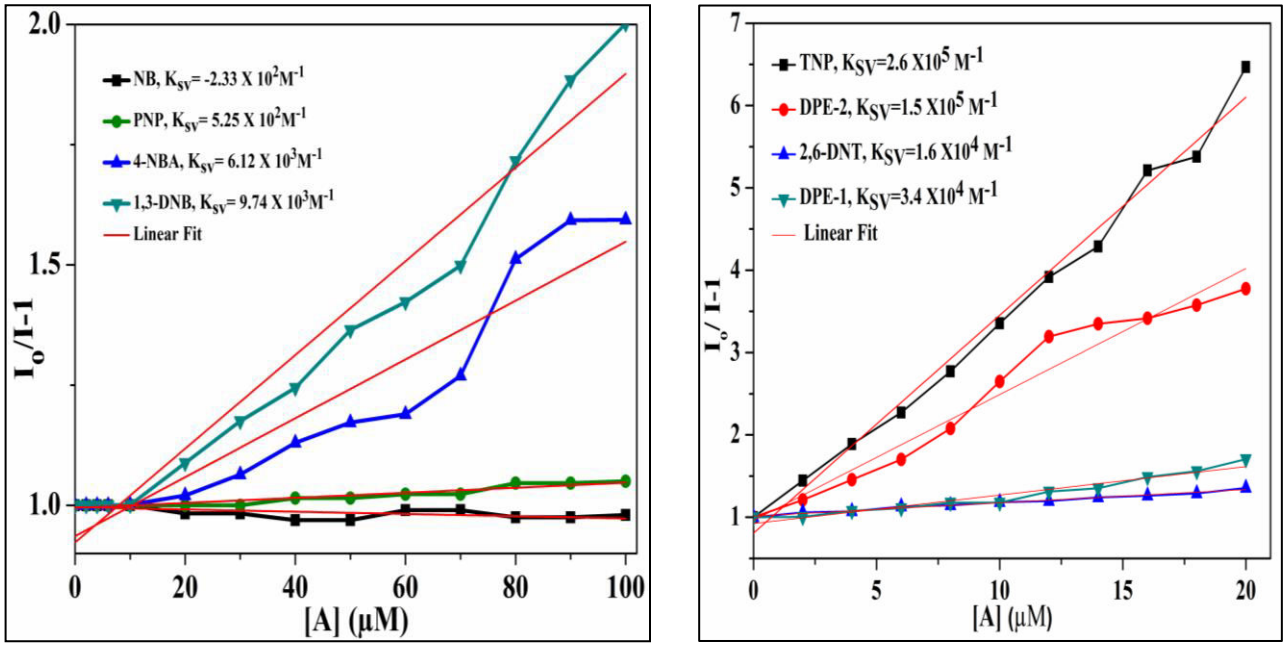

Fig.18. a) Stern-Volmer plot of (I_o/I)-1 (at 411 nm) *vs.* concentration of 1,3-DNB (upto 100 μM). b) Stern-Volmer plot of (I_o/I)-1 (at 411 nm) *vs.* concentration of TNP, DPE-2, 2,6-DNT and DPE-1 (upto 20 μM)

Explaining on the molecular level, the homogeneous dispersible nature of the MOF, **1**, enables molecular interaction between **1** and analytes leading to a significant amount of static quenching. After static quenching, there may be reduction in the amount of energy required to excite the OBA ligands of MOF, which may be due to one of the two possible mechanisms: (i) Absorption of the excitation energy by analytes to compete with OBA ligand, or (ii) Use of excitation energy for the transfer of electron from the ligand excited state to the LUMO of the analytes (nitro aromatics).

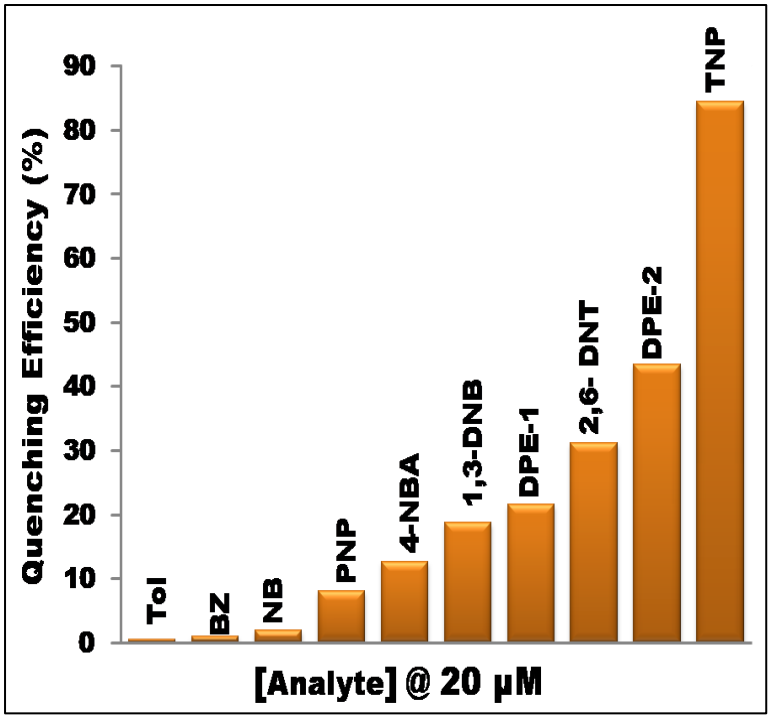

Fig.19. Percentage luminescence quenching at 411 nm of 1 with 20 µM of various nitro aromatics

Nitro aromatic compounds possess a low-lying π*-type LUMO due to electron withdrawing nitro group and its energy falls below the energy of conduction band (CB) of MOF. This leads to quenching effect once the nitro aromatic compound absorbs energy. This description/mechanism is based on the relative orbital energy levels of the coordination polymer and analyte. We also believe that more thoroughly studies are required in order to fully understand the origin of the quenching/enhancement effect.

Table 2: Summary of results for various nitro aromatic analytes

S.No.	Analyte	Quenching Coefficient (K_{SV})	Detection Limit (ppm)
1.	**TNP**	**2.6×10^5 M^{-1}**	**0.043**
2.	**DPE-2**	**1.5×10^5 M^{-1}**	**0.64**
3.	**2,6-DNT**	**1.6×10^4 M^{-1}**	**1.09**
4.	**DPE-1**	**3.4×10^4 M^{-1}**	**1.12**
5.	**1,3-DNB**	**9.74×10^3 M^{-1}**	**1.27**
6.	**4-NBA**	**6.12×10^3 M^{-1}**	**1.31**
7.	**PNP**	**5.25×10^2 M^{-1}**	**1.39**
8.	**NB**	**-2.33×10^2 M^{-1}**	**1.23**

DETECTION OF ORGANO PHOSPHATE PESTICIDES

The use of pesticides in agricultural sector followed by their seepage into soil is a big environmental concern nowadays. These harmful chemicals contaminate the water table and find a way to enter food chain due to the use of same water to fulfill daily human needs. On molecular level, most of the organophosphorous pesticides owe their toxicity to irreversibly bind the serine residue of acetylcholinesterases (AChE); [37] that is responsible for transmitting nerve impulses to the brain. Higher dosage or repeated exposure leads to neurodenegerative diseases. Thus, there is a need to detect these pesticides accurately in the systems and take necessary measures.

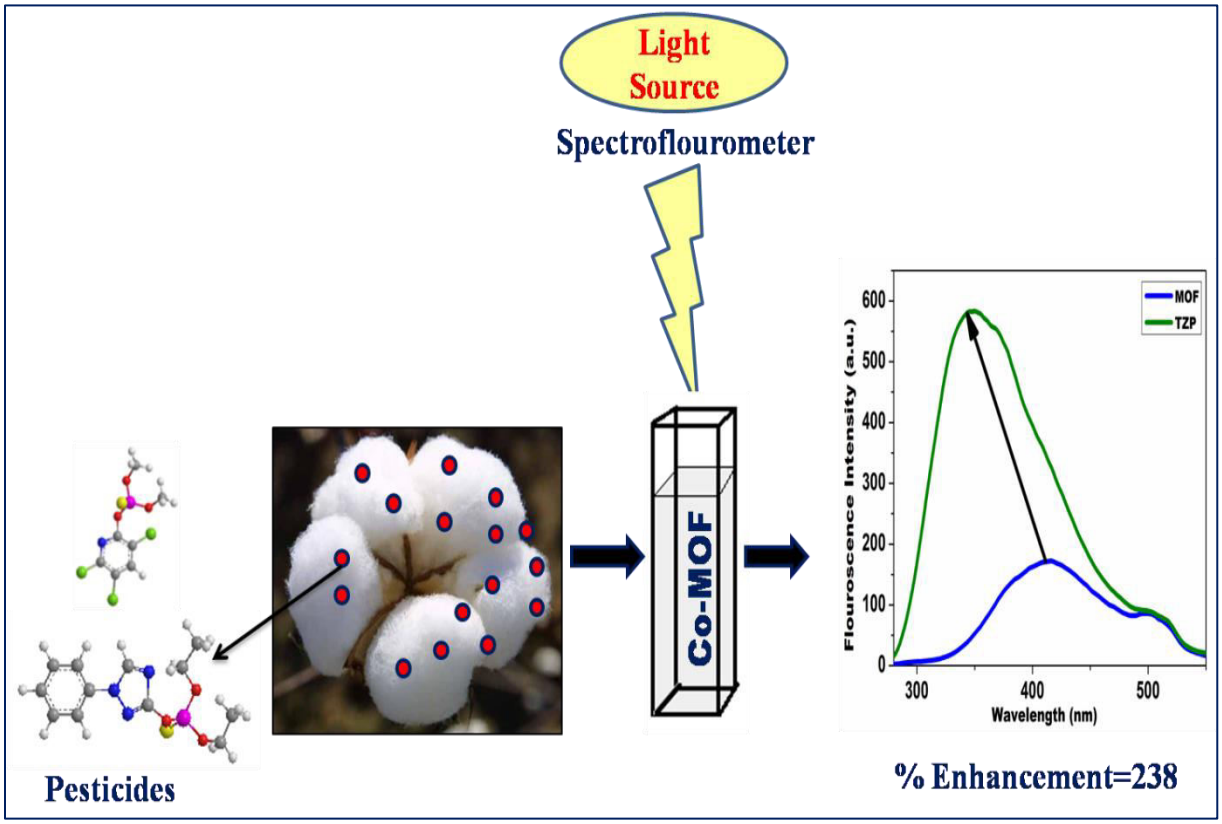

Gas chromatography (GC), [38-39] high performance liquid chromatography (HPLC) [40-41] and mass spectrometry[42] are routinely used techniques for the detection of such compounds. However, optical methods are more convenient due to their low cost, portability and ease of use. It was thus, envisioned to use Co-MOF for the detection of pesticides.

Four commercially available organophoshate pesticides, triazophos (TZP), chlorpyrifos (CPF), acephate (ACP) and malathion (MAL) were chosen for the study. Among all the organophosphorous pesticides, former two are aromatic while the later two are aliphatic (Fig. 20). Initial studies with all the four pesticides displayed that their aromatic nature induces the "turn-on" behavior while the aliphatic ones did not show any change in luminescence intensity.

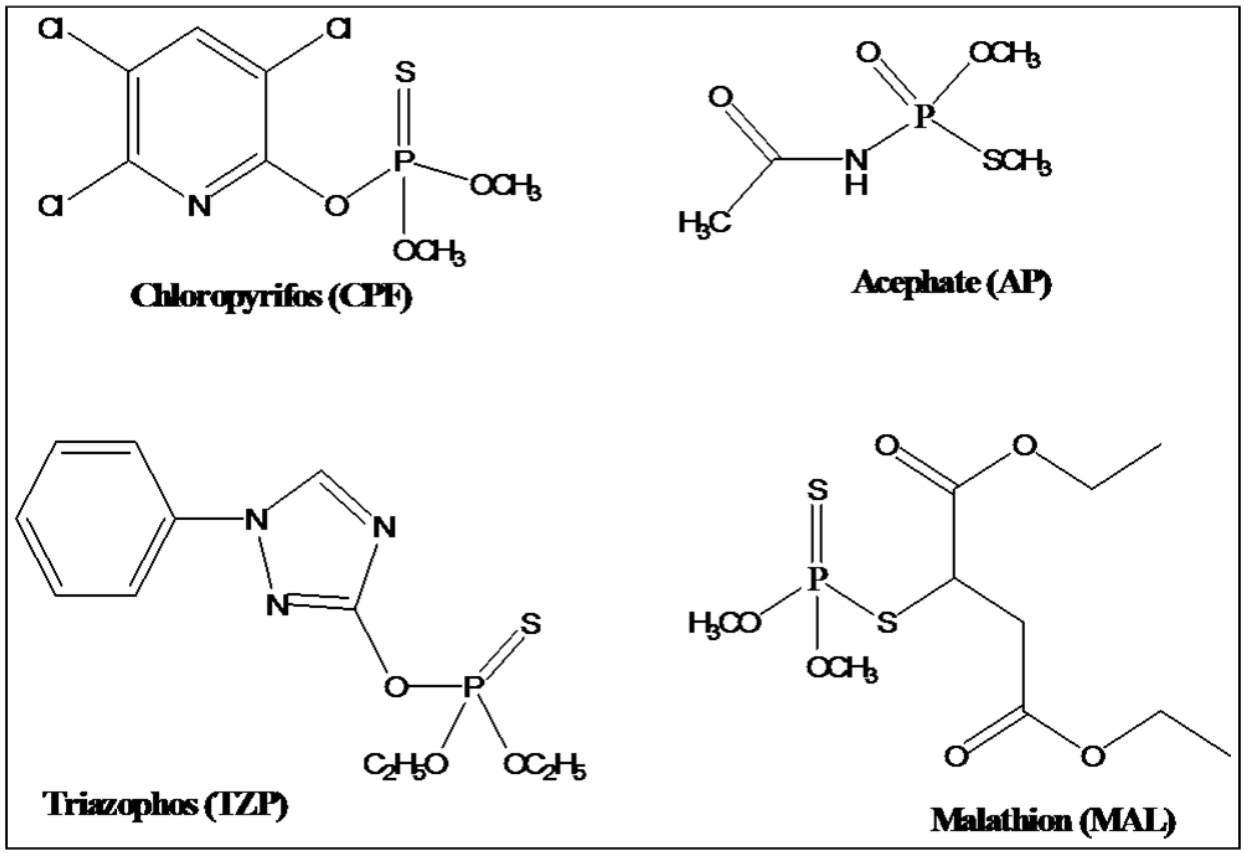

Fig. 20. Chemical structures of the aromatic organo-phosphorous pesticides (chloropyrifos and triazophos) and non-aromatic organo-phosphorous pesticides (acephate and malathion)

"Turn-on" phenomenon refers to evolution of a new peak from a blank background or increase in emission intensity due to the addition of analyte in the visible region. In this case, the selective binding of aromatic organo-phosphorous pesticides (guest) with CO-MOF (host) induces an increase in the emission of generally low emitting host. The observed luminescence turn-on behavior can be understood on the basis of acceptor-donor electron transfer mechanism (Fig. 21a). MOF, **1**, that has an extended network like structures (Fig.2) possess narrow energy bands because of highly localized electronic states and their valence band (VB) and conduction band

(CB) can be treated similar to that of molecular orbitals (MOs).[43] In case of electron rich aromatic pesticides such as CPF and TZP, LUMO have higher energy than CB of MOF. Hence when excited electrons are transferred from LUMO to CB of MOF, luminescence intensity is enhanced.

Fig. 21 b shows that triazophos shows luminescence turn-on behavior along with a red shift of about 70 nm. Chlorpyrifos however, also show turn-on behavior but without any shift (Fig. 22). The emission intensity of **1** increased to 238% of its initial intensity in case of TZP while 29% in case CPF in presence of 10 µM solution. On the other hand, two non-aromatic organophosphate-acephate and malathion did not show any change in emission intensity (Fig.22).

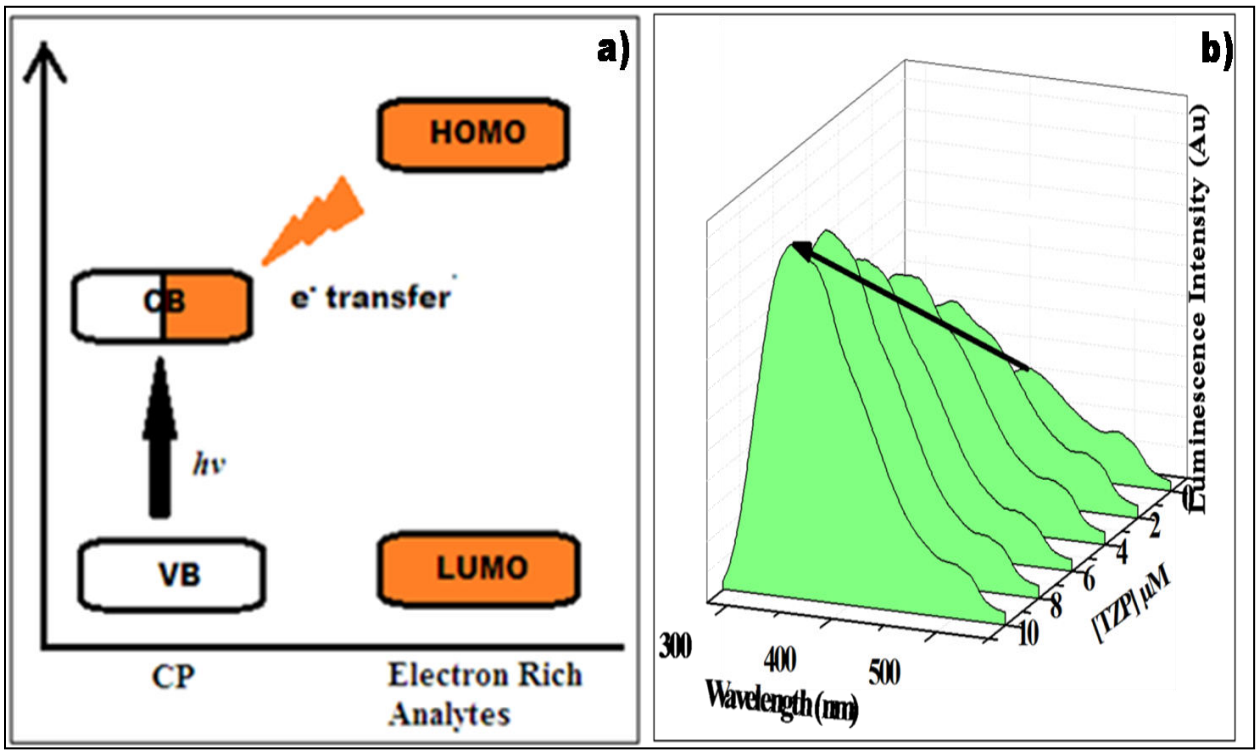

Fig. 21a) Schematic representation of photoluminescence turn-on behavior b) Emission spectra of **1** dispersed in water upon incremental addition of Triazophos solution (λ_{ex} = 255 nm)

The turn-on effect for TZP and CPF is mainly due to the presence of aromatic ring in their structure that increases electron donating effect of the pesticides. The luminescence turn-on behaviour for these two pesticides in water medium could be detected at a concentration as low as 0.62 and 0.7 ppm respectively for TZP and CPF.

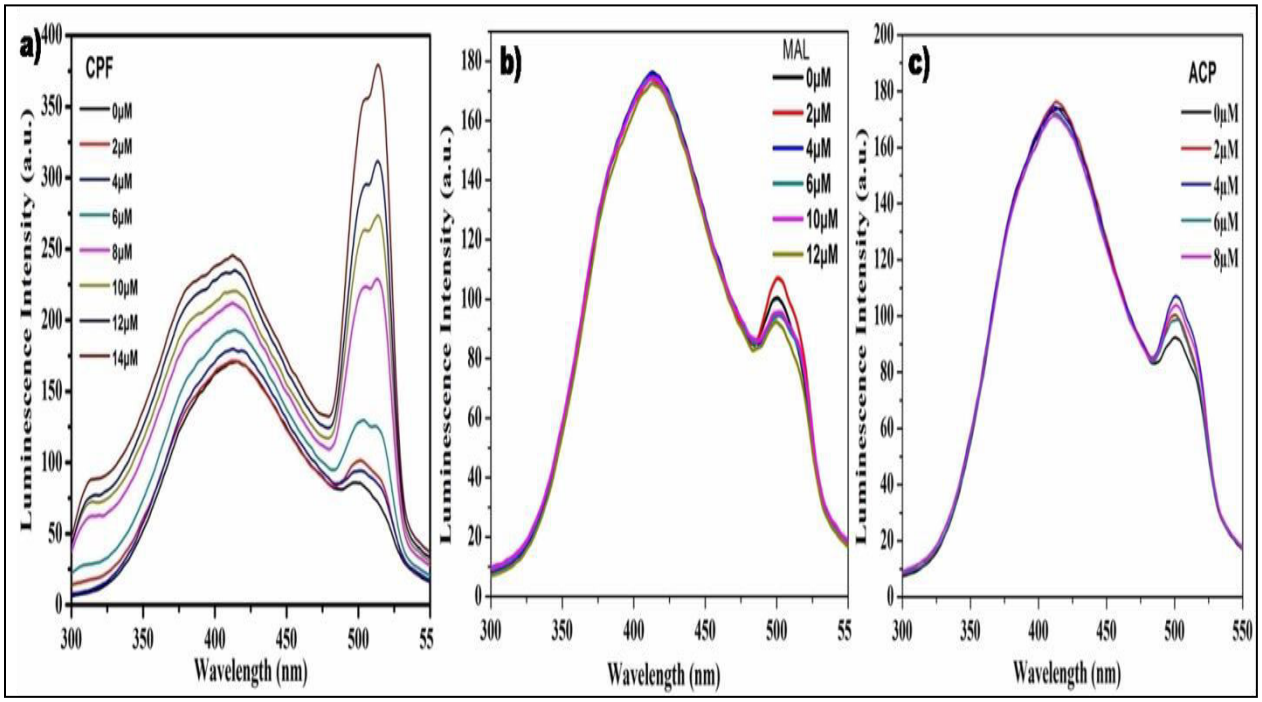

Fig. 22. Emission spectra of **1** dispersed in water upon incremental addition of a) Chlorpyrifos (CPF) b) Malathion (MAL) c) Acephate (ACP) (λ_{ex} = 255 nm)

It has been observed that more is the electron donating capacity of the analyte, more is the luminescence enhancement. TZP which possess an additional triazole ring shows more enhancements in the luminescence intensity as compared to the CPF whereas MAL and ACP showed no change in luminescence behavior of CP due to the absence of aromatic behavior. Thus, the present work demonstrates the ability of MOF (**1**) to selectively detect aromatic organo-phosphorous pesticides that can be useful in various poisoning and contamination related issues.

CATALYTIC REDUCTION OF NITRO AROMATIC COMPOUNDS (NACs)

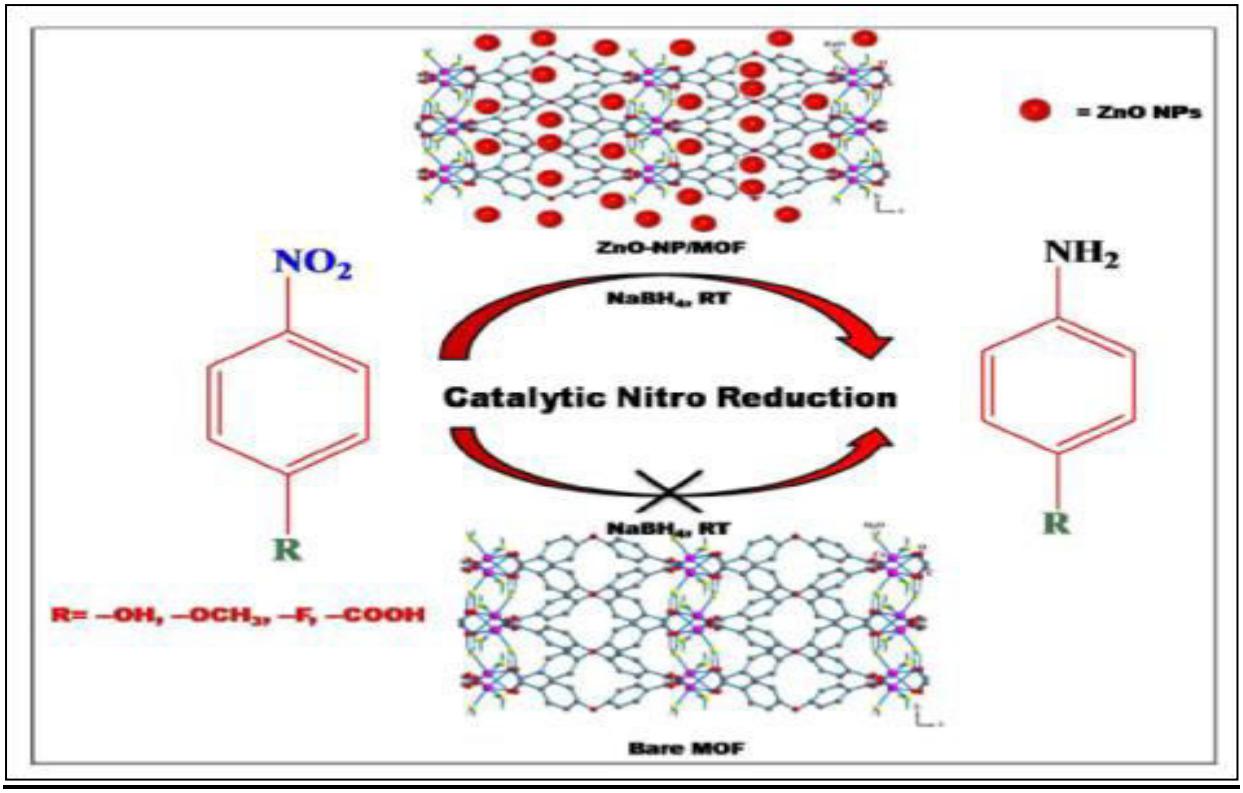

The application of nanoscience in diverse areas has led to a new revolution in the scientific society.[44-48] But the synthesis of nano particles has often been considered a herculean task due to lack of control on size distribution, possibility of agglomeration and low thermodynamic stability.[50] It is a well known fact that there is an onset of new physico-chemical properties as the particles enter the arena of nanometer range such as quantum-confinement effect and spectacular increase in the surface area of the materials.[49]. Therefore, to conserve and access such properties, there is a need of using some stabilizing agents or porous materials like silica,[51] zeolites,[52,53] alumina[54,55] and polymers[56] which can help in hampering their agglomeration and can also provide size confinement effect. Recently, metal organic frameworks (MOFs) are being used as potential candidates for incorporating or supporting nanoparticles due to their porous nature. Metal organic frameworks are basically coordination polymers comprising of metal nodes connected through mono to multidentate organic ligands which offer a wide room for their structural diversity. They have the highest surface areas[57- 59] reported till date as compared to other porous materials and large internal pore volumes with well defined pore sizes and

apertures. The cavity of a MOF not only provides a size limiting effect but also greatly helps in enhancing the thermal stability of NP whereas the NP helps to enhance the catalytic activity of the resulting composite. This synergistic effect provides them an edge over the other materials belonging to the related class.

Different methods have been reported for the synthesis of such composite materials. This includes wet impregnation,[60] chemical vapor deposition (CVD) method (commonly used for volatile precursors),[61,62] solid/mechanical grinding[63] and microwave assisted methods. During last few years, a number of noble metals such as Au,[64] Ag,[65] Pt,[66] Pd,[67] Ru,[68] have been reported to be embedded into the cavities of various MOFs with an aim of inducing or improving the catalytic,[69] magnetic[70] and electrochemical properties.[71] But the exorbitant cost of precursors and low shelf life of metal NPs pose a limitation to their wide use in various fields. To overcome this, the use of non noble metal or semiconductor NPs is widely encouraged. There are very rare examples in the literature where the use of semi conductor NPs is reported for such purposes hence there is a great need to explore this untrodden approach.

The reduction of nitro aromatics to the corresponding amines is one of the important organic reactions as many aromatic amines show biological properties and are profoundly used in dye and pharmaceutical industry.[72,73] Numerous methods can be found in the literature for the conversion of nitro compounds, such as catalytic hydrogenation[74] and metal-mediated reduction using Raney Ni, Pd/C etc.[75,76] but high cost and insufficiency of such metals are the major limiting factors for their large scale applications. Conventional methods using zinc metal usually employ harsh reagents such as NH_3, conc. HCl, aq. NaOH, elevated temperatures, prolonged reaction times and sometimes use of large portions of zinc metal. Some methods in an aqueous medium has also been reported to use 7.25 equiv. of zinc metal at 80°C.[77] On the other hand, modern day methodologies depend largely upon the use of nano-structured catalysts. Grirrane *et al*[78] achieved the reduction of nitro arenes by employing gold nanoparticles. However, the methods used high pressured hydrogen and elevated temperatures which make it an unfavourable approach due to safety issues. Therefore, employing nanoparticles loaded MOF for the reduction of nitro aromatics to their corresponding amines under ambient conditions was thought to be a logical approach.

Herein, we report the successful deposition of ZnO nanoparticles on a Co based MOF, $[Co(OBA)(H_2O)_2]$, **1**, used as a host matrix using wet impregnation method. The prepared

composites had different ratios of ZnO and behaved as efficient heterogeneous catalysts for the reduction of nitroarenes at ambient conditions. Size and shape of the resulting NPs were dominated by the metal loading ratios. To the best of our knowledge, this work presents the first report where the ZnO NPs incorporated with MOF, are behaving as an efficient catalyst without using any UV source that too under ambient conditions.

The reactions were performed at room temperature and were investigated primarily with the help of UV-Vis absorption spectroscopy (Fig. 24a) and confirmed by HPLC (Fig. 24b). Bare Co-MOF, ZnO nanoparticles and sodium borohydride alone were found incapable of causing the desired organic transformation reaction (Fig. 25). However, presence of ZnO loaded MOF as a catalyst facilitated the reduction at room temperature. A catalyst helps to overcome the kinetic barrier of reduction process to support the electron transfer chain.[79] This indicates that the synergistic effect of ZnO NPs and Co-MOF is playing a role for making the desired reduction reaction feasible.

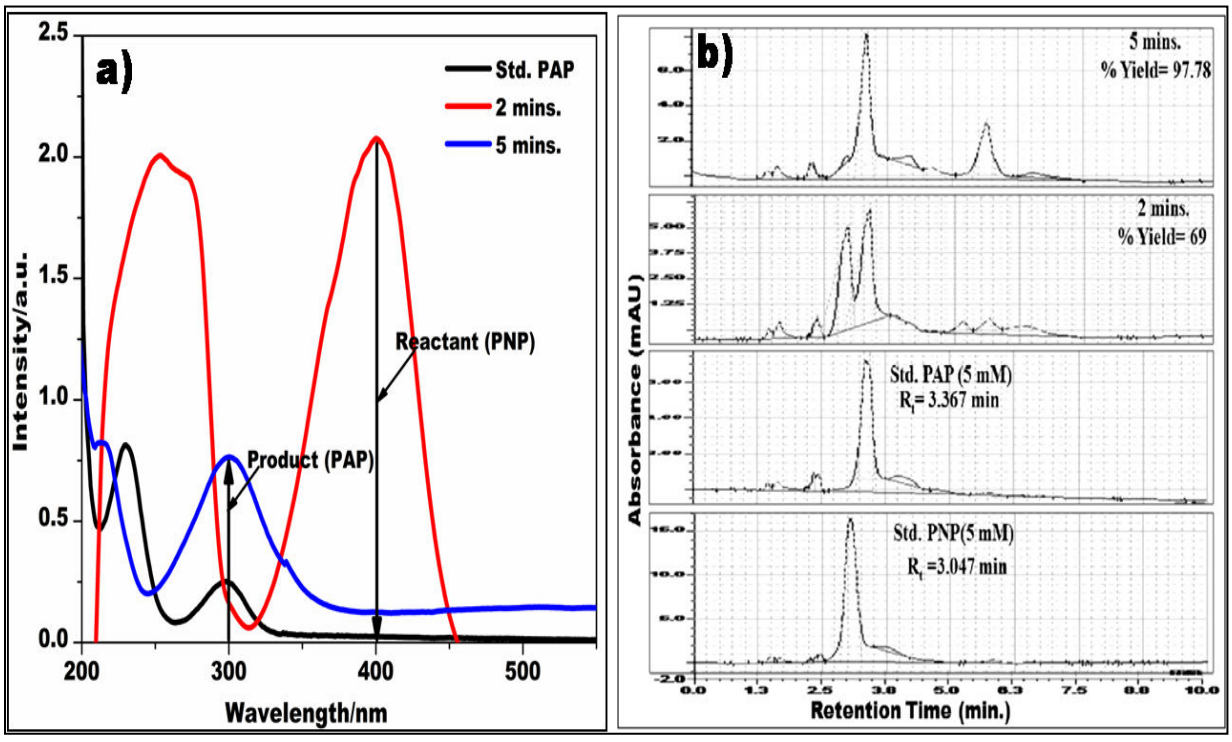

Fig. 24. An overlay of a) UV-Vis spectra and b) HPLC chromatograms for the catalytic reduction of p-Nitrophenol solution (5 mM) using ZnO/MOF-I indicating the respective % yields and the duration of reaction

The addition of $NaBH_4$ to the solution of PNP causes the peak of PNP (λ_{max} = 293 nm) to be red shifted due to the formation of phenolate ion (λ_{max}= 400 nm). Figure 24a shows the typical UV-Vis absorption spectra for the reduction of PNP. Followed by the addition of ZnO/MOF-I catalyst to the reaction mixture, the peak at 400 nm vanished and a new peak in the blue region appeared due to the corresponding amino compound (λ_{max}=300 nm). This was confirmed by

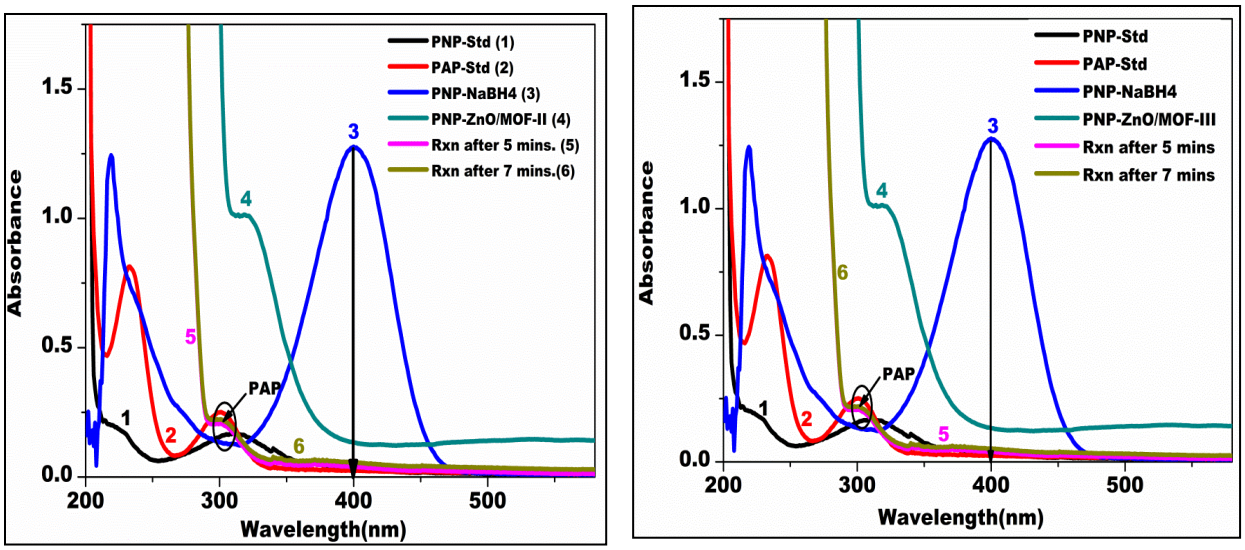

Fig.25. Absorption spectra for the catalytic reduction of p-Nitrophenol solution (5 mM) using three different composites : a) ZnO/MOF-II and b) ZnO/MOF-III

superimposing the spectrum of the pure amino compound under identical conditions as shown in Fig. 25. However, no change in the UV-Vis absorption was observed when PNP reacted with $NaBH_4$ in the absence of ZnO doped MOF or with ZnO/MOF-I catalyst alone in the absence of reducing agent. The reaction mixture was filtered using Millipore filter (pore size 0.22 μm) to separate the heterogeneous catalyst before analyzing the samples using UV-Vis spectrophotometer and HPLC (Fig. 24a and 24b).

The products were further quantified using HPLC [Fig.1-8 (Annexure-1)]. Fig. 24b shows the HPLC chromatogram indicating the progress of reaction (catalytic reduction of PNP) showing the % yields or % conversion, which was calculated using the general equation:

$$\% \text{ Yield} = [(A_0 - A_t)/ A_0] \text{ X } 100$$

where, A_0 = Initial Absorbance and A_t = Absorbance at any particular time

Time course studies revealed that the reaction mixture composition remained constant after 5 minutes indicating the completion of reaction using ZnO/MOF catalyst. The percentage conversion from PNP to PAP was highest in case of ZnO/MOF-I (97.78%) and lowest in case of ZnO/MOF-III (70.6%) (Table 4). This can be attributed to the increased surface area of ZnO NPs in case of ZnO/MOF-I due to their very small size.

Encouraged by the good results, reduction reactions of few other nitro aromatic compounds with different substituents such as methoxy, hydroxy, carboxylic acid, and fluoro (Table 4) were also studied successfully. Figure 26 shows the comparison of percentage conversion of all the reduction reactions using the three different composites. The reaction times, yields as calculated from HPLC analysis and rate constants have been summarized in Table 4.

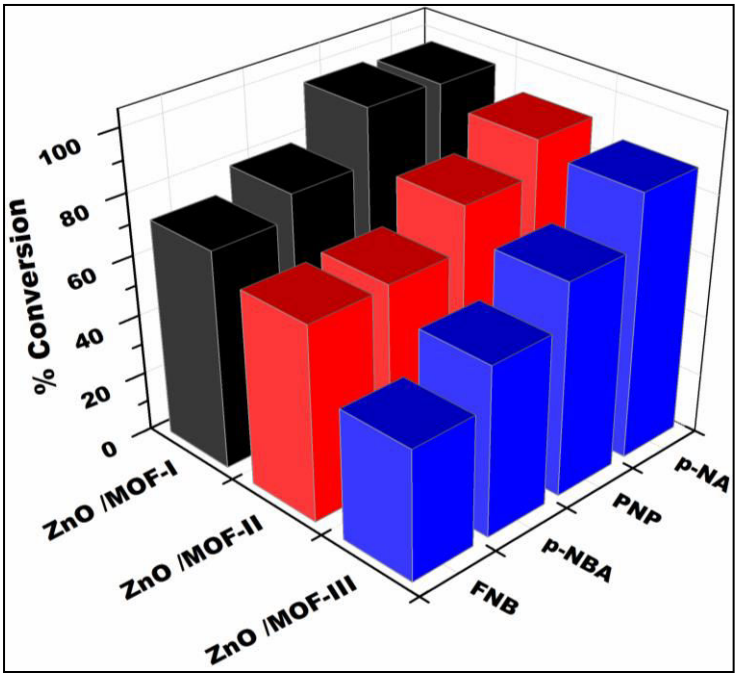

Fig. 26. Bar diagram summarizing the comparison of % conversion for all the three different composites

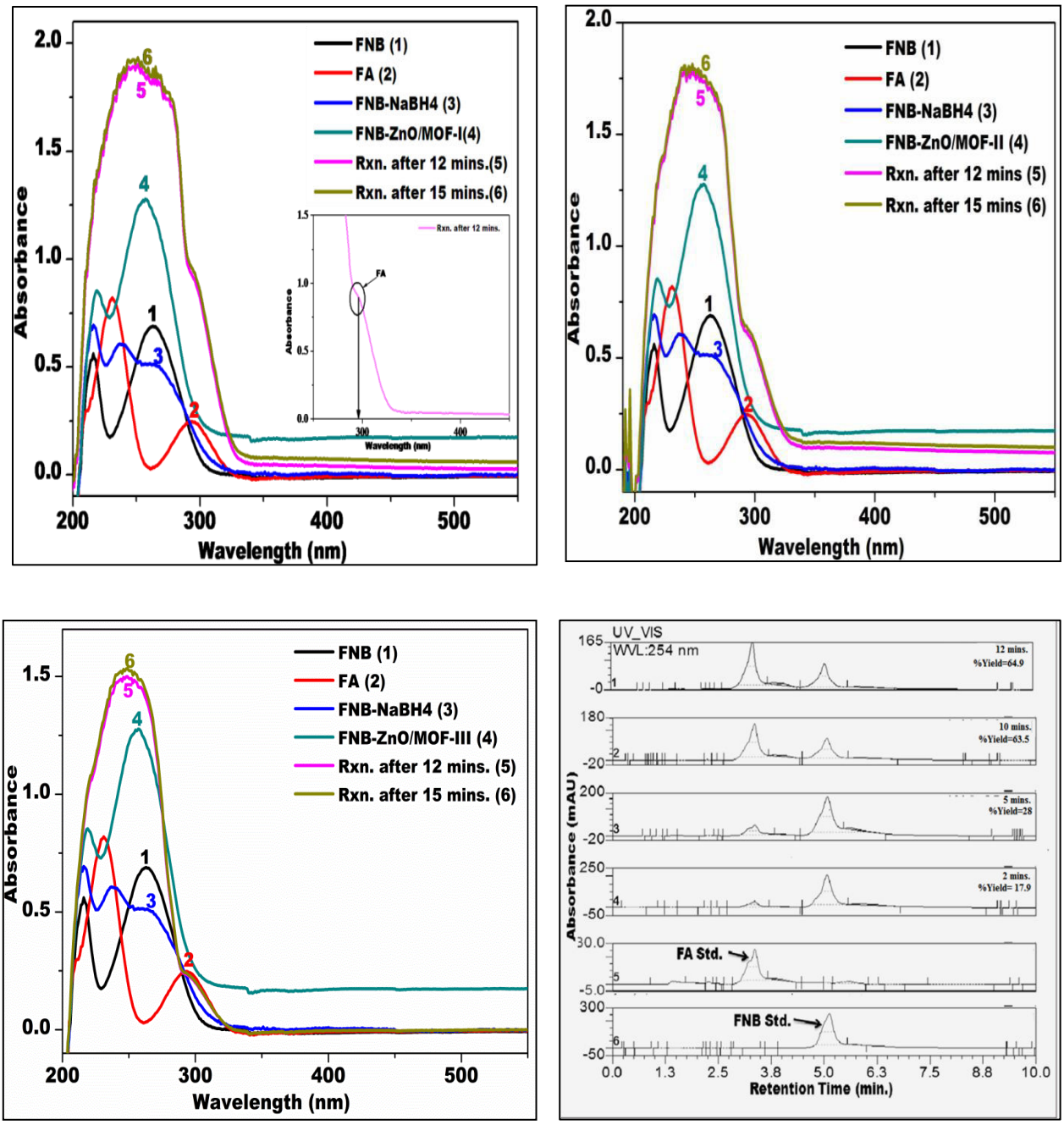

Fig.27. Absorption spectra for the catalytic reduction of 4-Flouro nitrobenzene (FNB) solution (5 mM) using a) ZnO/MOF-I, b) ZnO/MOF-II and c) ZnO/MOF-III d) An overlay of HPLC chromatograms for the catalytic reduction of 4-Flouro nitrobenzene solution (5 mM) using ZnO/MOF-II indicating the respective % yields and the duration of reaction

In order to understand the mechanistic details of the catalytic reduction, reduction of FNB was chosen as model reaction due to the longer duration of reaction as compared to the reduction of PNP. Moreover, the clear UV-Vis absorption spectrum due to non-overlapping peaks of both the reactants and products as opposed to the case of p-nitro benzoic acid and p-nitro anisole made it

a logical choice for such studies. The reactants were added in different sequences as given in table 3 and the impact was observed with the help of UV-Vis spectroscopy (Fig. 28). The reduction reactions were found to occur only according to sequence no-1 and 2 (Table-3). This observation proposed the formation of an intermediate complex that facilitates the reduction reaction between catalyst and the substrate. The reaction did not take place in the cases, where reducing agent was added without catalyst and the substrate forming a complex (Table-3, sequence no 3 to 6). Therefore, it can be concluded that the catalyst mediates the reduction process due to efficient adsorption of substrate (aromatic nitro compound) over the surface of catalyst. The reason behind adsorption is π- π stacking interactions between the nitro arene and the organic ligand of the MOF. This leads to the accumulation of substrate near the interface of ZnO NPs and MOF followed by the reduction by hydride ion from $NaBH_4$.

Table 3: Summary of order of addition of substrates for the catalytic reduction of 4-fluoro nitro benzene (FNB)

Sequence	Order of Addition			
	First	**Second**	**Third**	**Result**
1.	FNB	Cat.	$NaBH_4$	√
2.	Cat.	FNB	$NaBH_4$	√
3.	FNB	$NaBH_4$	Cat.	-
4.	$NaBH_4$	FNB	Cat.	-
5.	$NaBH_4$	Cat.	FNB	-
6.	Cat.	$NaBH_4$	FNB	-

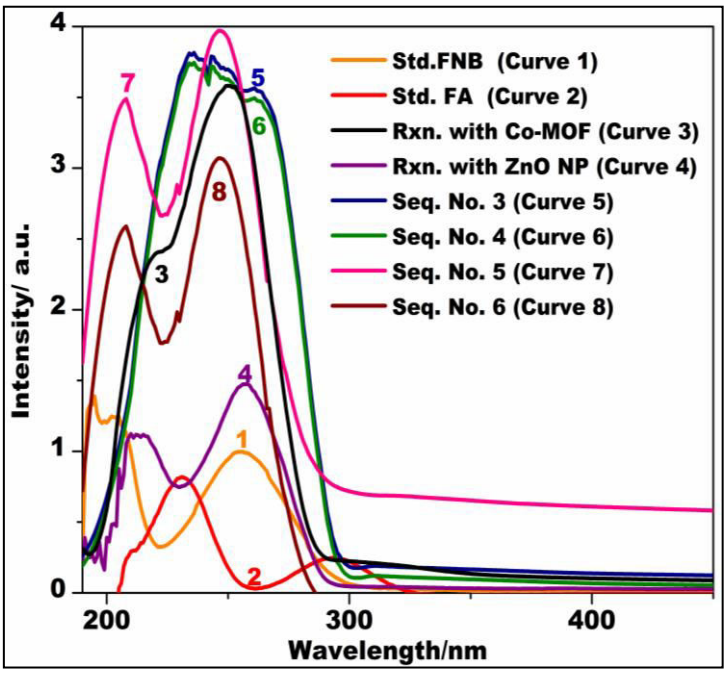

Fig. 28. UV-Vis spectrophotometric studies for showing the effect of order of addition of substrates for catalytic reduction of 4-fluoro nitro benzene (FNB) using ZnO/MOF-I as catalyst

Kinetics of the catalytic reductions was evaluated in terms of rate constants (Fig. 29). Plots of -ln (C/C_o) were drawn against time (t). Slopes of the straight lines were used to calculate rate constant values. Reaction kinetics during the initial period up to 180 seconds were considered for these plots, as the reaction kinetics tend to change after initial reaction and hence were not considered for the rate constant calculations. All the reactions were repeated five times as indicated by error bars in Fig. 29. It can be concluded that all the reduction reactions followed first order kinetics as indicated by linear plots for all the three catalyst. The observed results are in good agreement with the known fact that the catalytic property is dependent on its particle size. Smaller is the particle size, larger is the surface area with which it can interact with the reactants, hence greater is the catalytic activity.[80-83]

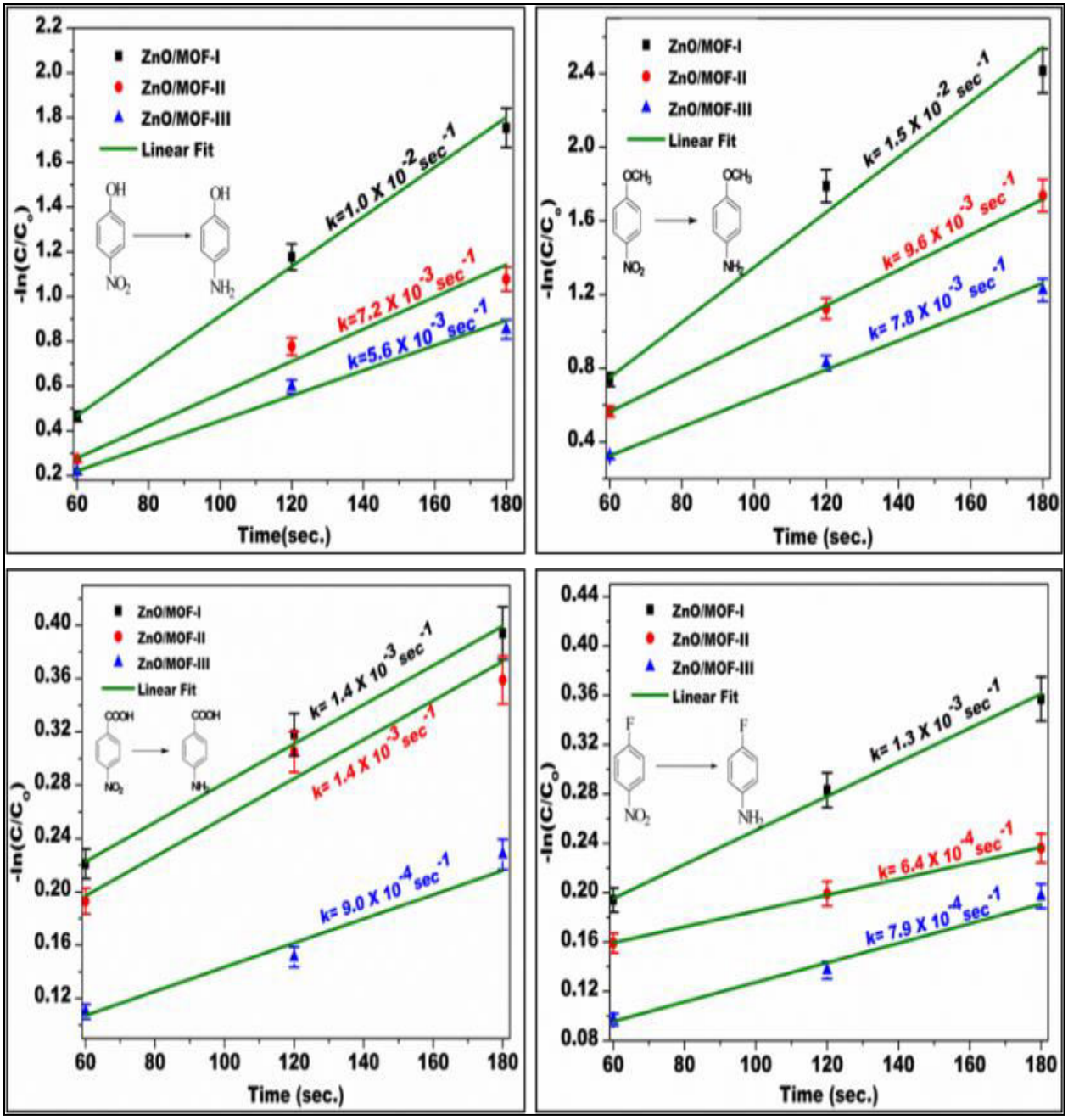

Fig. 29. Time course graph of reduction of (a) FNB (b) NBA (c) PNP & (d) NA [-ln (C/C_0)*vs* t] by ZnO/MOF-I, ZnO/MOF-II and ZnO/MOF-III catalysts

Comparison of catalytic performance of ZnO/MOF-I/II/III with reported catalysts

For quantitative comparison, the results obtained for the proposed catalysts (ZnO/MOF-I/II/III) are compared with the catalysts reported in the literature (Table 5). For this purpose, the reduction of PNP is selected as a model reaction and activity parameter (k') is used which is

Scheme 1 General representation of catalytic reduction of various nitro aromatic compounds

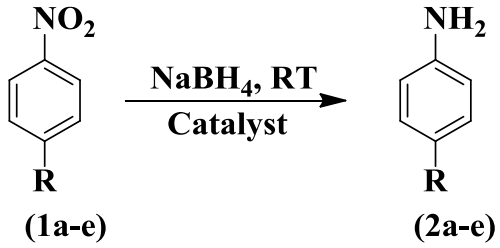

Table 4: Catalytic performance of the ZnO/MOF composites for the reduction reactions

Sr. No.	R	Reactant	Product	Catalyst	Time (min.)	Yield (%)	Rate constant, k (sec^{-1})
1.	F	1a	2a	ZnO/MOF-I	12	72.5	1.3×10^{-3}
				ZnO/MOF-II	12	64.9	6.4×10^{-4}
				ZnO/MOF-III	12	43.7	7.9×10^{-4}
2.	COOH	1b	2b	ZnO/MOF-I	15	80.1	1.4×10^{-3}
				ZnO/MOF-II	15	65.8	1.4×10^{-3}
				ZnO/MOF-III	15	56.5	9.0×10^{-4}
3.	OH	1c	2c	ZnO/MOF-I	5	97.78	1.0×10^{-2}
				ZnO/MOF-II	5	80.0	7.2×10^{-3}
				ZnO/MOF-III	5	70.6	5.6×10^{-3}
4.	OCH_3	1d	2d	ZnO/MOF-I	5	96.8	1.5×10^{-2}
				ZnO/MOF-II	5	91.0	9.6×10^{-3}
				ZnO/MOF-III	5	87.5	7.8×10^{-3}

defined as a ratio of rate constant, **k** and the total mass or weight of catalyst used, **m**.[84] As per the earlier reports shown in Table 5, Ag based catalysts- $Ag/Fe_3O_4@C$ [85] and Ag/SiO_2[86] have activity parameters of 0.86 sec^{-1} g^{-1} and 0.25 sec^{-1} g^{-1} respectively while Au/TiO_2 composite has k' value

of 0.12 sec^{-1} g^{-1}.[87] The catalytic activity of ZnO/MOF-I obtained is 20 sec^{-1} g^{-1} which is significantly greater than the Ag based composites mentioned above and is also greater than that of non-noble metal based hydrogel composites.[88-90] Out of the three nano-composites proposed in the current study, ZnO/MOF-I has better catalytic activity than ZnO/MOF-II and ZnO/MOF-III. This can be due to the quantum size effect of ZnO nanoparticles in ZnO/MOF-I thereby having highest surface area due to the smallest size of particles hence leading to the highest catalytic activity.[91] The composites showed the indirect relationship between the catalytic activity and the weight percentage of ZnO underlining the fact that there is a need of optimum concentration of ZnO nanoparticles for the maximum catalytic activity above which the catalytic tendency of the composite tends to decline. Hence ZnO/MOF-I shows the highest catalytic activity with optimum concentration of ZnO nanoparticles.

Table 5: Comparison of catalyst activity in terms of activity parameter with literature reports for PNP reduction

Sr. No.	Catalyst	k (sec^{-1})	k'=k/m (sec^{-1} g^{-1})	References
1.	**ZnO/MOF-I**	**1.0×10^{-2}**	**20**	**This work**
2.	**ZnO/MOF-II**	**7.2×10^{-3}**	**7**	**This work**
3.	**ZnO/MOF-III**	**5.6×10^{-3}**	**2.24**	**This work**
4.	$Ag/Fe_3O_4@C$	1.72×10^{-2}	0.86	85
5.	Ag/SiO_2	0.12×10^{-2}	0.25	86
4.	Au/TiO_2	0.71×10^{-2}	0.12	87
5.	p(AMPS)-Ni	9.38×10^{-4}	0.019	88
6.	p(AMPS)-Co	2×10^{-3}	0.04	89
7.	p(AMPS)-Cu	1.72×10^{-3}	0.172	90

ELECTROCATALYTIC STUDIES FOR OXYGEN EVOLUTION REACTION (OER)

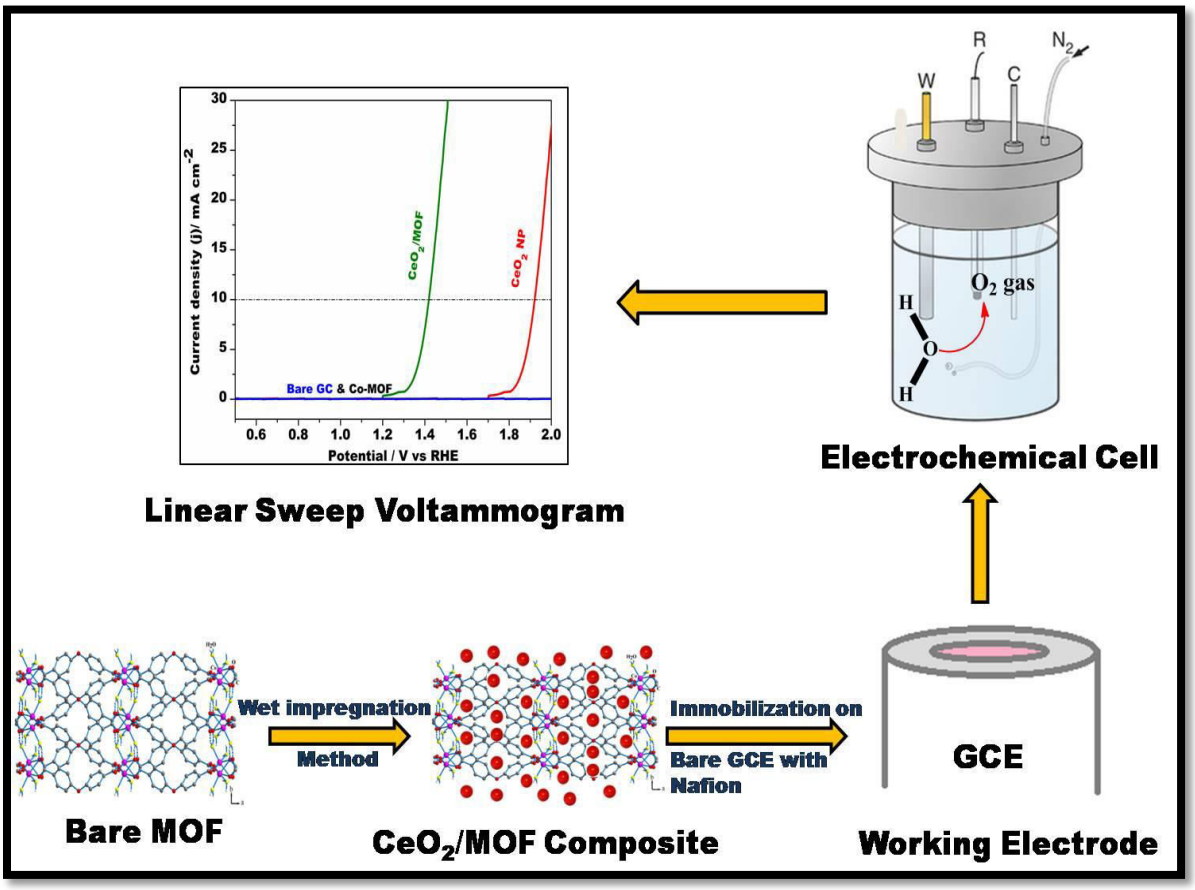

The increasing energy demands of a technologically advance society need to be met by the development of clean and sustainable energy devices such as fuel cells, metal-air batteries and water electrolyzers. In particular, water electrocatalysis or splitting is one of the most vital approaches for the fabrication of efficient energy storage and conversion devices to realize the dream of converting discontinuous renewable energy to the instant energy which can be produced as and when required. However, the slow kinetics of the water splitting reaction provides a great hindrance to the progress in the related field. Moreover, the best known catalysts that can reduce the overpotential of the two half cell reactions of water splitting process i.e. oxygen evolution reaction (OER) and hydrogen evolution reaction (HER)[92] are mainly derived from noble metals. Pt and Ir based catalysts have been known to be the most efficient for HER

and OER respectively.[92-95] Though noble metal based catalysts provide good activity but their sparse occurrence in the earth makes them an expensive alternate which limit their wide applicability for such purposes. Considering the high cost parameter, efforts have been much focused to replace such expensive catalysts with cheaper and earth abundant transition metal based electro catalysts,[96-98] especially derived from cobalt.[99-103] Therefore, cobalt based metal organic frameworks (MOFs) can be the fascinating candidates for such purposes owing to their inbuilt properties of high surface area and thermal stability. Moreover, their pores have been utilized for guest incorporation in order to modify and bestow them with altogether new properties in the area of catalysis,[104] magnetism,[105] and electrochemistry.[106] However, the low conductivity or insulating nature of Co based MOFs inhibit their applicability in electrochemical operations.[107] Hence, coupling them with conductive materials or nanoparticles is an attractive strategy that can endow them conductivity for the fabrication of a new generation electro catalysts. Metal oxide nanoparticles of ceria (CeO_2) are a promising alternate for conductive materials owing to its unique ability of getting easily interconverted between Ce(IV)↔ Ce(III) oxidation states.[6-8] Their use for oxygen ion conductivity and oxygen storage capacity has already been reported.[108] Hence, it was envisaged to utilize ceria nanoparticles in combination with Co-MOF for electrochemical applications.

Thus, this work presents a facile and easy wet impregnation protocol to load CeO_2 in the form of ceria nanoparticles onto Co-MOF (called as CeO_2/MOF composite, herein after). Co-MOF used in the present work is a known MOF which contains an aromatic organic linker, 4, 4'-oxy-bis (benzoic acid). The composite thus formed, has been characterized using techniques P-XRD, EDS, HR-TEM, XPS and Raman spectroscopy and investigated for electrocatalytic studies towards oxygen evolution reaction (OER). The resulting hybrid material exhibited satisfactory electrochemical performance with low overpotential of 180 mV at 10 mA cm^{-2} of current density and a small Tafel slope of 39 mV dec^{-1} which is better than the previously reported catalysts.[109]

The oxygen evolution reaction (OER) activity was examined for blank Co-MOF, ceria nanoparticles and CeO_2/MOF in 1.0 M KOH aqueous solution with the help of a standard three electrode system using linear sweep voltammetry (LSV) at a slow scan rate of 1 mV s^{-1} for the accurate analysis of Tafel slope. The potentials were referenced to a reversible hydrogen electrode (RHE). To confirm the evolution of oxygen, the samples were withdrawn from the

sealed reaction vessel (which was first evacuated and saturated with nitrogen) and were analyzed using gas chromatography (Fig. 30).

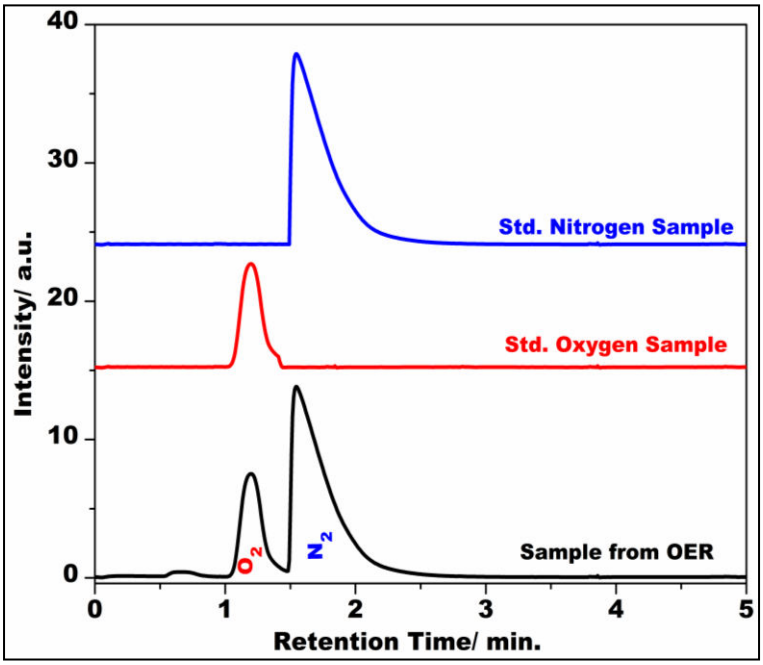

Fig. 30. Gas chromatograph for OER in 1.0 M KOH saturated with Nitrogen gas using CeO_2/MOF as an electrocatalyst

The ceria nanoparticles alone had a little activity (high overpotential of 0.7 V) and bare Co-MOF showed almost negligible catalytic tendency for OER whereas the ceria nanoparticles grafted/incorporated onto Co-MOF showed good activity (low overpotential of 0.18 V). This underlines the fact that the observed electrocatalytic activity is due to the synergistic effect of both the ceria nanoparticles and the Co-MOF where electron transfer is taking place from cerium to the cobalt coordination sphere as confirmed by XPS studies.

The electrocatalytic oxygen evolution starts at 1.23 V for CeO_2/MOF composite (vs reversible hydrogen electrode, RHE). Similarly for ceria nanoparticles, the current starts ascending at 1.69 V while the Co-MOF did not show any change (Fig. 31a). The overpotential (η) at the current density of 10 mA cm^{-2} is generally taken as key reference parameter for analyzing the oxygen evolution tendency in an electrocatalyst as it represents the current density of a realistic device.[110] The overpotential (η) for CeO_2/MOF composite was found to be low as 0.18 V revealing that the energy required for OER activity is very low. By plotting the overpotential (η) against log of current density (j) gives the Tafel plot (Fig. 31b), the slope of which helps to

determine the kinetic parameters of oxygen evolution reaction. The Tafel slope was found to be 39 mV dec^{-1}, which is quite low and a smaller Tafel slope signifies a faster increment in OER rate with increasing potential.

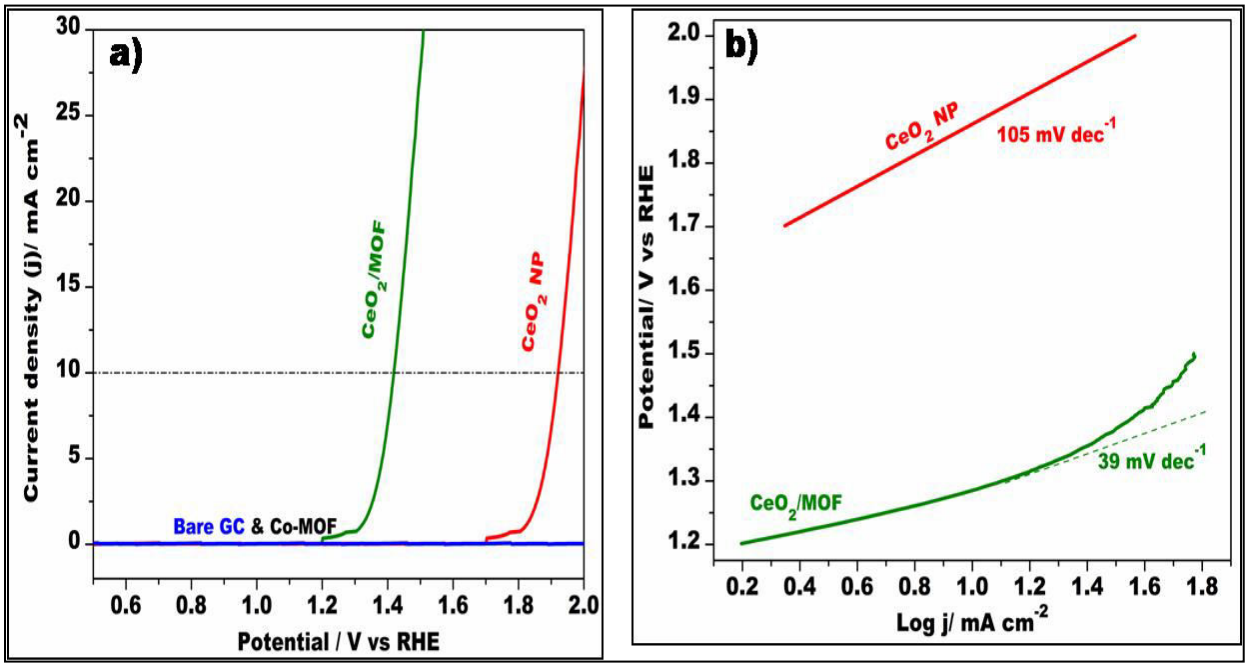

Fig. 31a) Linear sweep voltammetry (LSV) curves for glassy carbon electrode (GCE) modified with CeO_2/MOF (5mg), CeO_2 NPs, Co-MOF and bare GCE in O2-saturated 1.0 M KOH with a sweep rate of 1 mV s^{-1} b) Tafel plot of the catalyst CeO_2/MOF and CeO_2 NPs recorded at sweep rate of 1 mV s^{-1}

Electrochemical active surface area (A_{echem}) is another important parameter in order to estimate the efficiency of any electrocatalyst and can be easily evaluated from the relation i.e., $C_{dl} \propto v \times A_{echem}$ [111-114] where, C_{dl} stands for double layer capacitance (C_{dl}) and v is the scan rate applied. Hence, cyclic voltammetric studies were done for the measurement of electrochemical active surface area that showed the linear relationship between the current density and scan rate (Fig. 32 d). The slope gave C_{dl} which was calculated to be 24.157 mF cm^{-2} for CeO_2/MOF composite, 4.32 mF cm^{-2} (for Co-MOF) and 4.83 mF cm^{-2} (for CeO_2 NPs). Since double layer capacitance (C_{dl}) is in direct relation with the electrochemical active surface area, therefore it can be concluded that the incorporation of CeO_2 has effectively increased the active surface area. Hence, the superior activity towards OER can be justified in case of CeO_2/MOF composite in comparison to that of Co-MOF and CeO_2 NPs alone. The increase in active surface area further led to increase in electron transportation and also helped in improving permeation and flow of electrolyte in the electrode.[109]

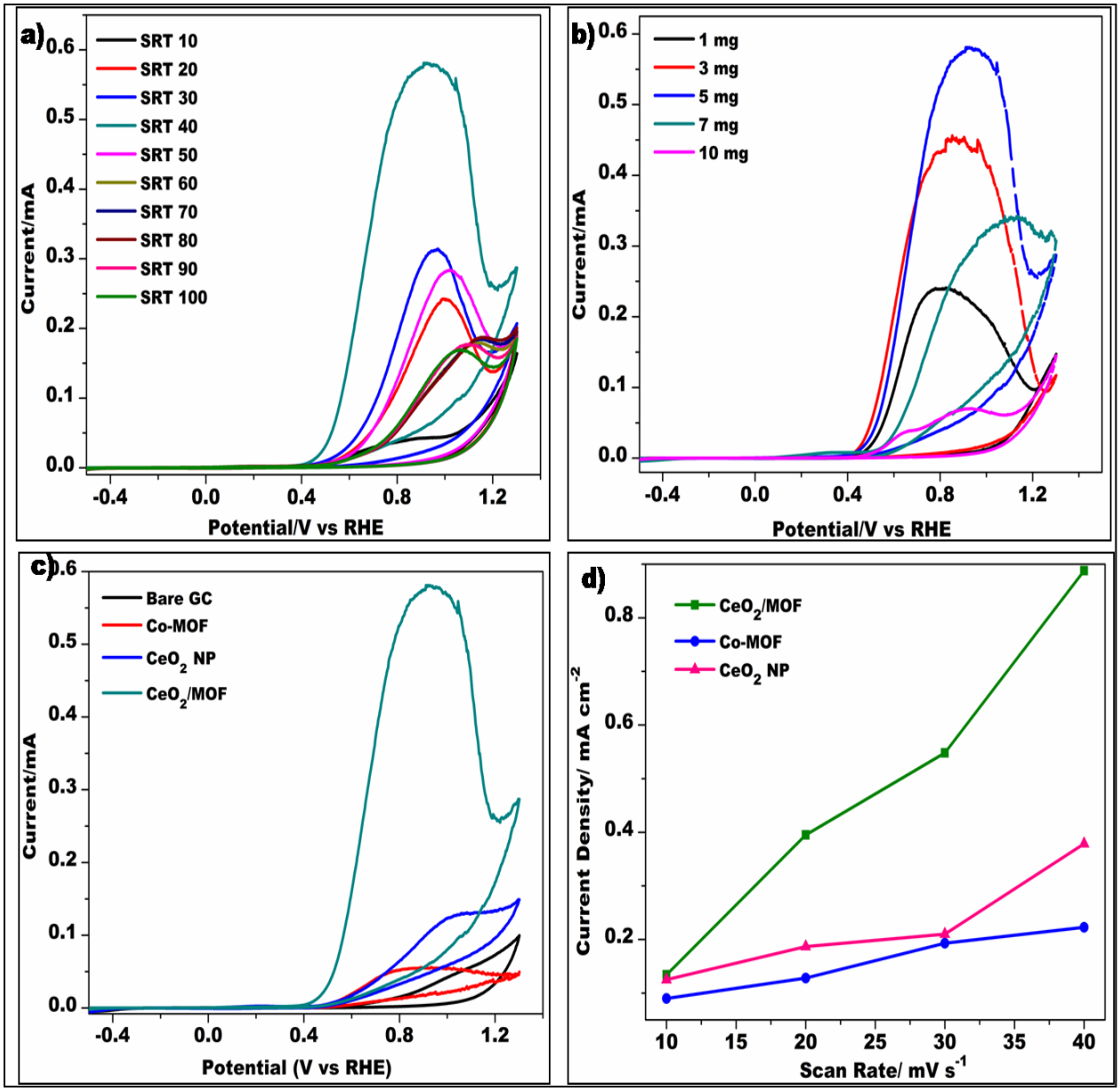

Fig. 32 a) Cyclic voltammogram for glassy carbon electrode (GCE) modified with CeO_2/MOF (5 mg) at different scan rates for OER in 1.0 M KOH b) Cyclic voltammogram graphs for glassy carbon electrode (GCE) modified optimized for different concentrations of CeO_2/MOF at scan rate of 40 mVs^{-1} for OER in 1.0 M KOH c) Cyclic voltammogram graphs for glassy carbon electrode (GCE) modified with CeO_2/MOF, CeO_2 NP, Co-MOF and bare GCE at scan rate of 40 mVs^{-1} for OER in 1.0 M KOH d) Plot for the estimation of C_{dl} and relative electrochemically active surface area

Longer stability of a catalyst towards OER is a critical factor for the realization of future oriented energy storage and conversion devices. Thus, chronoamperometric tests were done over the time period of 16 hours to check for the stability of the electrocatalyst (fig.33). No significant change in current was observed with the current value varying between 0.30 to 0.25 mA at the beginning and the end of 16 hours. Hence, it can be concluded that the composite afforded good stability

without significant current loss. Taking all the above observations into account, the efficiency of CeO_2/MOF (as an electrocatalyst in terms of activity and kinetics) can be defined on the grounds of four major parameters- lower overpotential at current density of 10 mA cm^{-2} (0.18 V), smaller Tafel slope (39 mV dec^{-1}) , high electrochemical surface area (24.157 mF cm^{-2}) and longer durability.

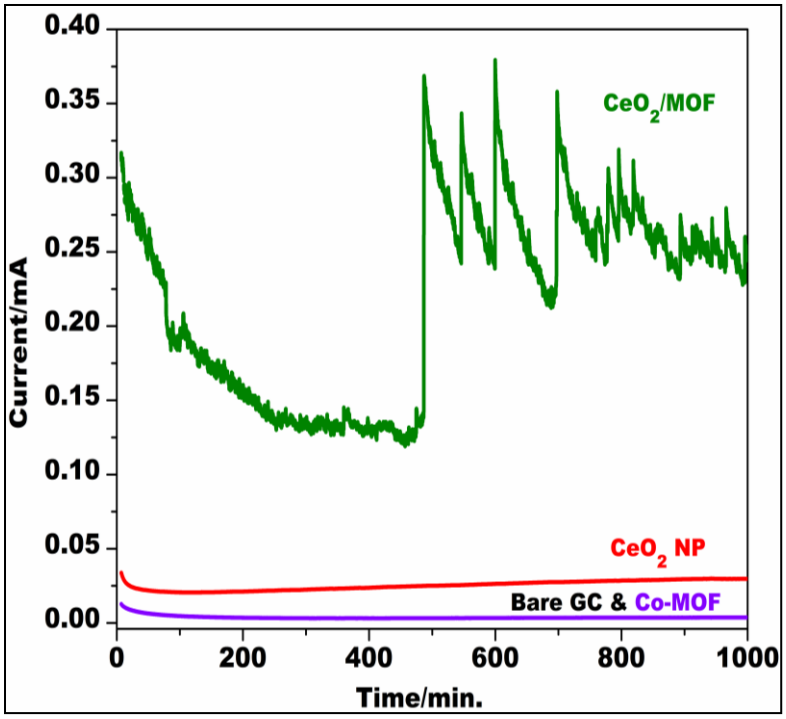

Fig.33. Chronoamperometric responses of OER using modified glassy carbon electrode with CeO_2/MOF, CeO_2 NP, Co-MOF and bare GCE in 1.0 M KOH

Table 6: OER activities of some previously reported electrocatalysts in alkaline solutions with a current density at 10 mA cm^{-2}

Sr. No.	Catalyst	Electrolyte	Tafel slope (mV/dec)	η (mV)	References
1.	Co-MOF@CNTs	1.0 M KOH	69	340	8
2.	MOF-derived Co_3O_4C-NA	1.0 M KOH	61	1520	111
3.	Fe/Ni-BTC MOF	0.1 M KOH	47	270	115
4.	$Ni_xFe_{3-x}O_4$	1.0 M KOH	53	400	116
5.	$Co_xFe_{3-x}O_4$	1.0 M KOH	57	420	116
6.	20 wt% Ir/C	0.1 M KOH	-	380	117
7.	20 wt% Ru/C	0.1 M KOH	-	390	117
8.	Co-P/NC	1.0 M KOH	52	354	117
9.	**CeO_2/MOF**	**1.0 M KOH**	**39**	**180**	**This work**

For quantitative comparison, the kinetic and catalytic activity of the CeO_2/MOF composite was compared with that of the other reported electrocatlysts. It can be clearly seen from Table 6, the overpotential value of 180 mV and Tafel slope of 39 mV dec^{-1} is markedly lower than that of the previously reported MOF based (Co-MOF@CNTs,[8] MOF-derived Co_3O_4C-NA [111] and Fe/Ni-BTC MOF[115]), mixed oxide based ($Ni_xFe_{3-x}O_4$, $Co_xFe_{3-x}O_4$)[116] and noble metal based (Ir/C, Ru/C)[117] electrocatalysts. Thus the composite material under consideration (i.e. CeO_2/MOF) can be ranked amongst the good catalysts for OER activity.

References:

1. Mahata, P.; Drazneiks, C. M.; Roy, P.; Natarajan, S., *Cryst. Growth Des.* **2013**, *13***,** 155.
2. Aijaz, A.; Karkamkar, A.; Choi, Y. J.; Tsumori, N.; Rönnebro, E.; Autrey, T.; Shioyama, H.; Xu, Q. *J. Am. Chem. Soc.* **2012**, *134*, 13926.
3. Jiang, H. L.; Liu, B.; Akita, T.; Haruta, M.; Sakurai, H.; Xu, Q. *J. Am. Chem. Soc.* **2009**, *131*, 11302.
4. Bai, S.; Hu, J.; Li, D.; Luo, R.; Chen, A.; Liu, C. C. *J. Mater. Chem.* **2011**, *21*, 12288.
5. Strohmeier, B. R.; Evans, W. T.; Schrall, D. M. *J. Mater. Sci.* **1993**, *28*, 1563.
6. Liu, X. W.; Zhou, K. B.; Wang, L.; Wang, B. Y.; Li, Y. D. *J. Am. Chem. Soc.* **2009**, *131*, 3140.
7. Esch, F.; Fabris, S.; Zhou, L.; Montini, T.; Africh, C.; Fornasiero, P.; Comelli, G.; Rosei, R. *Science* **2005**, *309*, 752.
8. Qi, J.; Chen, J.; Li, G. D.; Li, S. X.; Gao, Y.; Tang, Z. Y. *Energy Environ. Sci.* **2012**, *5*, 8937.
9. Yang, H.; Huang, C.; Tang, A.; Zhang, X.; Yang, W. *Mater. Res. Bulletin* **2005**, *40***,** 1690.
10. Yu, K. L.; Ruan, G. L.; Ben, Y. H.; Zou, J. J. *Mater. Sci. Engg. B* **2007**, *139***,** 197.
11. Zhang, Y.; Bo, X.; Nsabimana, A.; Han, C.; Li, M.; Guo, L. *J. Mater. Chem. A* **2015**, *3*, 738.
12. Babitha, K. K.; Sreedevi, A.; Priyanka, K. P.; Sabu, B.; Varghese, T. *Ind. J. Pure App. Phys.* **2015***, 3*, 596.
13. Lee, J.; Farha, O. K.; Roberts, J.; Scheidt, K. A.; Nguyen, S. T.; Hupp, J. T. *Chem. Soc. Rev.* **2009**, *38*, 1450.
14. Collins, D. J.; Zhou, H. C. *J. Mater. Chem.* **2007**, *17*, 3154.
15. Li, J. R.; Ma, Y.; McCarthy, M. C.; Sculley, J.; Yu, J.; Jeong, H. K.; Balbuena, P. B.; Zhou, H. C. *Coord. Chem. Rev.* **2011**, *255*, 1791.
16. Horcajada, P.; Serre, C.; Maurin, G.; Ramsahye, N. A.; Balas, F.; Vallet-Regi, M.; Sebban, M.; Taulelle, F.; Ferey, G. *J. Am. Chem. Soc.* **2008**, *130*, 6774.
17. An, J. Y.; Geib, S. J.; Rosi, N. L. *J. Am. Chem. Soc.* **2009**, *131*, 8376.
18. Reineke, T. M.; Eddaoudi, M.; Fehr, M.; Kelley, D.; Yaghi, O. M. *J. Am. Chem. Soc.* **1999**, *121*, 1651.
19. Zhang, Z.; Xiang, S.; Rao, X.; Zheng, Q.; Fronczek, F. R.; Qian, G.; Chen, B. *Chem. Comm.* **2010**, *46*, 7205.

20. Harbuzaru, B. V.; Corma, A.; Rey, F.; Jorda, J. L.; Ananias, D.; Carlos, L. D.; Rocha, J. *Angew. Chem. Int. Ed.* **2009**, *48*, 6476.
21. White, K. A.; Chengelis, D. A.; Gogick, K. A.; Stehman, J.; Rosi, N. L.; Petoud, S. *J. Am. Chem. Soc.* **2009**, *131*, 18069.
22. Kreno, L. E.; Leong, K.; Farha, O. K.; Allendorf, M.; Duyne, R. P. V.; Hupp, J. T. *Chem. Rev.* **2012**, *112*, 1105.
23. Hu, Z.; Deibert, B. J.; Li, J. *Chem. Soc. Rev.* **2014**, *43*, 5815.
24. Thomas, S. W.; Joly, G. D.; Swager, T. M. *Chem. Rev.* **2007**, *107*, 1339.
25. He, G.; Peng, H.; Liu, T.; Wang, M.; Zhang, Y.; Fang, Y. *J. Mater. Chem.* **2009**, *19*, 7347.
26. Nagarkar, S. S.; Desai, A. V.; Ghosh, S. K. *Chem. Comm.* **2014**, *50*, 8915.
27. Singha, D. K.; Majee, P.; Mondal, S. K.; Mahata, P. *Eur. J. Inorg. Chem.* **2015**, *2015*, 1390.
28. Roy, B.; Bar, A. K.; Gole, B.; Mukherjee, P. S. *J. Org. Chem*. **2013**, *78*, 1306.
29. Furton, K. G.; Myers, L. J. *Talanta* **2001**, *54*, 487.
30. Eiceman, G. A.; Stone, J. A. *Anal. Chem*. **2004**, *76***,** 390.
31. Luggar, R. D.; Farquharson, M. J.; Horrocks, J. A.; Lacey, R. J. *X-Ray Spectro*. **1998**, *27***,** 87.
32. Hakansson, K.; Coorey, R. V.; Zubarev, R. A.; Talrose, V. L.; Hakansson, P. *J. Mass Spectro*. **2000**, *35*, 337.
33. Sylvia, J. M.; Janni, J. A.; Klein, J. D.; Spencer, K. M. *Anal. Chem.* **2000**, *72*, 5834.
34. Kandpal, M.; Bandela, A. K.; Hinge, V. K.; Rao, V. R.; Rao, C. P. *ACS Appl. Mater. Interfaces* 2013, **5**, 13448.
35. Moros, J.; Laserna, J. J. *Anal. Chem.* 2011, **83**, 6275.
36. Hallowell, S. F. *Talanta* 2001, **54**, 447.
37. Gallo, M. A.; Lawryk, N. J., in: *Handbook of Pesticide Toxicology*, Vol. 2, Hayes, W. J., Laws, E. R., Ed., Academic Press, San Diego, **1991**, 917.
38. Stan, H. J. *J. Chromatogr.* **2000**, *892*, 347.
39. Chen, P. S.; Huang, S. D. *Talanta* **2006***, 69*, 669.
40. Leandro, C. C.; Hancock, P.; Fussell, R. J.; Keely, B. J. *J. Chromatorgr. A* **2006**, *1103*, 94.

41. Zhang, G. L. *J. Anhui Agric. Sci.* **2003**, *31*, 663.
42. Kazemi, M.; Tahmasbi, A. M.; Valizadeh, R.; Naserian, A. A.; Soni, A. *Agri. Sci. Res. J.* **2012**, *2*, 512.
43. Mahata, P.; Natarajan, S.; Panissod, P.; Drillon, M. *J. Am. Chem. Soc.* **2009**, *131***,** 10140.
44. Mullane, A. P. O.; Ippolito, S. J.; Sabri, Y. M.; Bansal, V.; Bhargava, S. K. *Langmuir* **2009**, *25*, 3845.
45. Dotzauer, D. M.; Bhattacharjee, S.; Wen, Y.; Bruening, M. L. *Langmuir* **2009**, *25*, 1865.
46. Schmid, G.; Corain, B. *Eur. J. Inorg. Chem.* **2003**, 3081.
47. Sabri, Y.; Ippolito, S.; Mullane, A. O.; Tardio, J.; Bansal, V.; Bhargava, S. *Nanotech.* **2011**, *22*, 305501.
48. Pasqua, L.; Cundari, S.; Ceresa, C.; Cavaletti, G. *Med. Chem.* **2009**, *16***,** 3054.
49. Yanhong, L.; Dejun, W.; Qidong, Z.; Min, Y.; Qinglin, Z. *J. Phys. Chem. B* **2004**, *108*, 3202.
50. Domènech, B.; Munoz, M.; Muraviev, D. N.; Macanas, J. *Nanoscale Res. Lett.* **2011**, *6*, 406.
51. Sun, J.; Ma, D.; Zhang, H.; Liu, X.; Han, X.; Bao, X.; Weinberg, G.; Pfander, N.; Su, D. *J. Am. Chem. Soc.* **2006**, *128*, 15756.
52. Mandal, S.; Roy, D.; Chaudhari, R. V.; Sastry, M. *Chem. Mater.* **2004**, *16*, 3714.
53. Yang, M.; Fujino, T. *Chem. Phys. Lett*. **2013**, *576*, 61.
54. Kumar, A. P.; Kumar, B. P.; Kumar, A. B. V. K.; Huy, B. T.; Lee, Y. *Appl. Surf. Sci.* **2013**, *265*, 500.
55. Yin, D.; Qin, L.; Liu, J.; Li, C.; Jin, Y. *J. Mol. Cat. A: Chem.* **2005**, *240*, 40.
56. Smuleac, V.; Bachas, L.; Bhattacharya, D. *J. Membrane Sci.* **2010**, *346*, 310.
57. Wang, C.; deKrafft, K. E.; Lin, W. *J. Am. Chem. Soc.* **2012**, *134*, 7211.
58. Furukawa, H.; Ko, N.; Go, Y. B.; Aratani, N.; Choi, S. B.; Choi, E.; Yazaydin, A. O.; Snurr, R. Q.; O'Keeffe, M.; Kim, J.; Yaghi, O. M. *Science* **2010**, *329*, 424.
59. Xuan, W.; Zhu, C.; Liu, Y.; Cui, Y. *Chem. Soc. Rev.* **2012**, *41*, 1677.
60. Liu, H.; Liu, Y.; Li, Y.; Tang, Z.; Jiang, H. *J. Phys. Chem. C* **2010**, *114***,** 13362.
61. Park, Y. K.; Choi, S. B.; Nam, H. J.; Jung, D.Y.; Ahn, H. C.; Choi, K.; Furukawa, H.; Kim, J. *Chem. Comm.* **2010**, *46*, 3086.
62. Esken, D.; Turner, S.; Lebedev, O. I.; Tendeloo, G. V.; Fischer, R. A. *Chem. Mater*. **2010**, *22*, 6393.
63. Ishida, T.; Nagaoka, M.; Akita, T.; Haruta, M. *Chem. Eur. J.* **2008**, *14*, 8456.

64. Li, Z.; Zeng, H. C. *Chem. Mater.* **2013**, *25*, 1761.
65. Müller, U.; Lobree, L.; Hesse, M.; Yaghi, O. M.; Eddaoudi, M. WO 03/101975, **2003**.
66. Proch, S.; Herrmannsdörfer, J.; Kempe, R.; Kern, C.; Jess, A.; Seyfarth, L.; Senker, J. *Chem. Eur. J.* **2008**, *14*, 8204.
67. Sabo, M.; Henschel, A.; Fröde, H.; Klemm, E.; Kaskel, S. *J. Mater. Chem*. **2007**, *17*, 3827.
68. Schröder, F.; Esken, D.; Cokoja, M.; Van den Berg, M. W. E.; Lebedev, O. I.; Van Tendeloo, G.; Walaszek, B.; Buntkovsky, G.; Limbach, H. H.; Chaudret, B.; Fischer, R. A. *J. Am. Chem. Soc.* **2008**, *130*, 6119.
69. Gu, X.; Lu, Z. H.; Jiang, H. L.; Akita, T.; Xu, Q. *J. Am. Chem. Soc.* **2011**, *133*, 11822.
70. Lu, G.; Li, S.; Guo, Z.; Farha, O. K.; Hauser, B. G.; Qi, X.; Wang, Y.; Wang, X.; Han, S.; Liu, X.; DuChene, J. S.; Zhang, H.; Zhang, Q.; Chen, X.; Ma, J.; Loo, S. C. J.; Wei, W. D.; Yang, Y.; Hupp, J. T.; Huo, F. *Nature Chemistry* **2012**, *4*, 310.
71. Hosseini, H.; Ahmar, H.; Dehghani, A.; Bagheri, A.; Fakhari, A. R.; Amini, M. M. *Electrochimica Acta* **2013**, *88*, 301.
72. Shono, T.; Matsumara, A.; Kanazawa, T. *Tet. Lett.* **1983**, *24*, 4577.
73. Khattab, A. T.; Gaffer, E. H. *Col. Tech*. **2016**, *132*, 460.
74. Smith, G. V.; Notheisz, F. *Heterogeneous Catalysis in Organic Chemistry*, Academic Press, New York, **1999**, 71.
75. Allen, C. F. H.; VanAllan, J. *Org. Synth.* **1955**, 63.
76. Bavin, P. M. G. *Org. Synth.* **1973**, 30.
77. Tsukinoki, T.; Tsuzuki, H. *Green Chem.* **2001**, *3*, 37.
78. Grirrane, A.; Corma, A.; García, H. *Science* **2008**, *322*, 1661.
79. Bai, S.; Hu, J.; Li, D.; Luo, R.; Chen, A.; Liu, C. C. *J. Mater. Chem.* **2011**, *21*, 12288.
80. Park, Y. K.; Choi, S. B.; Nam, H. J.; Jung, D.-Y.; Ahn, H. C.; Choi, K.; Furukawa, H.; Kim, J. *Chem. Comm.* 2010, **46**, 3086.
81. D. Esken, S. Turner, O. I. Lebedev, G. V. Tendeloo and R. A. Fischer, *Chem. Mater*., 2010, **22**, 6393.
82. F. Schröder, D. Esken, M. Cokoja,; M. W. E.van den Berg, O. I. Lebedev, G. V. Tendeloo, B. Walaszek, G. Buntkowsky, H.-H. Limbach, B. Chaudret and R. A. Fischer, *J. Am. Chem. Soc.*, 2008, **130**, 6119.

83. S. Proch, J. Herrmannsdörfer, R. Kempe, C. Kern, A. Jess, L. Seyfarth and L. Senker, *Chem.-Eur. J.*, 2008, **14**, 8204.
84. Pradhan, N.; Pal, A.; Pal, T. *Colloids and Surfaces A: Physicochem. Eng. Aspects* **2002**, *196***,** 247.
85. Baruah, B.; Gabriel, G. J.; Akbashev, M. J.; Booher, M. E. *Langmuir* **2013**, *29***,** 4225.
86. Zhu, M. Y.; Wang, C. J.; Meng, D. H.; Diao, G. W. *J. Mater. Chem. A* **2013**, *1*, 2118.
87. Wang, M.; Tian, D.; Tian, P. P.; Yuan, L. J. *Appl. Surf. Sci.* **2013**, *283*, 389.
88. Ismail, A. A.; Hakki, A.; Bahnemann, D. W. *J. Mol. Catal. A: Chem.* **2012**, *358*, 145.
89. Tang, S. C.; Vongehr, S.; He, G. R.; Chen, L.; Meng, X. K. *J. Colloid Interface Sci.* **2012**, *375***,** 125.
90. Sahiner, N.; Ozay, H.; Ozay, O.; Aktas, N. *Appl. Catal. A: Gen.* **2010**, *385***,** 201.
91. Sahiner, N.; Ozay, H.; Ozay, O.; Aktas, N. *Appl. Catal. B: Environ.* **2010**, *101*, 137.
92. Zou, X.; Zhang, Y. *Chem. Soc. Rev.* **2015**, *44*, 5148.
93. Zhao, Y.; Hernandez-Pagan, E. A.; Vargas, N. M.; Dysart, J. L.; Mallouk, T. E. J. *Phys. Chem. Lett.* **2011**, *2*, 402.
94. Zou, X.; Goswami, A.; Asefa, T. *J. Am. Chem. Soc.* **2013**, *135*, 17242.
95. McCrory, C. C. L.; Jung, S.; Ferrer, I. M.; Chatman, S. M.; Peters, J. C.; Jaramillo, T. F. *J. Am. Chem. Soc.* **2015**, *137*, 4347.
96. Gorlin, Y.; Jaramillo, T. F. *J. Am. Chem. Soc.* **2010**, *132*, 13612.
97. Gong, M.; Li, Y.; Wang, H.; Liang, Y.; Wu, J. Z.; Zhou, J.; Wang, J.; Regier, T.; Wei, F.; Dai, H. *J. Am. Chem. Soc.* **2013**, *135*, 8452.
98. Long, X.; Li, J.; Xiao, S.; Yan, K.; Wang, Z.; Chen, H.; Yang, S. *Angew. Chem. Int. Ed.* **2014**, *126*, 7714.
99. Artero, V.; Chavarot-Kerlidou, M.; Fontecave, M. *Angew. Chem. Int. Ed.* **2011**, *50*, 7238.
100. Smith, R. D. L.; Prevot, M. S.; Fagan, R. D.; Trudel, S.; Berlinguette, C. P. *J. Am. Chem. Soc.* **2013**, *135*, 11580.
101. Bajdich, M.; García-Mota, M.; Vojvodic, A.; Nørskov, J. K.; Bell, A. T. *J. Am. Chem. Soc.* **2013**, *135*, 13521.
102. Zhang, M.; Respinis, M. D.; Frei, H. *Nat. Chem*. **2014**, *6*, 362.
103. Zhuang, Z.; Sheng, W.; Yan, Y. *Adv. Mater.* **2014**, *26*, 3950.
104. Gu, X.; Lu, Z. H.; Jiang, H. L.; Akita, T.; Xu, Q. *J. Am. Chem. Soc.* **2011**, *133*, 11822.

105. Lu, G.; Li, S.; Guo, Z.; Farha, O. K.; Hauser, B. G.; Qi, X.; Wang, Y.; Wang, X.; Han, S.; Liu, X.; DuChene, J. S.; Zhang, H.; Zhang, Q.; Chen, X.; Ma, J.; Loo, S. C. J.; Wei, W. D.; Yang, Y.; Hupp, J. T.; Huo, F. *Nature Chemistry*, 2012, 4, 310.
106. Hosseini, H.; Ahmar, H.; Dehghani, A.; Bagheri, A.; Fakhari, A. R.; Amini, M. M. *Electrochimica Acta* **2013**, *88*, 301.
107. Lu, X.; Zhao, C. *J. Mater. Chem. A* **2013**, *1*, 12053.
108. Feng, K. J.; Yang, Y. H.; Wang, Z. J.; Jiang, J. H.; Shen, G. L.; Yu, R. Q. *Talanta* **2006**, *70*, 561.
109. Fang, Y.; Li, X.; Li, F.; Lin, X.; Tian, M.; Long, X.; An, X.; Fu, Y.; Jin, J.; Ma, J. *J. Power Sources* **2016**, *326*, 50.
110. Luo, J.; Im, J.-H.; Mayer, M. T.; Schreier, M.; Nazeeruddin, M. K.; Park, N.-G.; Tilley, S. D.; Fan, H. J.; Grätzel, M. *Science* **2014**, *345*, 1593.
111. Ma, T. Y.; Dai, S.; Jaroniec, M.; Qiao, S. Z. *J. Am. Chem. Soc.* **2014***, 136*, 13925.
112. Li, Y.; Hasin, P.; Wu, Y. *Adv. Mater.* **2010**, *22*, 1926.
113. Benck, J. D.; Chen, Z. B.; Kuritzky, L. Y.; Forman, A. J.; Jaramillo, T. F. *ACS Catal.* **2012**, *2,* 1916.
114. Li, P.; Jin, Z.; Xiao, D. *J. Mater. Chem. A* **2014**, *2*, 18420.
115. Wang, L.; Wu, Y.; Cao, R.; Ren, L.; Chen, M.; Feng, X.; Zhou, J.; Wang, B. *ACS Appl. Mater. Interfaces* **2016**, *8*, 16736.
116. Feng, Y.; Wei, J.; Ding, Y. *J. Phys. Chem. C* **2016**, *120*, 517.
117. Gorlin, Y.; Jaramillo, T. F. A. *J. Am. Chem. Soc.* **2010**, *132*, 13612.

CHAPTER-5

CONCLUSIONS

To summarize, a two-dimensional metal organic framework, $[Co(OBA)(H_2O)_2]$ [(OBA =4,4'-oxybis(benzoate)], **1,** was synthesized by a known procedure.[1] MOF-1 so synthesized was characterized by P-XRD and modified further by incorporating zinc oxide and ceria nanoparticles using wet impregnation method. The frameworks of the resulting composites retain their structural integrity which was confirmed by powder X-Ray diffraction (PXRD), scanning electron microscopy (SEM), energy dispersive X-ray (EDX) spectroscopy, high resolution transmission electron microscopy (HR-TEM), microwave plasma-atomic emission spectroscopy (MP-AES), X-Ray photoelectron spectroscopy (XPS) and Raman spectroscopic methods. The detailed structural investigation of ZnO/MOF composites revealed the size (4-8 nm for ZnO/MOF-I to 80-90 nm for ZnO/MOF-III), loading ratios of nanoparticles (0.51 wt % to 2.57 wt %), species of zinc present and the chemical bonding between the nanoparticles and MOF. Similarly, structural analysis of ceria doped MOF composite using powder X-Ray diffraction (PXRD), scanning electron microscopy (SEM), energy dispersive X-ray (EDX) spectroscopy, high resolution transmission electron microscopy (HR-TEM), X-Ray photoelectron spectroscopy (XPS) and Raman spectroscopic methods confirmed the size and loading ratio of ceria nanoparticles. Also the species of cerium present and the type of interactions between the ceria nanoparticles and the MOF were revealed.

The synthesized MOF and its modified forms were further investigated for the potential applications. MOF-1 was found to useful for the detection of nitro aromatics when it quenched the emission spectra of MOF-1. Among the various nitro aromatics used for these studies, the response of 2, 4, 6-trinitrophenol- a well known explosive compound found in landmines was found to have maximum quenching coefficient of $2.6 \times 10^{-5}\ M^{-1}$ with the lowest detection limit of 0.043 ppm.

The same MOF was found to behave as an efficient luminescent sensor for aromatic organo-phosphorous pesticides. Chlorpyriphos and triazophos were detected by "turn-on" luminescence phenomenon in the concentrations as low as 0.6 and 0.7 ppm respectively. Triazophos increased the original emission intensity of MOF-1 by 238% of its original value while the chlorpyriphos increased the same by 29%.

The accessibility and catalytic activity of the embedded ZnO nanoparticles into Co-MOF was checked through the reduction of nitroarenes by $NaBH_4$ under ambient conditions. The use of a simple and a mild reducing agent, $NaBH_4$ in methanol with ZnO/MOF catalysts (having varied weight ratios of ZnO) facilitated the reactions which were monitored using UV-Vis spectroscopy and HPLC. The percentage conversion from PNP to PAP was highest in case of ZnO/MOF-I (97.78%) and lowest in case of ZnO/MOF-III (70.6%). This can be attributed to the increased surface area of ZnO NPs in case of ZnO/MOF-I due to their very small size. With this work, we established and validated the possibility of inducing the catalytic activity to the MOF using cheap ZnO nanoparticles for the first time substituting the corrosive and reactive catalysts as used conventionally.

The same Co-MOF when loaded with ceria nanoparticles was investigated thoroughly for oxygen evolution reaction (OER) after casting a thin film on glassy carbon electrode. This electrocatalyst showed high activity with lower overpotential value of 180 mV at 10 mA cm^{-2}, higher electrochemical surface area and a small Tafel slope of 39 mV dec^{-1}. Moreover, the thin film of electrocatalyst maintains its electrochemical stability and activity over a long period of 16 hours. Hence, the current synthetic strategy and approach towards more electrochemical reactions may pave a new path towards the futuristic energy storage and conversion devices.

References:

1. Mahata, P.; Drazneiks, C. M.; Roy, P.; Natarajan, S., *Cryst. Growth Des.* **2013**, *13*, 155.

ANNEXURE-1

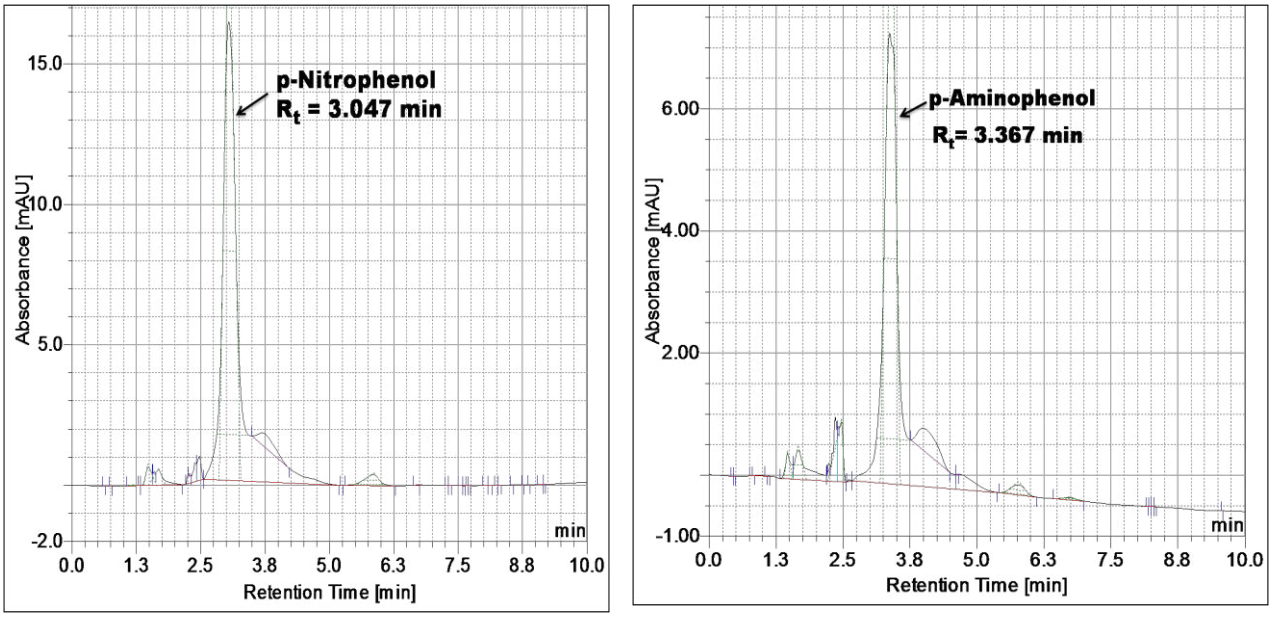

Fig.1. HPLC chromatograms of Standard p-nitro phenol and p-amino phenol

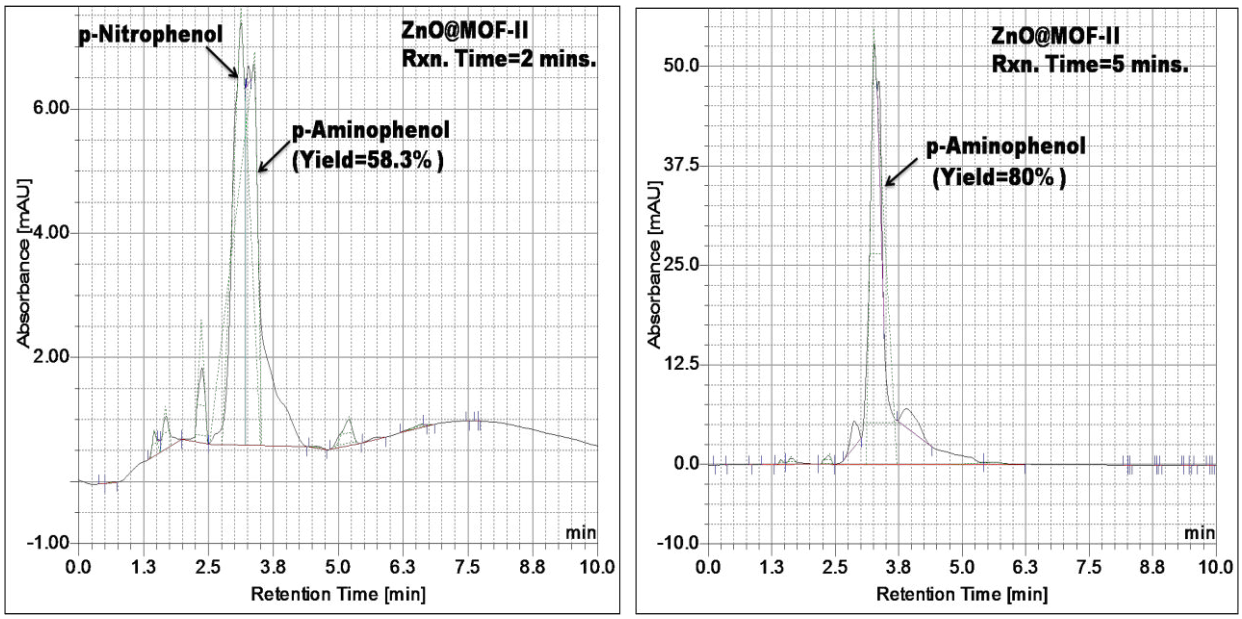

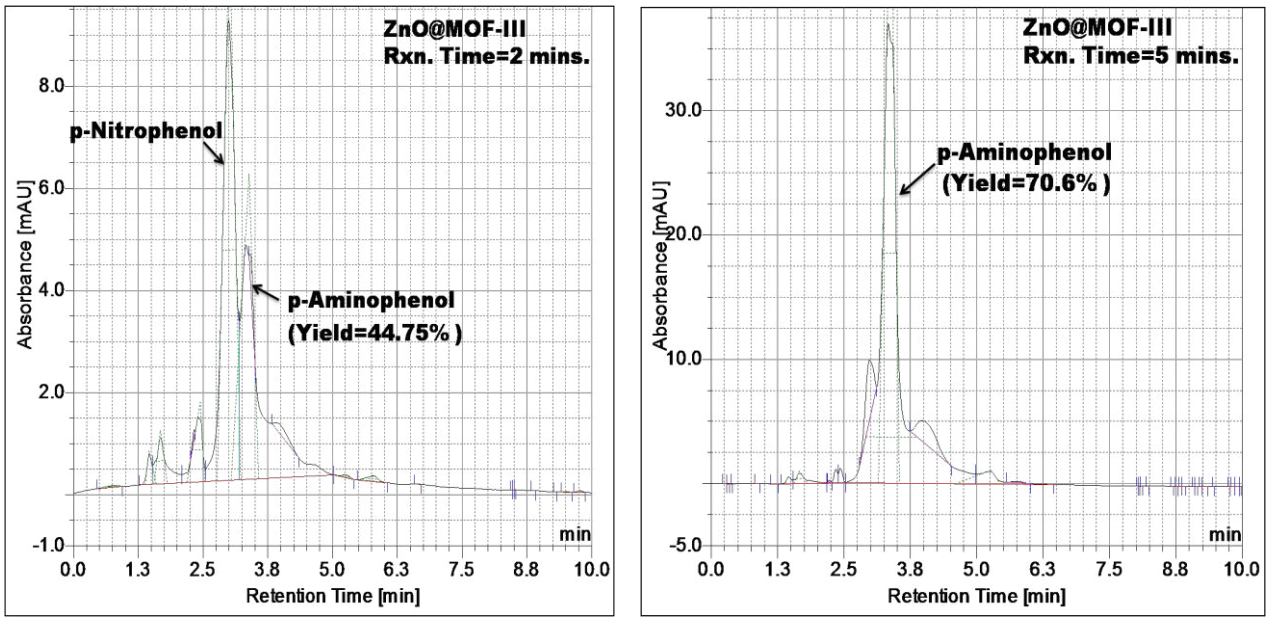

Fig. 2. HPLC chromatograms for the catalytic reduction of p-nitro phenol using ZnO/MOF-II and ZnO/MOF-III

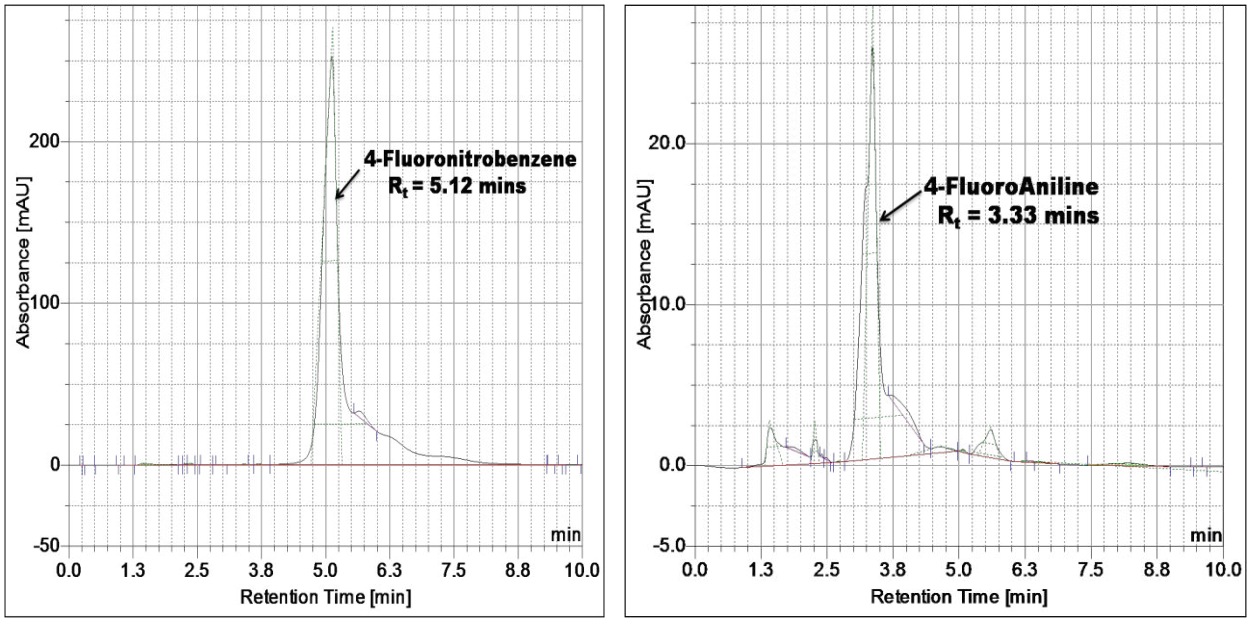

Fig. 3. HPLC chromatograms of Standard 4-flouro nitro benzene and 4-flouroaniline

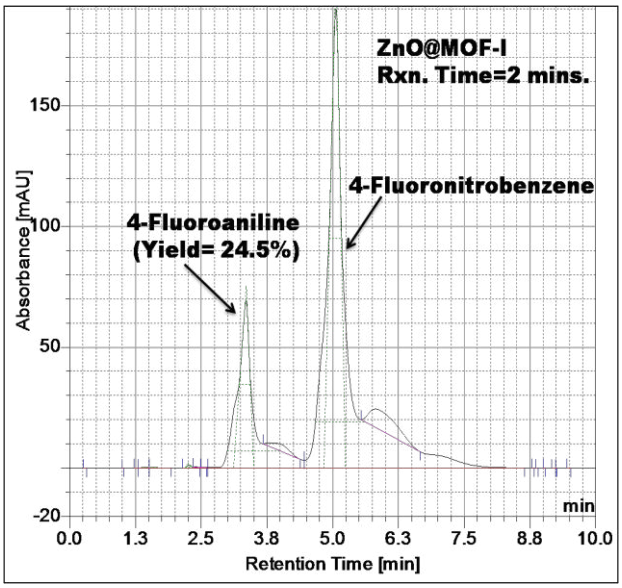
ZnO@MOF-I
Rxn. Time=2 mins.
4-Fluoroaniline
(Yield= 24.5%)
4-Fluoronitrobenzene
Absorbance [mAU]
Retention Time [min]
min

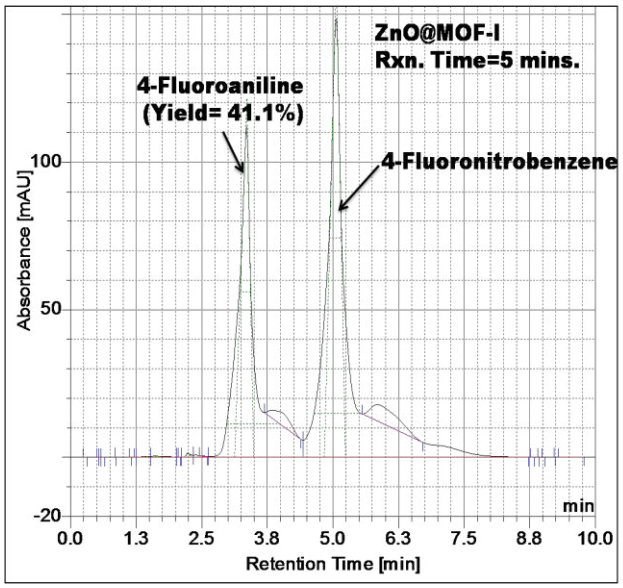
ZnO@MOF-I
Rxn. Time=5 mins.
4-Fluoroaniline
(Yield= 41.1%)
4-Fluoronitrobenzene
Absorbance [mAU]
Retention Time [min]
min

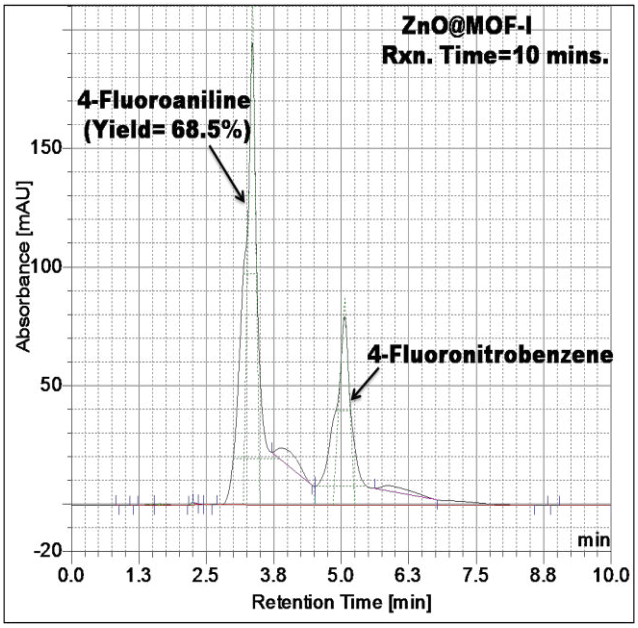
ZnO@MOF-I
Rxn. Time=10 mins.
4-Fluoroaniline
(Yield= 68.5%)
4-Fluoronitrobenzene
Absorbance [mAU]
Retention Time [min]
min

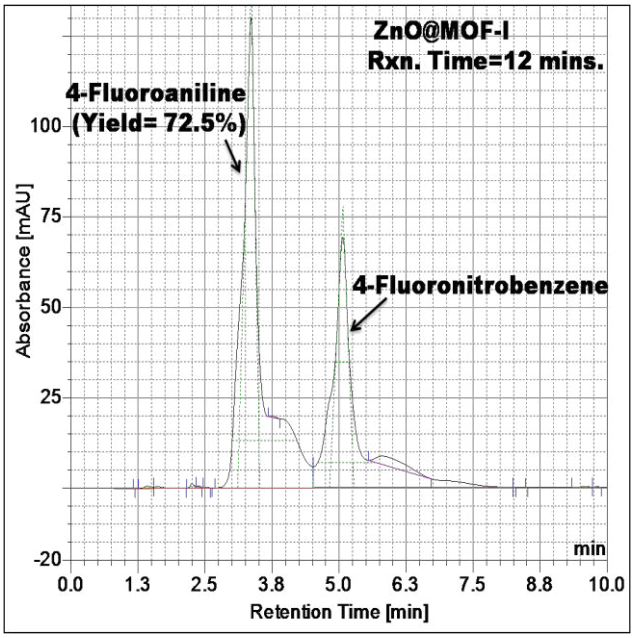
ZnO@MOF-I
Rxn. Time=12 mins.
4-Fluoroaniline
(Yield= 72.5%)
4-Fluoronitrobenzene
Absorbance [mAU]
Retention Time [min]
min

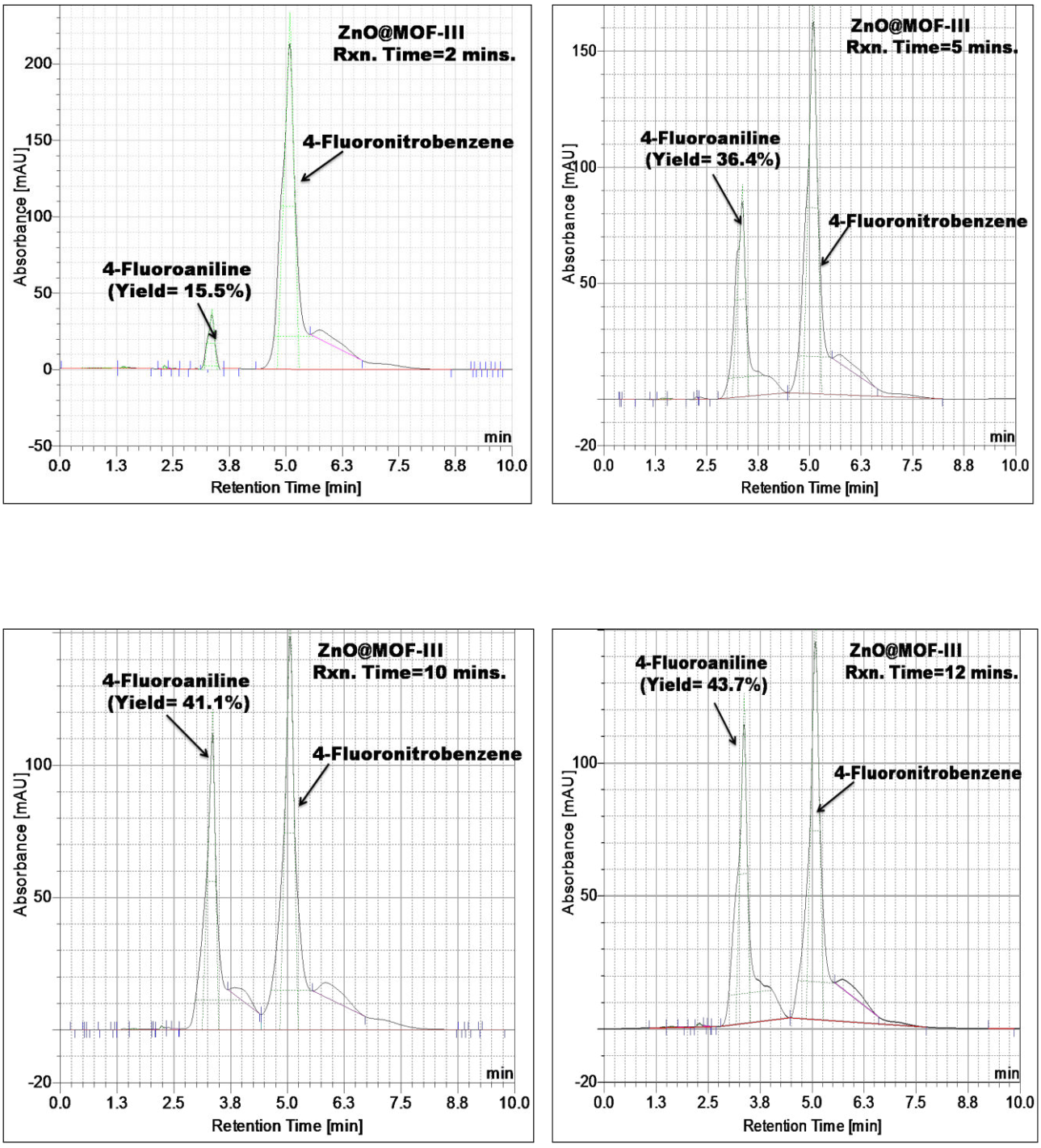

Fig.4. HPLC chromatograms for the catalytic reduction of 4-flouro nitro benzene using ZnO/MOF-I and ZnO/MOF-III

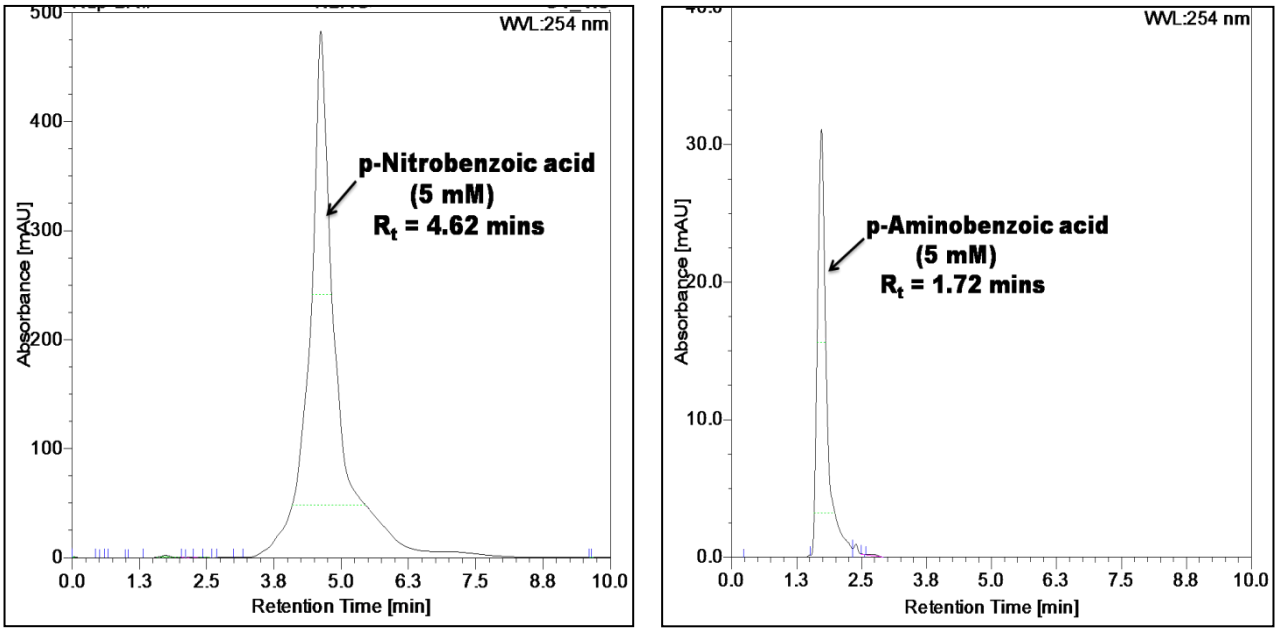

Fig.5. HPLC chromatograms of Standard p-nitro benzoic acid and p-amino benzoic acid

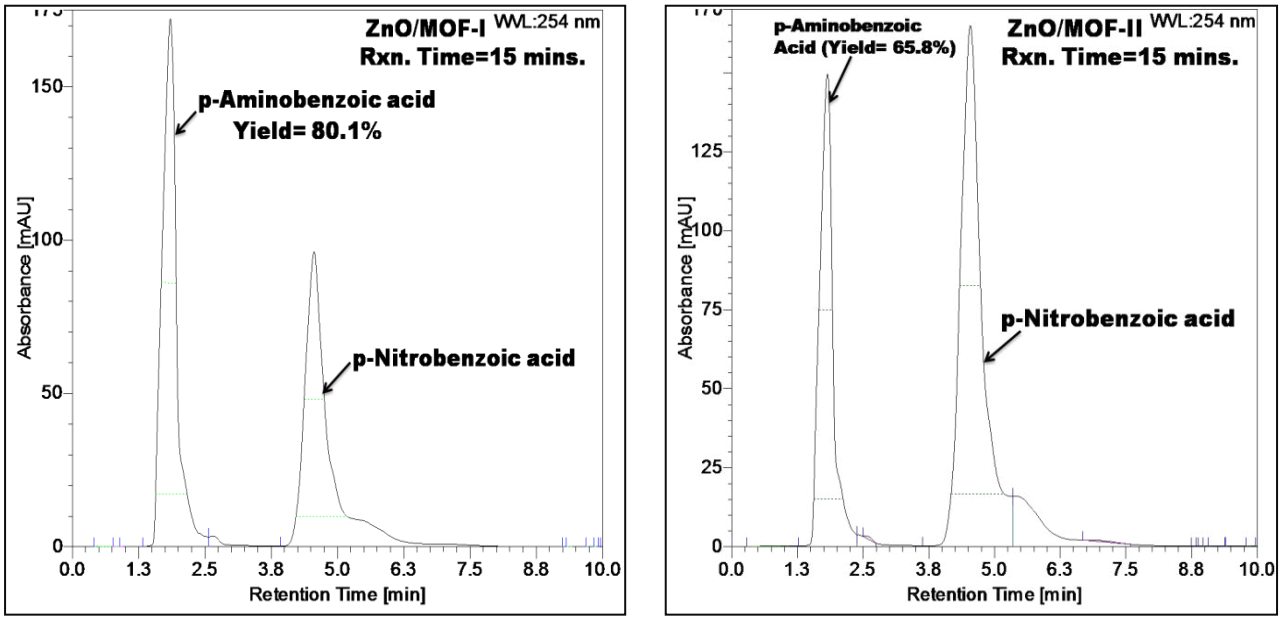

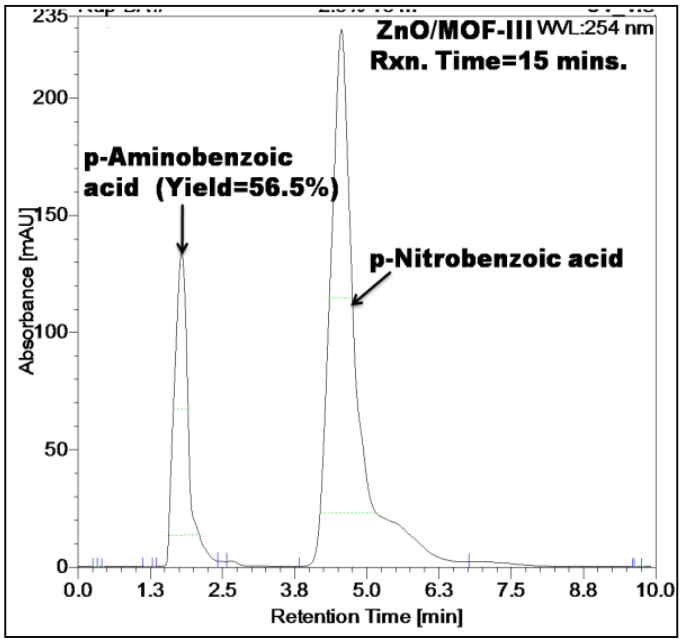

Fig.6. HPLC chromatograms for the catalytic reduction of p-nitro benzoic acid using ZnO/MOF-I, ZnO/MOF-II and ZnO/MOF-III

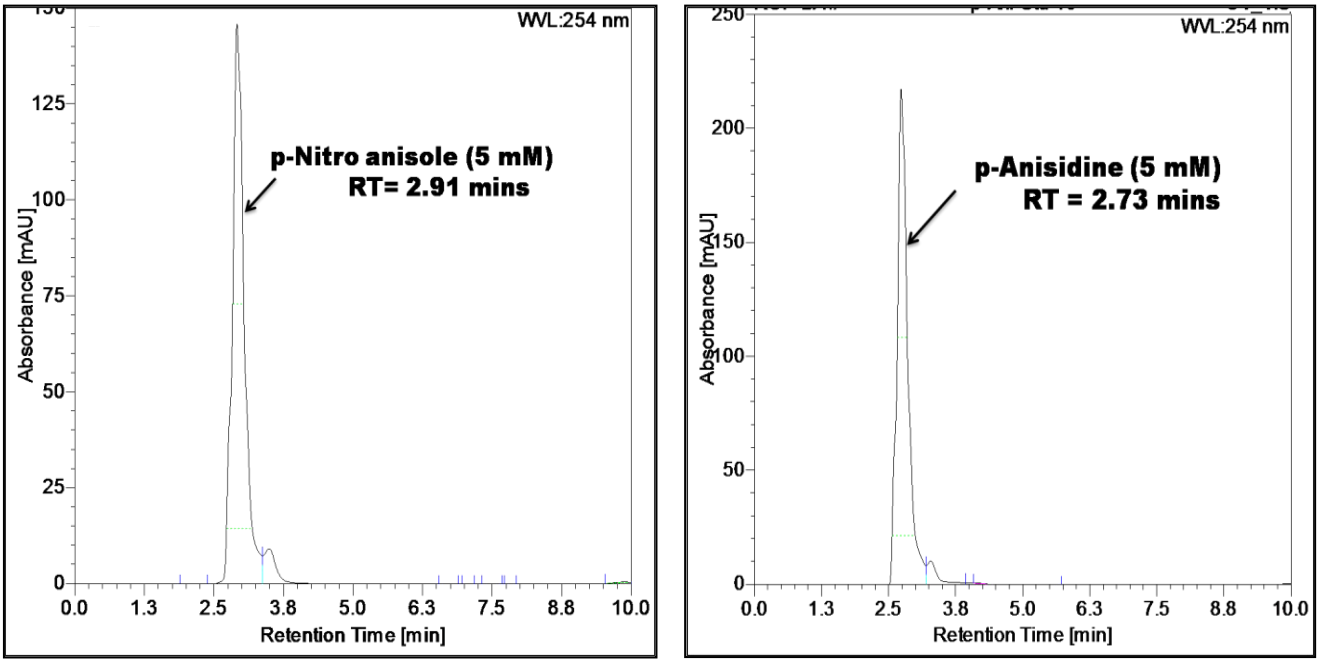

Fig.7. HPLC chromatograms of Standard p-nitro anisole and 4-anisidine

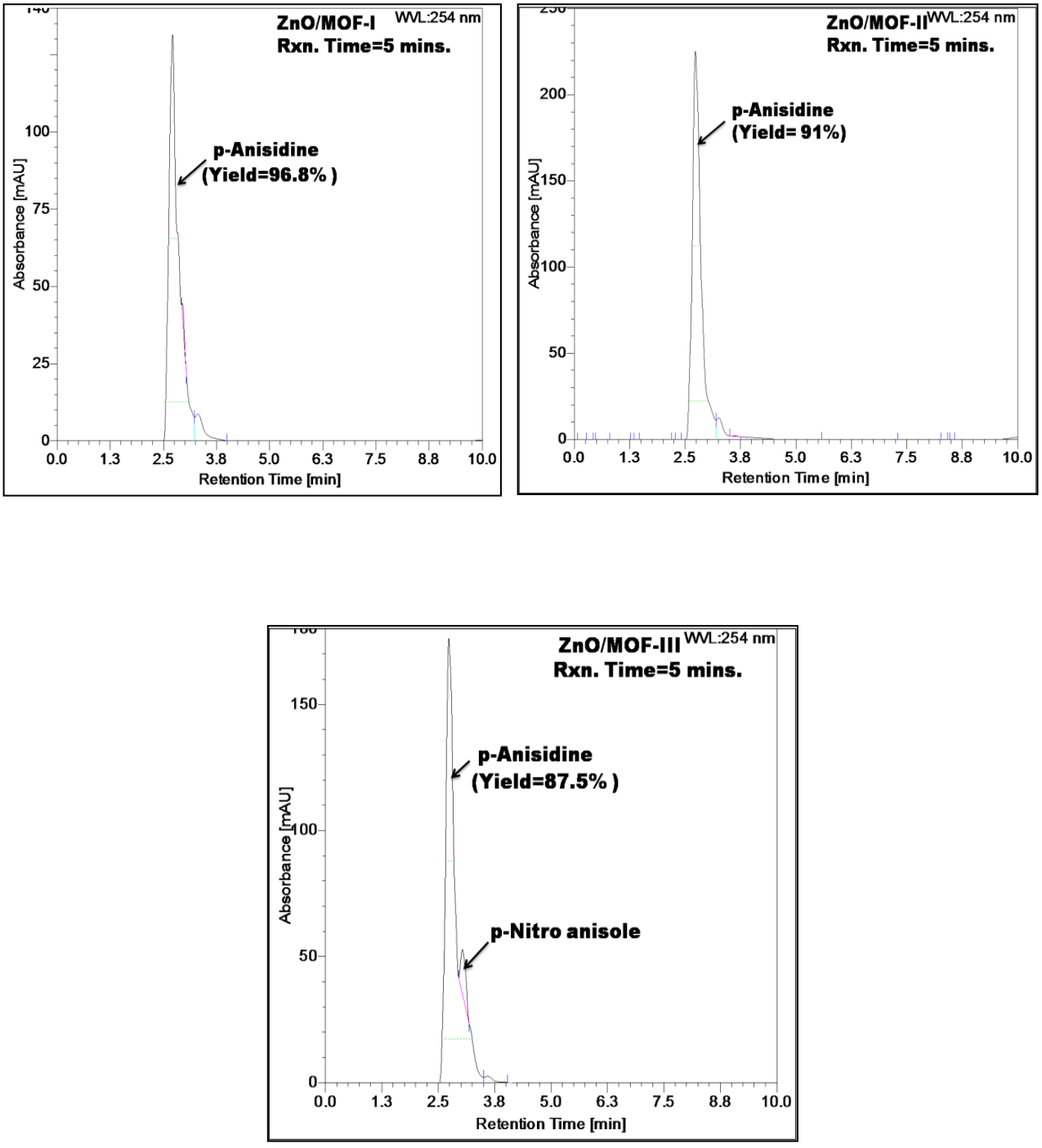

Fig. 8. HPLC chromatograms for the catalytic reduction of p-nitro anisole using ZnO/MOF-I, ZnO/MOF-II and ZnO/MOF-III

LIST OF PUBLICATIONS

Papers in SCI/referred journals

1. Rupinder Kaur, Susheel K. Mittal*, Manmohan Chhibber and Partha Mahata, **Luminescence Based Detection of Trinitrophenol and Aromatic Organophosphorous Pesticides Using a Coordination Polymer,** *J. Mex. Chem. Soc*., **2017**, 61(4), 336-341.
2. Rupinder Kaur, Susheel K. Mittal*, Manmohan Chhibber and Partha Mahata, **Induction of Catalytic Activity in ZnO Loaded Cobalt Based MOF for the Reduction of Nitroarenes,** *Chemistry Select,* **2018**, 3, 3417– 3425.
3. Rupinder Kaur, Susheel K. Mittal*, Manmohan Chhibber and Partha Mahata "**Cobalt based metal organic framework with incorporated ceria nanostructures for efficient oxygen evolution"** (Manuscript under preparation)

Papers/ Posters in Conferences

1. **Poster presentation** at *17th CRSI National Symposium for Chemistry* held at NCL, Pune, 6-8 Feb, 2015.
2. **Poster presentation** at *Synergistic Aspects of Chemical and Other Sciences (SACOS-2015)* held at Punjabi University, Patiala, 19-20 Feb, 2015.
3. Attended ***"TEQIP Sponsored- Short Term Course on Advanced Materials & Characterization Techniques"*** held at NIT, Jallandhar from 01-07 June, 2015.
4. **Poster presentation** at *National Conference on New Frontiers in Chemistry- From Fundamentals to Applications (NFCFA-2015)* held at BITS Pilani, KK Birla Campus, Goa, 18-19 Dec, 2015.
5. **Poster presentation** at *18th CRSI National Symposium for Chemistry* held at Panjab University, 5-7 Feb, 2016.